The distribution of dwarf galaxies and black holes in the local cosmic density field

Emmanuel Detsis

Doctor of Philosophy
University of Edinburgh
2005

To my parents who were and always are there for me.

Declaration

I declare that this thesis was composed by myself and that the work contained therein is my own, except where explicitly stated otherwise in the text.

(*Emmanuel Detsis*)

Table of Contents

Chapter 1

Introduction

1.1 The Universe from basic principles

The nature of the universe is undoubtedly one of the most important questions that the human race has tried to answer. The question "why am I here?" and "where is here?" is still being vehemently argued. If the first question is almost impossible to answer from a scientific point of you, at least there is hope to get an answer for the second one. Not surprisingly, the answer is not complete yet, although we now claim to have a good picture of how the universe is.

The main characteristic of the universe is that it is homogeneous and isotropic. There are striking differences in small scales of course, like stars in comparison to empty space or even the Milky Way when compared to the intergalactic void, but on larger scales there is very little deviation from the mean density of the universe nor is there a preferred direction for the distribution of matter. The idea of a universe with such characteristics is indeed old.

As a philosophical argument, it was initially put forth by Giordano Bruno in two of his philosophical dialogues in 1584, in which we advocates an infinite, homogeneous universe without any preference in position (so the earth itself is simply one heavenly body amongst others). This was an extension of the Heliocentric system of Copernicus and was inspired more from personal and philosophical beliefs than any scientific observations.

The notions of homogeneity and isotropy but not infinity (in the sense that the universe is extended forever) were present in the cosmology of Einstein when he formulated his general theory of relativity in the beginning of the 20th century (de Sitter, 1916; Einstein, 1920). This was a mathematical description of the universal geometry and one of the landmarks of modern physics. The formulation of general relativity marks the beginning of modern cosmology and is the basis that any model of the universe must be based upon.

The theoretical foundation therefore had been set and observational proof had to wait for technology to catch up with theory. After the completion of several major surveys that mapped a large portion of the sky and a large number of galaxies (Shapley & Ames, 1932; Zwicky *et al.*, 1968; Shane & Wirtanen, 1967) the main universal characteristics of homogeneity and isotropy where verified observationally as well.

Of course the presence of structure in the universe cannot be ignored and the question arises as to how did structure formed in such a universe. This is one of the fundamental questions of modern cosmology and in order to proceed with any specialised description of the universe and its contents it is imperative to outline, at least in general, the current cosmological model that will serve as the foundation that the remaining thesis will be build upon.

1.1.1 The metric

The equation that describes the relation of the coordinates of the four dimensions, three spatial and one time coordinate, in a spacetime continuum is called the metric. More specifically, the metric gives the spacetime separation between two events in a universe. The metric is the foundation for any description since it defines the geometry of the continuum. For a universe that is homogeneous and isotropic the spacetime interval that is applicable is called Robertson-Walker metric.

The Robertson-Walker metric has many forms, although perhaps the most widely used is

$$c^2 d\tau^2 = c^2 dt^2 - R^2(t)[dr^2 + f_k^2(r) d\phi^2] \ , \tag{1.1}$$

where c is the speed of light, $d\tau$ is the proper interval, R is the scale factor (which is time dependant) and measures how the universe changes with time, either by contracting or expanding, dr and $d\phi$ are the spatial parts of the metric and the function f_k is a function of the curvature of the universe and has the following form, depending on the geometry

$$f_k(r) = \begin{cases} \sin r & k = 1 \quad \text{positive curvature} \\ \sinh r & k = -1 \quad \text{negative curvature} \\ r & k = 0 \quad \text{no curvature} \end{cases} \tag{1.2}$$

It is important to note the the coordinate r is a comoving coordinate, which means that it remains constant as the universe expands. The frame of reference in this case is locked in the Hubble flow, so the coordinates do not change as the universe expands. The true distance between two points may change over time due to the expansion, but their comoving distance will remain the same.

The curvature of the universe can have three states without violating the need for an isotropic and homogeneous universe. The tree states define the geometry of spacetime and if the universe will be open (infinite) or closed (finite).

- The $3D$ space of a positively curved universe has the $2D$ analogue of a sphere. The surface has no visible boundaries but it is finite; in this case, the universe is closed.
- For a negatively curved universe, an analogue is hard to imagine. A saddle region has negative curvature in $2D$ space. The universe in this case is infinite and open.
- No curvature denotes a universe that has all the characteristics of Euclidean space. It is infinite and extends to all directions.

1.1.2 Expansion of the universe

There is much observational evidence to support the case that the universe is not static but it is in fact expanding. Since the universe itself is expanding, then a single observer positioned at some part of the universe will note that the cosmos appears to be moving away from his position. A mass distribution that is homogeneous and isotropic (for these properties have to be maintained) gives rise to a velocity field that can only have the form

$$v = H \cdot r \ . \tag{1.3}$$

The equation can be rewritten with the help of the scale factor as

$$H = \frac{\dot{R}}{R} \ . \tag{1.4}$$

This is *Hubble's Law* that states that galaxies move away with a velocity that is linearly dependant on their distance from us. This observation was the first to support the case for an expanding universe, as stated in Hubble & Humason (1931) and perhaps the most striking. The constant H is the Hubble constant and its value it is still an issue of investigation in cosmology. The value of H_0 (the value of H in the present epoch) has been calculated within a small error margin by two key cosmology projects as $H_0 = 72 \pm 8\,\mathrm{km\,s^{-1}Mpc^{-1}}$, from the Hubble Space Telescope key project to measure the Hubble constant (Freedman *et al.*, 2001) and $H_0 = 72 \pm 5\,\mathrm{km\,s^{-1}Mpc^{-1}}$ (Spergel *et al.*, 2003), from the Wilkinson Microwave Anisotropy Probe.

1.1.3 Redshift

The discovery that galaxies have different velocities was made by spectral analysis of their emitted light and the fact that their spectrum appears to be redshifted. By identifying various features (normally well known emission or absorption lines of elements) in the spectrum of an object and comparing with laboratory data on the same features, the velocity that the object is moving can be recovered. For a source that is moving away from the observer, the light would appear to have shifted to longer wavelengths or redshifted (from the fact that visible light would appear slightly redder). This is the well known *Doppler effect*. There is a subtle difference when applied to galaxies though. A galaxy can have a relative velocity towards an observer and even appear to be *blue shifted* if it is moving towards the observer, but the *cosmological redshift* is due to the expansion of the universe. In a universe where space is expanding, the light that travels through it is stretched as well, making its wavelength longer. If a photon is emitted with frequency ν_e from a source that is moving away with velocity u with $u \ll c$, it would be observed to have a different frequency ν_o due to the doppler effect. The redshift is defined (for $u \ll c$) as

$$1 + z = \frac{\nu_e}{\nu_o} = 1 + \frac{v}{c} \ . \tag{1.5}$$

If a galaxy, that is moving away from an observer with the Hubble flow, emits a photon at time t_0 that is picked up at t_1, then the comoving distance is given by the metric as

$$d_0 = \int_{t_0}^{t_1} \frac{c}{R(t)} dt \ . \tag{1.6}$$

If a second photon is emitted from the source after δt_0 and picked up after δt_1, then once more the comoving distance is

$$d_1 = \int_{t_0+\delta t_0}^{t_1+\delta t_1} \frac{c}{R(t)} dt \ . \tag{1.7}$$

The comoving distance does not change with time though, so $d_1 = d_0$. Equation 1.7 can be broken in different integrals as

$$d_1 = \int_{t_0}^{t_0+\delta t_0} \frac{c}{R(t)} dt + d_0 - \int_{t_0}^{t_0+\delta t_0} \frac{c}{R(t)} dt \ , \tag{1.8}$$

therefore

$$\int_{t_1}^{t_1+\delta t_1} \frac{c}{R(t)} dt = \int_{t_0}^{t_0+\delta t_0} \frac{c}{R(t)} dt \ . \tag{1.9}$$

Since the time difference between the emission of the two photons is very small, R is constant for the emission and reception. Therefore,

$$\frac{\delta t_0}{R_0} = \frac{\delta t_1}{R_1} \Longleftrightarrow \frac{\delta t_0}{\delta t_1} = \frac{R_0}{R_1} \ . \tag{1.10}$$

This relation should hold for the photon frequencies as well, so it follows that

$$\frac{\nu_0}{\nu_1} = \frac{R_0}{R_1} \ , \tag{1.11}$$

and the redshift due to the expansion of the universe will be given as

$$1 + z = \frac{R_0}{R_1} \ . \tag{1.12}$$

It is normal practise to create a dimensionless scale factor

$$a(t) = \frac{R(t)}{R_0} \ , \tag{1.13}$$

where R_0 is the value of the scale factor at the present epoch. Using this notation

$$a(t) = (1 + z)^{-1} \ . \tag{1.14}$$

1.1.4 Distance - Redshift relation

In Newtonian physics if a spherically symmetric object with radius r is placed at position O, the gravitational field generated by this object at any point beyond the radius of the object can be replaced by the gravitational field generated by a point with the same mass as the object placed at O. The gravitational field at a point $x < r$ can be replaced by a point at O with mass equal to the mass of the object encompassed by a sphere with radius x. This implies that the gravitational field inside a spherical shell is zero. In 1923 Birkhoff proved that the same holds in general relativity. This allows to use the energy conservation argument for the expanding universe, therefore the formula

$$\frac{(\dot{R}r)^2}{2} - \frac{GM}{Rr} = const \tag{1.15}$$

must hold true. The constant at the right hand side is given by general relativity and substituting the mass M for the case of a sphere with $M = \rho\frac{4}{3}\pi(rR)^3$ equation 1.15 transforms to

$$\dot{R}^2 - \frac{8\pi G}{3}\rho R^2 = -kc^2 \ , \tag{1.16}$$

where the density ρ includes contributions from all components to the universe (matter, radiation and vacuum). For a universe without curvature, $k = 0$ and from 1.16 and 1.4, the critical density is given by

$$\rho_c = \frac{3H^2}{8\pi G} \ . \tag{1.17}$$

This critical density gives an insight to the geometry of the universe. If the density of the universe ρ has a value higher than the critical density ρ_c then the universe is said to be spatially closed. If $\rho < \rho_c$, then the universe is spatially open.

The relation between the density of the universe and the critical density is given by the dimensionless parameter

$$\Omega \equiv \frac{\rho}{\rho_c} = \frac{8\pi G\rho}{3H^2} \ . \tag{1.18}$$

Very often, Ω is split into the various contributors to the density and then becomes

$$\Omega = \Omega_m + \Omega_r + \Omega_\Lambda \ , \tag{1.19}$$

where Ω_m is the contribution from the matter in the universe, Ω_r is due to radiation and Ω_Λ is the contribution of the cosmological constant. For an expanding universe, the densities will change as space grows bigger, so the density becomes

$$\rho(a) \propto \Omega_m a^{-3} + \Omega_r a^{-4} + \Omega_\Lambda \ , \tag{1.20}$$

in order to account for the thinning out of the density (the a^{-3} term for both matter and radiation) and the redshifting of the radiation frequency (the extra a^{-1} term for the radiation). The contribution from the cosmological constant remains fixed and is not affected by the expansion.

Since the values of many cosmological parameters change with every breakthrough that is made, it is desirable to be able to scale results for the different cosmology used in each case. Thus, the introduction of the h parameter that scales the Hubble constant.

$$h = \frac{H_0}{100\,\mathrm{km\,s^{-1}Mpc^{-1}}} \ , \tag{1.21}$$

where H_0 is the current value of the Hubble constant. Manipulating 1.16

$$H^2 = \frac{8\pi G\rho}{3} - \frac{kc^2}{R^2} \ , \tag{1.22}$$

and substituting for the various contributions

$$\frac{8\pi G\rho}{3} = H_0^2(\Omega_\Lambda + \Omega_m a^{-3} + \Omega_r a^{-4}) \ , \tag{1.23}$$

and

$$\frac{kc}{H^2R^2} = \Omega - 1 \ , \tag{1.24}$$

equation 1.22 then becomes

$$H^2(a) = H_0^2[\Omega_v + \Omega_m a^{-3} + \Omega_r a^{-4} - (\Omega - 1)a^{-2}] \ . \tag{1.25}$$

The radial equation for a photon is

$$Rdr = cd\tau = c\frac{dR}{\dot{R}} = \frac{c}{H}\frac{dR}{R} \tag{1.26}$$

and substituting the a factor with the redshift

$$R_0 dr = \frac{c}{H_0}[(1-\Omega)(1+z)^2 + \Omega_\Lambda + \Omega_m(1+z)^3 + \Omega_r(1+z)^4]^{-1/2}dz \ . \tag{1.27}$$

1.1.5 Some tools of cosmography

The prime objective of galaxy surveys is to give the positions of galaxies in the universe along with their magnitude, a measure of their luminosity. Hence the most frequent equations in an analysis are the ones dealing with the distance to a galaxy and its luminosity.

Equation 1.27 gives the comoving distance element. In a more compact form and integrating over z, it can be rewritten as

$$D_c = \frac{c}{H_0}\int_0^z \frac{dz}{E(z)} \ , \tag{1.28}$$

which gives the comoving distance to redshift z (Hogg, 2000), with $E(z)$ being

$$E(z) = \sqrt{(1-\Omega)(1+z)^2 + \Omega_\Lambda + \Omega_m(1+z)^3 + \Omega_r(1+z)^4} \ . \tag{1.29}$$

The angular diameter distance is defined as the ratio of the transverse size of an object to its angular size. It transforms angular separations in a telescope image to physical size at the source. For a universe without curvature (as it is used in all calculations in this thesis) it has the form

$$D_A = (1+z)^{-1}D_c \ . \tag{1.30}$$

Another important quantity is the luminosity distance, which is defined as

$$D_L = \sqrt{\frac{L}{4\pi S}} \ , \tag{1.31}$$

where L and S are the bolometric luminosity and flux of the object respectively. The luminosity distance depends on the comoving distance as follows

$$D_L = (1+z)D_c \ . \tag{1.32}$$

If the monochromatic flux of an object at redshift z is of concern (since it is very difficult to integrate over all frequencies to get the bolometric quantities), the equation for it is

$$S_\nu(\nu_0) = \frac{L_\nu\big((1+z)\nu_o\big)}{4\pi D_c(1+z)} \ . \tag{1.33}$$

Finally, the comoving volume element at redshift z is given by

$$dV = \frac{c}{H_0}\frac{(1+z)^2 D_A^2}{E(z)}d\Omega\, dz \ . \tag{1.34}$$

1.2 CDM cosmology

The metric of the universe and its equation of state is of course useful to know, but it still does not answer the question of what is in the universe, more specifically what are the values of the Ω_x factors. The initial guess was that the nature of Ω_m would be pretty straightforward to define, as galaxies make up the universe, but apparently not all is what it seems.

1.2.1 Evidence for the existence of Dark Matter

Observational proof that there is something missing in the universal picture came as soon as large catalogues were made. After the study of kinematics in the large galaxy clusters Coma and Virgo, it was found that the calculated total mass of the cluster was orders of magnitude larger than the one expected. The velocities of the individual galaxies were far to great for the clusters to be gravitationally bound by just the mass that was observed (Smith, 1936; Zwicky, 1937), but the velocities could be explained if there was some mass in a non luminous form.

The question about the existence of this mysterious for of matter arose later as well after the study of the rotational curves of galaxies (Freeman, 1970; Ostriker *et al.*, 1974; Rubin *et al.*, 1980; Burstein & Rubin, 1985). The velocity profiles of stars at the edge of a galactic disk were found to deviate from the expected rotational curve for a galaxy that contains most of its mass in the centre and has its limits at the edges of the luminous disk. The profiles could be explained if the galaxy exhisted within a halo of dark matter which continued after the luminous edge of the galaxy.

1.2.2 The mass of the universe

One of the most fundamental questions in cosmology is the amount of mass in the universe. In the local universe, the numerical density of galaxies per luminosity (the luminosity function of galaxies) has been well established from redshift surveys (at least for the local universe) and has the form

$$\phi(L)dL = \phi_* \left(\frac{L}{L_*}\right)^{-\alpha} e^{-L/L_*} \frac{dL}{L_*} \ . \tag{1.35}$$

This is often called the Schechter Luminosity Function, since it was first introduced by Schechter (1976). The integration of the luminosity function over all luminosities will give the luminosity density of the local universe

$$\int \phi(L)dL = \phi_* L_* \Gamma(2-\alpha) = \rho_L \ . \tag{1.36}$$

In the blue band, the value for the luminosity density as given by Efstathiou *et al.* (1988) is

$$\rho_L = 1.93 \pm 0.7 \times 10^8 h L_\odot \ , \tag{1.37}$$

where $L_\odot$ is the luminosity of the sun. If the luminosity density is divided with the critical density, it produces the necessary *mass to light ratio* to close the universe, which has a value of

$$\left(\frac{M}{L}\right)_{\text{critical}} \sim 1.5 \pm 0.5 \times 10^3 h \ . \tag{1.38}$$

This is a very large value. Even large values of mass to light ratios for galaxies do not exceed $M/L \sim 10^2$ (Tully, 2005). So in order to have a closed universe, there is a need for the existence of dark matter.

1.2.3 The nature of dark matter

The nature of dark matter is a puzzle and it will remain so, until some direct observation of the DM particle or particles in the laboratory. So far, results have been negative (Akerib *et al.*, 2004). There are many theories concerning the nature of dark matter. The cosmology that is widely adopted these days in the Cold Dark Matter (CDM) model, initially proposed by Peebles (1982) or even more explicitly, ΛCDM, a cold dark matter model that incorporates a cosmological constant (Gnedin, 1996; Efstathiou *et al.*, 2002). The name cold implies that the particles of the CDM have no thermal velocities. These particles are nonbaryonic and collisionless and had decoupled while they were non relativistic after the big bang.

It is not know which particles make up the dark matter and there are two main theories concerning their nature. The first school of thought proposes that the DM consists of Weakly Interacting Massive Particles or WIMPs, as they are widely known. These are elementary particles that, as the name suggests, interact though gravity and the weak nuclear force only (Pretzl, 2002; Kamionkowski & Kurylov, 2005). The other theory put forth advocates that the missing matter is made up by large objects that are not bright enough to be detected, like black holes, brown dwarves and planets, a class of objects known as Massive Astrophysical Compact Halo Objects (MACHOs) as an answer to the previous idea (Waldrop, 1993; de Paolis *et al.*, 1998; Yoo *et al.*, 2004).

1.3 Formation of structure

The ultimate test of any theory is of course to reproduce the observational facts. In the case of dark matter models, the observational verification would be the reproduction of the structure that is present in the universe today. Not only does the model have to account for the general universal characteristics of homogeneity and isotropy at large scales, but the presence of clusters of galaxies and galaxies themselves have to be accounted for. The CDM model is a hierarchical model where small objects clump together to form larger configurations. Structure starts from the base up. The main idea is that primordial fluctuations in a smooth density field would grow and create underdense and overdense regions that will then become the dark matter haloes upon which galaxies are formed.

1.3.1 Press Schechter approach

The number of gravitationally bound structures $f(M)dM$ is called the mass function. The integral mass function $F(M)$ denotes the number of objects with masses greater than M. The formation of objects under gravity is a very complex non-linear problem but the overall number of bound objects can be approximated for an initial *linear* density field, therefore calculating $F(M)$ can become possible.

If an initial density field $\rho(x)$ exists, that is homogeneous and isotropic in large scales but has overdense and underdense regions locally, there would be regions with overdensity $1 + \delta_R = \rho/\langle\rho\rangle$ larger than a critical value δ_c that would be expected to form gravitationally bound objects after their collapse.

If the initial random field has a Gaussian form and the overdense regions are smoothed over with a window function W_R with a smoothing radius R, the regions with density higher than the critical density will eventually form objects with mass $M \propto \bar{\rho}R^3$, with $\bar{\rho}$ being the mean density of the initial field. The precise relation depends on the smoothing function and for a Gaussian function is given by

$$M = (2\pi)^{\frac{3}{2}}\bar{\rho}R^3 \ . \tag{1.39}$$

The probability that a point will lie inside one of the overdense regions for the Gaussian field is given by

$$p(\delta > \delta_c|R) = \frac{1}{2}\left[1 - \mathrm{erf}\left(\frac{\delta_c}{\sqrt{2}\sigma(\mathrm{R})}\right)\right] \ , \tag{1.40}$$

where erf is the error function

$$\mathrm{erf(x)} = \frac{2}{\sqrt{\pi}}\int_0^{\mathrm{x}} \mathrm{e}^{-\mathrm{t}^2}\mathrm{dt} \ , \tag{1.41}$$

so the integral mass function will be

$$F(M) = \int_{\delta_c}^{\infty} P(\delta, R) d\delta = 1 - \mathrm{erf}\left(\frac{\delta_c}{\sigma(\mathrm{M})\sqrt{2}}\right) \quad , \tag{1.42}$$

the mass function is

$$f(M) = \frac{\partial F(M)}{\partial M} \quad , \tag{1.43}$$

the comoving number density is

$$\frac{M f(M)}{\bar{\rho}} = \left|\frac{\partial F}{\partial M}\right| \quad , \tag{1.44}$$

so this gives

$$N(M)dM = -\left(\frac{\bar{\rho}}{M}\right)\left(\frac{1}{2\pi}\right)^{1/2}\left(\frac{\delta_c\, d\sigma}{\sigma^2\, dM}\right)\exp\left(-\frac{\delta_c^2}{2\sigma^2}\right) dM \quad , \tag{1.45}$$

or

$$\frac{M^2 f(M)}{\bar{\rho}} = \frac{dF}{dlnM} = \left|\frac{d\,\ln\sigma}{d\,\ln M}\right| \sqrt{\frac{2}{\pi}}\frac{\delta_c}{\sigma}\exp\left(-\frac{\delta_c^2}{2\sigma^2}\right) \quad , \tag{1.46}$$

where $M^2 f(M)/\bar{\rho}$ is the multiplicity function. Equation 1.46 was the inspiration for the general galaxy luminosity function in its Schechter form since equation 1.35 was developed around the same time (Schechter, 1976).

The Press-Schechter theory has been expanded since then but the basis of the theory remain the same. One of the problems of the theory is the prediction of the number of low mass objects. Theory predicts a higher number of objects than the number seen by simulations of hierarchical clustering. In an attempt to account for this discrepancy Sheth *et al.* (2001) and Sheth & Tormen (2002) have proposed a model where the spherical collapse of dark matter haloes is replaced by an ellipsoidal collapse, thus allowing for better agreement between theory and simulation.

1.4 Galaxy Formation

So far the formation of structure concerns dark matter and not the galaxies that are visible in the universe. But the stuff of galaxies, namely baryons, were present during the creation of the dark matter haloes and after the creation of sufficiently large haloes, galaxy formation starts taking place.

Modelling the galactic distribution is a very complex procedure because of the nature of the problem and one successful approach is semi-analytical models, that combine theory with computer simulations. Their strength lies in the fact that

they can utilise the computational power of modern computers with some theoretical approximations to speed up and simplify the problem, as well as increase the resolution, so that actual galaxy structures can be observed. These models are quite elaborate and depend on many parameters (Kauffmann *et al.*, 1993; Cole *et al.*, 2000) but are nevertheless very educational because they incorporate many areas of modern astrophysics.

The other approach is to do a full N-body simulation of the universe, or an area thereof, by modelling the behaviour of dark matter. The achieved resolution though is not high enough to allow for individual galaxies to be examined. The results from simulations of this kind have been quite successful in replicating the clustering properties of galaxies in the observed universe (Pearce *et al.*, 1999). Overall both methods agree reasonable well on their results as shown by Benson *et al.* (2001).

1.4.1 Gas and dark matter

When dark matter halos merge to form larger objects, any present gas is heated to the virialized temperature of the halo. This is in essence the transformation of the kinetic energy of the gas into heat and for a gas cloud with mean molecular weight μ this translates to

$$kT_v = \frac{1}{2}\mu m_p V_c^2 \ , \tag{1.47}$$

where k is the Boltzmann's constant and m_p the proton mass. V_c is the circular velocity of the gas that has settled onto a disk. The reason for the formation of such a disk is that the angular momentum that the gas gains during the DM halo mergers is conserved. The rotation helps the gas avoid gravitational collapse and heats it to the virialized temperature T_v. The gas disk then starts to cool inside the gravitational well of the DM halo, a time where star formation begins taking place.

The shape of the gas regions is also governed by any cases of halo merging, an incident that may result in significant burst of star formation for the emerging galaxies. A combination of two halos can also reshape the disk and transform it into a spherical halo.

1.4.2 Star formation and feedback

After the creation of the first stars, there are three separate regions that can be identified in the galactic disk: The already formed stars, the dense gas that has cooled down and in which stars are formed and finally the still hot gas component.

The stars that are formed from the cooled gas, start radiating and heating up the remaining cold gas bringing it up to the temperature of the hot component. As well as radiation from stars, supernovae that explode enrich the interstellar medium with heavier metals and in turn transfer energy onto the interstellar medium, again heating the cold gas (Efstathiou, 2000). Stars and supernovae also give the necessary energy to material to escape the protogalactic disk in a form of wind. The heating up of the cool gas and the escape of material from the disk affects the star formation rate. This process is called feedback, since the new born stars change the parameters that led to their creation, influencing the star formation process in a feedback loop.

Feedback from stars is a very important process because it prevents the creation of very small DM haloes and helps explain the absence of dwarf galaxies. The number of low mass haloes predicted from Press-Schechter theory has the form

$$\frac{dN(m)}{dm} \approx m^{-(9-n)/6} \ , \tag{1.48}$$

which for any reasonable values of n predicts a low mass slope much steeper than the observed faint end of the galaxy luminosity function (Efstathiou *et al.*, 1988; Loveday *et al.*, 1992; Loveday, 1997; Zucca *et al.*, 1997). Without a feedback mechanism to prevent the collapse of small haloes the theory would strongly contradict observations in that range.

1.4.3 Biasing of the galaxy distribution

The way galaxies form relative to the Dark Matter Haloes is a very important question. It is not easy to answer because detailed observations of dark matter in the universe cannot be done directly despite some hints from gravitational lensing. Therefore simulations of the DM are performed in order to understand its properties. The distribution of galaxies in the universe is much easier to observe but nevertheless there remains a grey area between the simulations and the galaxies, namely as to how precisely do galaxies form in the sea of dark matter. It is not trivial to solve, since the simulations are better suited to monitor the dark matter whereas observations are confined to the galaxies only.

The borderline area between the dark matter and the galaxy formations is known as the biasing of the galaxy distribution. The definition of the bias parameter b is

$$\left(\frac{\Delta\rho}{\rho}\right)_{\mathrm{DM}} = b\left(\frac{\Delta\rho}{\rho}\right)_{\mathrm{galaxies}} \ , \tag{1.49}$$

where ρ indicates density. The development of the bias parameter was deemed

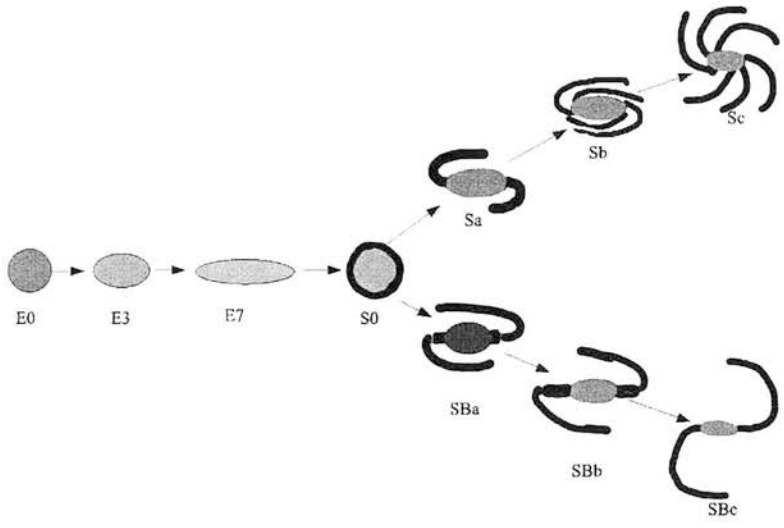

Figure 1.1: The Hubble sequence of galaxies. From ellipticals to the left to spirals and barred spirals. Irregulars are not included since they have to predetermined shape.

necessary because of the fact that different galaxy types are seen to cluster in different ways, therefore they could not all be correct tracers of the mass distribution. Latest results indicate that at least on large scale, galaxies overall trace the matter distribution with a bias parameter equal to one hence they are good tracers of the mass (Verde *et al.*, 2002). On smaller scales the difference of galaxy clustering according to their type is still present.

1.4.4 Galaxy types

The galaxies that can be seen in the universe are not uniform of course. There are many different types and there are many classification schemes. The standard galactic sequence is considered the Hubble sequence (Hubble, 1926), the oldest and still the more widely used. It is based on the morphology of galaxies and divided the galaxies in the following categories

- **Elliptical Galaxies:** Galaxies that have an ellipsoid form and are categorised according to their ellipticity, from almost circular (E0) to greatly flattened (E7). Stars can be seen throughout the galaxy.
- **Lenticular Galaxies:** S0 and SB0 are galaxies that display a bulge component (looking like an E0 galaxy) in the centre and a disk around it but

have no spiral structure.

- **Spiral Galaxies:** Disk galaxies that have spiral structure. They consist of a central bulge component and a disk with a pattern of spiral arms. The distinction between spirals concerns how big the bulge is and how tight the spiral arms are around the galaxy, ranging from Sa that have a large bulge component and tight spiral arms to Sc that have a small bulge and very loose spiral arms.

- **Barred Spirals Galaxies:** They are very similar to spiral galaxies but they also display a bar running through the disk.

- **Irregular Galaxies:** Galaxies with a more chaotic and asymmetric appearance.

There is a misconception regarding this sequence. The ellipticals are often referred to as early types or early galaxies and the spirals as late types. Initially that was because it was believed that it represented the development of a galaxy. It would start as an elliptical and later develop a disk. This is not the case any more. The present school of thought is that a galaxy is formed as a spiral first and by merging the disk component gets stripped and an elliptical is formed. Nevertheless the separation to early types and late types still remains but now it refers to the position of the galaxies in the sequence; early types are to the left, late types towards the right.

1.5 Black Holes in the Universe

There are other entities that take part in the feedback process as well as the supernovae and radiating stars. These are the active galactic nuclei, that produce enormous energy that impacts on the interstellar medium and drive the feedback process. The term active galactic nuclei takes its name from the fact that in those particular galaxies the non-thermal energy output exceeds the thermal energy output from stars, gas and interstellar medium at some band or bands, thus the presence of other processes apart from thermal radiation makes the galaxy active. It is also observed that most of this energy is generated in the central part of the galaxy, thus the combined term active nuclei. The current paradigm for an AGN, is of disk accreting onto a supermassive black hole ($\geq 10^8 M_\odot$) (Urry & Padovani, 1995).

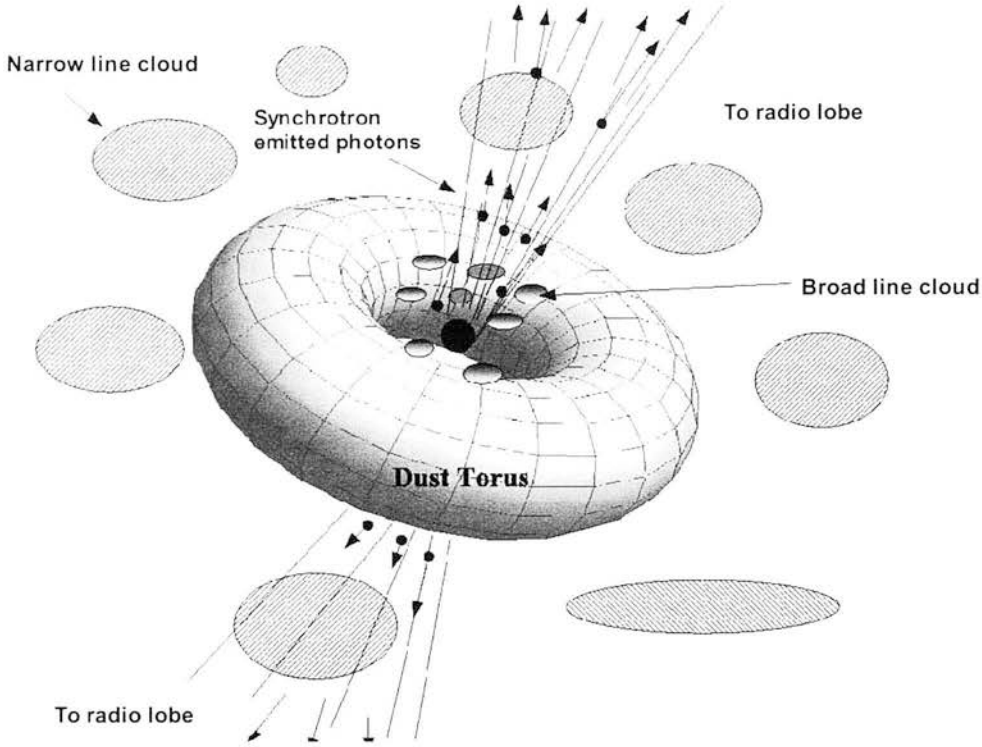

Figure 1.2: A schematic of an Active Galactic Nuclei. The black hole in the centre is surrounded by a disk of material that is accreting on to the centre.

1.5.1 AGN schematics

Active nuclei have been the subject of many studies and even more changes concerning their nature. Since the realisation by Seyfert (1943) that some extragalactic nebulae exhibit strong emission lines and they form a distinct group from normal galaxies (later named Seyfert galaxies), the riddle of their nature kept becoming more complex with time.

Radio emission from some of these sources was detected and the first picture of their nature began to form in the late 50s. Woltjer (1959) argued that

- They are small in size, less than 100 pc.
- Their lifetimes must be of the order of 10^8 years.
- Their mass must be very high, of the order $10^8 M_\odot$

From radio surveys, a new class of objects were added to the picture; Quasars or quasi-stellar radio sources. Star like objects that exhibited strong radio emission (Matthews & Sandage, 1963), which were later found to have very high redshift (Schmidt, 1963). If the redshift was a measurement of their distance form the earth then these star like objects must have an enormous luminosity,

brighter even than luminous galaxies. Eventually Seyfert galaxies and quasars were recognised as part of the same sequence of objects as reported by Weedman (1976), with the creation of a unified model for all the Active Galaxies (Antonucci, 1993; Urry & Padovani, 1995).

1.5.2 Black Hole Masses

There is of course no limit to the mass of a black hole, at least theoretically. Any mass that is contained in a small enough volume can create a black hole. The radius for the configuration is given from the Schwarzschild radius:

$$r_s = \frac{2Gm}{c^2} \ , \tag{1.50}$$

where G is the gravitational constant, c the speed of light and m the mass in question. The masses of the Black Holes that reside in Active Galactic Nuclei are quite large as can be verified by an approximation via the Eddington Luminosity.

If a source has luminosity L and radius R, then in order to be stable and isotropic while radiating at maximum efficiency, radiation pressure must be countered by gravity. So for a point at distance r

$$|F_R| \leq |F_G| \ . \tag{1.51}$$

The radiation pressure from photons with frequency ν is given by

$$P_R = \frac{F}{c} = \frac{L}{4\pi r^2 c} \ , \tag{1.52}$$

where F is the radiation flux at point r.

The cross-section for the interaction between a photon and an electron with mass m_p is the Thomson cross section σ_e, so equation 1.51 becomes for an electron proton pair

$$\frac{\sigma_e L}{4\pi r^2 c} \leq \frac{GMm_p}{r^2} \ , \tag{1.53}$$

and thus the Eddington luminosity is

$$L_E = \frac{4\pi G c m_p}{\sigma_e} M \ . \tag{1.54}$$

The Eddington luminosity can provide a lower limit for the mass of an object if the assumption is made that the object accretes at maximum efficiency. That would be the minimum mass required to produce the observed luminosity. In most cases the Eddington limit is not reached, so equation 1.54 can be recast as

$$\frac{\sigma_e L}{4\pi G c m_p} \leq M \ . \tag{1.55}$$

If the substitution is made for the constant $\sigma_e = 6.652 \times 10^{-29}\mathrm{m}^2$, $G = 6.672 \times 10^{-11}\mathrm{Nm}^2\mathrm{kg}^{-2}$, $m_p = 1.673 \times 10^{-27}\mathrm{kg}$, $c = 2.997 \times 10^8\mathrm{ms}^{-1}$ and introduce the solar mass $M_\odot = 1.989 \times 10^{30}\mathrm{kg}$, then the equation takes the practical form:

$$M \geq 10^8 M_\odot \times \frac{L}{1.2 \times 10^{39}\mathrm{W}} \ . \tag{1.56}$$

For typical AGN luminosities of the order $L_{\mathrm{AGN}} \sim 10^{38}\mathrm{W}$ (Netzer *et al.*, 1996), the mass of the central black hole is in the order of 10^8 solar masses. Since the Eddington limit demands accretion at the highest efficiency the actual mass is somewhat larger as can be verified by more direct mass measurements for some galaxies (Peterson, 1993).

1.5.3 The relation of the central black hole and the host galaxy

Despite the current success of the unified model in explaining the various observations of AGN, there are still numerous questions remaining answered. Most important perhaps is the fundamental question of what triggers an AGN or how does a galaxy develop an active centre. As an indication to a possible answer to this question, Richstone *et al.* (1998) introduced a relation between the host galaxy bulge luminosity and the AGN's black hole mass, an equation also known as the Magorrian relation. It was also observed that the stellar velocity dispertions of the galactic bulge were depended on the mass of the central black hole (Ferrarese & Merritt, 2000), a fact that confirmed that the existence of the AGN is interlaced with the host galaxy.

Unfortunately the origin of the Magorrian relation is yet unclear. It is obvious that the galaxy and the central black hole evolve in an interacting way and the two relations provide some powerful constraints in any theoretical models of galaxy evolution. One such model that predicts those two correlations was proposed by Kauffmann & Haehnelt (2000). In this model, black holes evolve through merger activity. If two galaxies with comparable mass merge then their black holes combine to form a bigger BH that accretes a fraction of the merger-remnant gas, over a short period of time. Other models assume that the BH was created first after the collapse of the dark matter halo and before star formation had taken place in the bulge (Silk & Rees, 1998). The black hole then accretes and generates a quasar-wind, which could shape the gas in the proto galaxy, and influence the velocity of the stars in the bulge, giving them the necessary velocities for the $M_{\mathrm{bh}} - \sigma$ relation. These are surprisingly the only models that account for the observational correlation between the black hole mass and the host galaxy

properties and clearly the consensus on the coexistence of black holes with galaxies is not settled yet.

1.6 Radio Galaxies

1.6.1 The discovery of radio galaxies

The discovery of radio emission from extraterrestrial sources is another story of accidental discovery. In 1932-33, Carl Jansky was looking for sources of static interference in transatlantic radio communications when he recorded a source of unknown origin. Initially Jansky believed that it was radio output from the sun but eventually it was determined that it came from the Galaxy and the constellation of Sagittarius. The discovery made quite a sensational impact but no additional research was made into the subject, since the static was not strong enough to interfere with radio communications. Fortunately scientists were impressed enough to start projects of their own and seven years later the first map of the galactic radio emission was constructed by Grote Reber (Reber, 1940, 1944). An extragalactic object was identified as the source of radio emission in 1954 (Baade & Minkowski, 1954). This source (Cygnus A, the brightest radio galaxy today) was also found to have a redshift of $z = 0.057$ and a strange appearance, initially mistaken for two different galaxies but later shown to be in fact a single galaxy with two lobes on either side, from which the radio emission originated (Jennison & Latham, 1959). This discovery introduced a new species of galaxies; High redshift galaxies that were radio active.

1.6.2 Categories of radio sources

Radio galaxies come in two main categories; extended and compact radio sources. Extended sources extend beyond the limits of the host galaxy and are the largest structures known in the universe, with intrinsic sizes reaching the > 100 kpc scales. Radio emission in extended sources originates more than 1 kpc from the nucleus of the galaxy. In contrast, compact sources are much smaller with cores that do not extend more that a few parsecs, while the extended radio emission comes well within 1kpc from the nucleus. Because of the size difference, compact sources can be variable in their energy output in time scales of several months, whereas extended sources remain constant. As well as size difference, there are also spectral differences. The spectral indix α is defined from the equation for the flux density $S_\nu \propto \nu^{-\alpha}$ at frequency ν. The spectra of compact radio sources

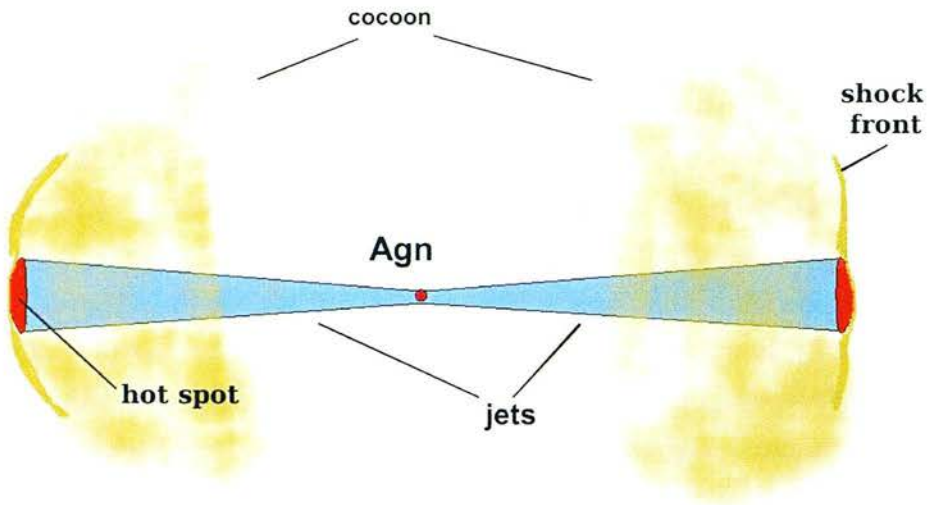

Figure 1.3: A simple drawing of a double radio galaxy. The hot-spots and AGN are the sources of radio emission. The jets are beams of relativistic electron-positron plasma and the cocoon is made of intergalactic or interstellar material that has been shocked by the jets.

have flat spectrum indices in the range $\alpha \in (0, 0.5)$ whereas extended sources have steep spectra where $\alpha \in (0.7, 1.2)$.

Another commonly encountered separation of objects according to their radio emission is the distinction of active galactic nuclei in two main categories, based in the presence of radio emission. The first category encompasses radio loud AGN, named thus due to their radio exceeding values of $L_{\rm rad} \geq 10^{24}{\rm WHz}^{-1}{\rm sr}^{-1}$.The second class of AGN includes objects with radio luminosity $L_{\rm rad} \leq 10^{24}{\rm WHz}^{-1}{\rm sr}^{-1}$ and they are collectively called radio quiet AGN. It is important to note that radio quiet AGN are not necessary objects with no radio emission but simply galaxies where the radio luminosity is quit low.

1.6.3 Radio emitting processes in galaxies

Radio emission from AGN differs in nature from radio emission from normal galaxies. The term normal galaxies applies to all galaxies that do not have an AGN in the centre, or it is dormant. This is an important distinction since the physical processes are quite different. Radio emission from normal galaxies comes from mainly two sources (Condon, 1992):

- Free-free emission from HII regions. The free electrons are deflected by the ion nuclei resulting in the emission of a photon. The interstellar matter in these clouds is ionised due to supernovae activity.

- Synchrotron radiation from relativistic electrons in magnetic fields. The electrons are accelerated to relativistic speeds in supernovae explosions and after travelling through the galaxy eventually lose energy in the presence of a magnetic field producing radiation.

In the case of an active galactic nucleus, the radio part of the radiation is synchrotron radiation in nature, but it is produced in relativistic jets. The standard picture (Scheuer, 1974) for double radio galaxies consists of two relativistic continuous beams that originate from the central black hole, are made up of electrons or positrons and expand into the interstellar and intergalactic medium. At the point where the jet reaches the material of the intergalactic or interstellar medium a shock front is formed. Those two points (one for either beam) are the hot spots identified in radio maps. The shocked material forms a cocoon around the hot spot where matter from the jet is deposited. This cocoon form the extended lobes that are observed in the double radio galaxies. The expansion of the cocoon produces a bow show in the intergalactic material.

1.7 Thesis outline

The first chapter of this thesis takes a closer look in the galaxy luminosity function and especially the faint end. By combining two galaxy surveys, the 2dFGRS survey, a redshift survey that includes $\approx 250,000$ galaxies and the MGC survey, a very deep optical survey that reaches up to $m_{\mathrm{MGC}} = 23.5$ an attempt is made to better define the faint end of the galaxy luminosity function. By the use of the 2dFGRS galaxies as centres, since their distance is known, and the faint MGC galaxies as satellite galaxies of those centres, one can assign distances to the faint galaxies and therefore be able to probe the faint end of the luminosity function.

In the second chapter, the central black hole mass function of the 2dFGRS survey is computed. Recent findings suggest that there is a black hole in the centre of every galaxy and utilising the Magorrian relation between the luminosity of the bulge and the black hole mass, the black hole masses for a large percentage of the 2dFGRS survey are calculated. A relationship is developed between galaxy colour and Hubble type which translates to a relationship between the colour and the dominance of the galactic bulge. The galactic bulge properties are calculated

with the use of the b_j and r_f colours from the SCSS survey that are included in the 2dFGRS release.

In the third chapter the 2dFGRS survey is combined with the NVSS radio survey in order to retrieve radio fluxes for the 2dFGRS galaxies. The radio luminosity of the survey is calculated and relationship between black hole mass and radio luminosity is examined. By the use of two prominent lines in the 2dFGRS spectra, an attempt is made to distinguish between radio output due to the AGN in the galactic centre and radio output from the galaxy. Finally, the probability of black hole mass given radio luminosity is computed.

In the final chapter, the local numerical density is calculated for the 2dFGRS survey. The survey is then split according to the local density and a comparison between the different luminosity functions of the populations is made. The black hole mass distribution is examined according to the local density and a statistical analysis in performed in order to determine if galaxies with radio output belong to the same population as normal galaxies.

Chapter 2

The faint end of the galaxy luminosity function

2.1 Introduction

The numerical description of large scale structure in modern cosmology makes use of two simple yet powerful quantities. The correlation function of galaxies and the luminosity function of galaxies. These are perhaps the most basic and important measurements of structure and distribution of galaxies. The luminosity function of galaxies is a mathematical tool that describes the numerical distribution of galaxies of various luminosities in a cosmological volume, whereas the correlation function of galaxies is a mathematical representation of the level and strength of clustering among galaxies.

Since those methods are statistical tools in essence, as with all statistics, it is necessary to use large samples of galaxies in order to achieve better accuracy. The large redshift surveys of recent years are proving invaluable in advancing modern astrophysics and cosmology. In an attempt to add fainter galaxies in a redshift sample, a combination of a redshift survey with a very deep optical survey can provide information on the behaviour of fainter galaxies, that are not bright enough to provide a spectroscopic redshift. This chapter describes one such use of galaxy catalogues in an attempt to better define the galaxy luminosity function at the faint end.

The method to be employed is based on the assumption that dwarf galaxies are clustered around brighter galaxies, therefore they are expected to lie at approximately the same distance. Using a bright galaxy with measured redshift as the centre of a cluster of faint galaxies , one can assign distances to galaxies that were too faint to be included in a redshift survey. This method of determining the luminosity function was first proposed by Phillipps & Shanks (1987) and further

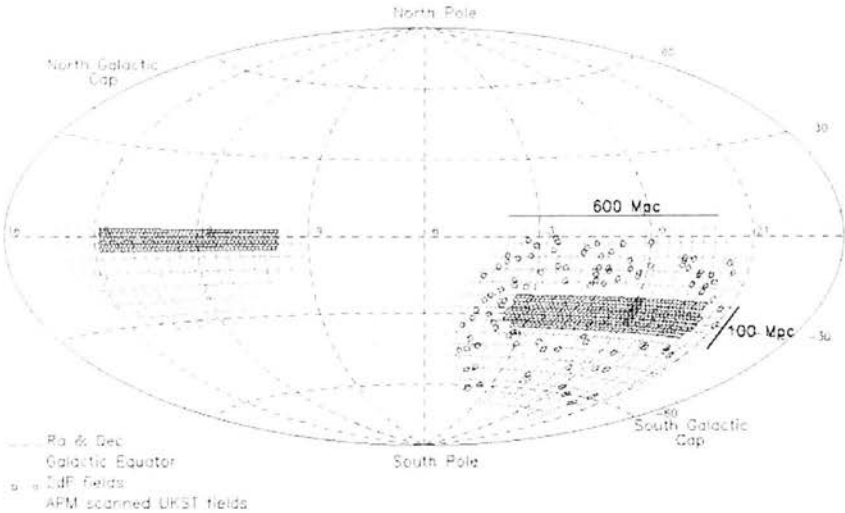

Figure 2.1: A map of the 2dFGRS survey showing the distribution of the observed fields in the sky. (Adopted from the 2dFGRS home page on the web). The survey is split in 2 main areas, defined by the galactic hemisphere that they are in, as well as many random fields around the SGP strip. The selected galaxies were drawn from the APM survey (red squares) area and cover around 1500 square degrees.

developed by Loveday (1997).

2.2 The Data

2.2.1 The 2 Degree Field Galaxy Redshift Survey

The 2dFGRS survey is one of the largest redshift surveys that has been undertaken in recent years. The survey has yielded spectra and redshifts of approximately 250,000 galaxies (Lewis *et al.*, 2002; Colless *et al.*, 2001). It uses the 2dF multi-fibre spectrograph on the Anglo-Australian Telescope, which is capable of observing 400 objects simultaneously in a 2 degree diameter field. The survey covers approximately 2000 square degrees in the sky and is split into three strips. The North Galactic Pole strip , the South Galactic Pole strip plus some randomly distributed fields. The survey has a median redshift depth of $\bar{z} = 0.11$ and contains galaxies brighter than $b_j = 19.45$ selected from the APM survey. The b_j magnitude of the 2dFGRS is a photographic B magnitude using IIIa-J plates. The 2dF spectra have a two-pixel resolution of 9 Åand cover the range between 3600-8000 Å. It is one of the largest complete redshift surveys and even though the SDSS survey at its latest release contains more galaxies (Abazajian *et al.*, 2005) the mask of the SDSS is not yet understood completely and there

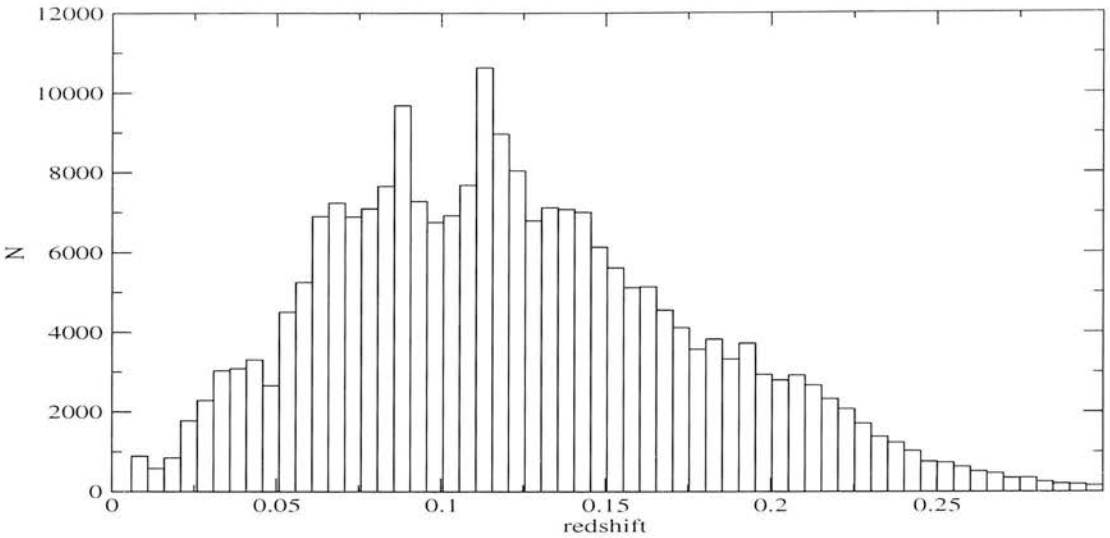

Figure 2.2: Redshift distribution for the 2dFGRS survey. Almost all galaxies have redshift lower than 0.3. The existance of the two peaks around $z = 0.1$ is of special interest; there is no contribution from those structures in the 2-point correlation function, although higher order correlation functions are heavily influenced by their presence (Gaztañaga *et al.*, 2005).

are several more issues pending, still making the 2dFGRS an invaluable tool to the astronomical community that has been the source of major breakthroughs in astronomy and cosmology.

The survey is now finished and it is available on the world wide web. The input catalogue for this work was the best spectroscopic observations catalogue which consists of 245591 galaxies.

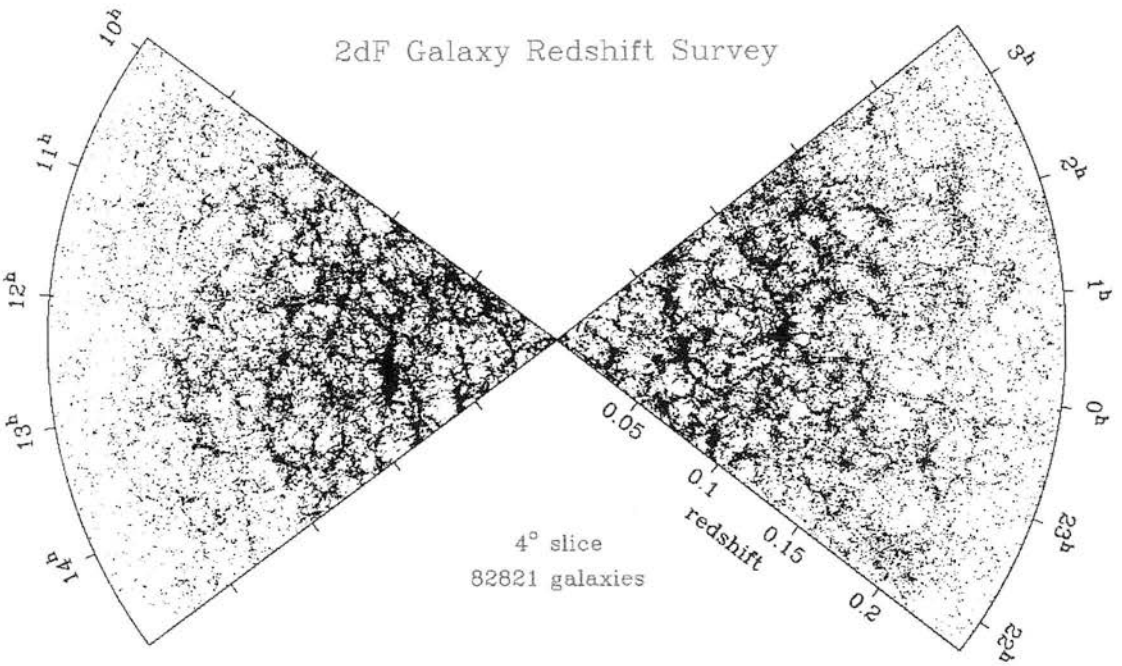

Figure 2.3: a redshift cone plot showing the distribution of the 2dFGRS galaxies in right ascension and redshift. The plot was made using a small slice of declination (around $\sim 2^o$) from the NGP and SGP respectively.

2.2.2 The Millennium Galaxy Catalogue Survey

The MGC survey (Liske *et al.*, 2003) is a deep blue band survey that covers a narrow strip ($\sim$ 37.5 square degrees) inside the 2dFGRS North Galactic strip. The MGC goes as deep as $b_{\rm MGC} \leq 24$ magnitude and is fully contained within the 2dFGRS as well as the Sloan Digital Sky Survey. More details can be found in Liske *et al.* (2003).

The MGC survey was conducted using the The Wide Field Camera instrument on the Isaac Newton Telescope. The WFC camera consists of four CCD chips with dimensions of 2048×4096 pixels each. They are arranged as shown in figure 2.4.The MGC survey consists of 144 pointings of the camera covering a long and thin RA strip along the equator. The first field is centred on RA = 150°, DEC = 0° and each consecutive field is centred 30′ off the previous one. The last field is centred on RA = 221.5° and DEC = 0°. The Millennium Galaxy Catalogue provides information on the position and apparent magnitude of 2×10^6 faint galaxies.

2.2.2.1 The geometry of the MGC

One of the most useful tools in the analysis of catalogues of galaxies is the ability to reproduce random surveys that follow certain properties of the original but have a given random element, for example, the galaxies of the random survey have a random placement and are uncorrelated with each other.

The geometry of the MGC survey initially appears quite simple; the survey is just a narrow strip along the NGP of the 2dFGRS. But in a clean sample from which bad areas have been removed [1], various holes appear that need to be incorporated in the analysis lest they skew the results. This results in a quite complicated geometry.

Coupled with poor documentation and lack of any mention of calibration coordinates for the CCD pixels, constructing a mask for the MGC catalogue was a more complicated task than expected. The coordinates for the various holes and overscan regions are given in CCD coordinates and as centre for the configuration of the 4 CCDs the system assumes the centre of CCD 4. There was insufficient information regarding the regions between the CCDs and adjustment had to be done empirically.

[1] This could be due to many reasons. Defective pixels on a CCD, various defects of the optics (vignetting on the edges for example), contamination from cosmic rays, bright stars and over exposed items and the occasional bad night that degrades the quality of certain observational runs.

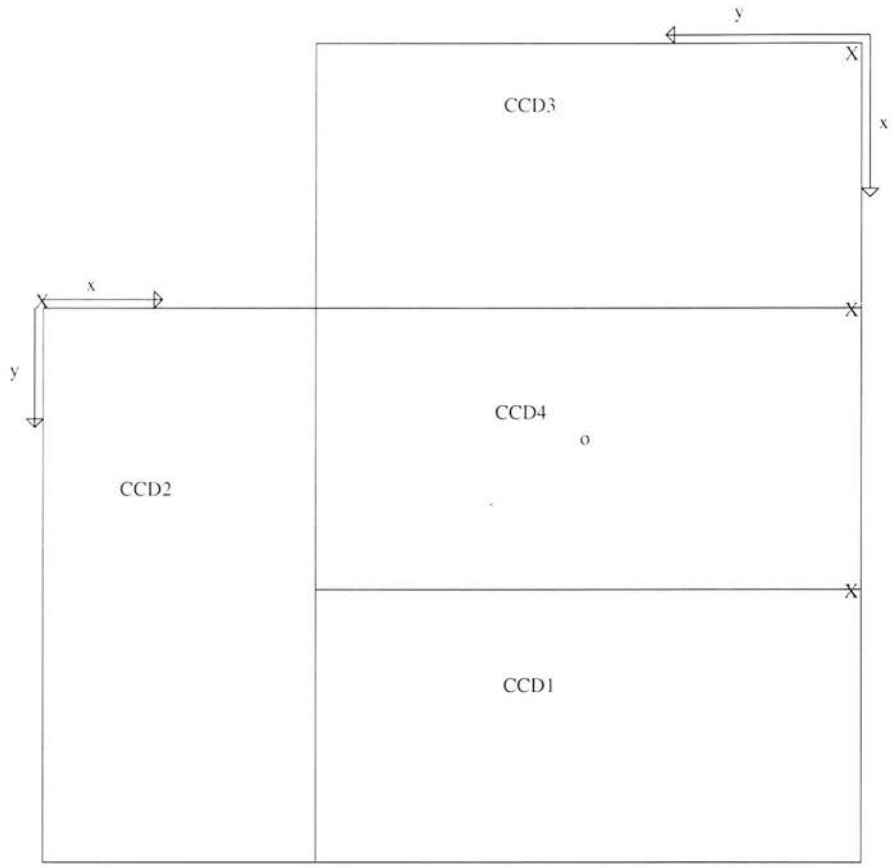

Figure 2.4: The configuration of the 4 CCDs on the WFC camera. The beginning of the CCD axis is noted for each one as well as the centre of the MGC frames, which coincides with the middle of CCD4. This configuration was centred on RA = 150°,DEC = 0° and there were 143 consecutive pointings, each 30′ towards increasing RA coordinates.

To avoid any mask regions that were ignored in the development of the software the following measures were taken:

- First, the MGC survey itself passes through the mask until no rejections occur.
- If a solution to some rejections can not be found, it is imperative that the rejected points are not included in any analysis
- Finally, an optical examination of a number of randomly selected fields revealed the presence of areas that were not catalogued. These were removed by hand.

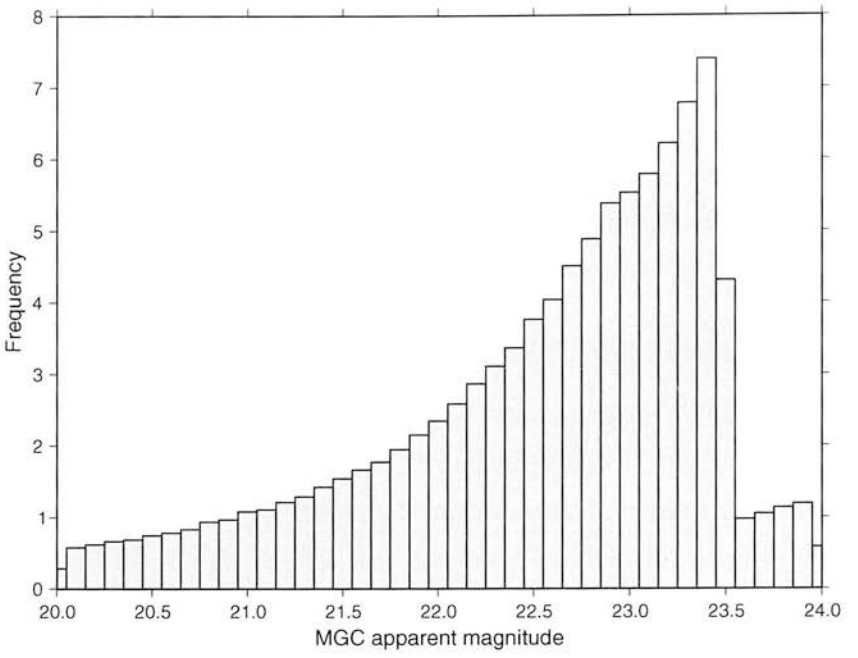

Figure 2.5: The apparent magnitude distribution for the MGC survey. The source is the faint sources catalogue that excludes all areas that had some imperfection (Liske *et al.*, 2003). The magnitudes fainter than $m_{\rm MGC} = 23.5$ were not used in the calculations.

2.3 Cross-correlation method

2.3.1 The luminosity function of galaxies

The most common representation for the distribution of galaxies according to their properties, is the galaxy luminosity function. The galaxy luminosity function is defined as the co-moving number density of galaxies per unit magnitude per unit volume as:

$$\phi(M) = \frac{\Delta N}{\Delta M \Delta V} \text{ or } \phi(L) = \frac{\Delta N}{\Delta V \Delta L} \ . \tag{2.1}$$

The most common parametrisation of the luminosity function is the Schechter function, proposed by Schechter (1976):

$$\phi(L)dL = \phi^* \left(\frac{L}{L^*}\right)^a e^{-\frac{L}{L^*}} \frac{dL}{L^*} \ , \tag{2.2}$$

or, in a more useful form, using absolute magnitudes:

$$\phi(M) = 0.4 \ln 10 \, \phi^* [10^{0.4(M^*-M)}]^{(1+a)} e^{-10^{0.4(M^*-M)}} \ , \tag{2.3}$$

where $L^*(M^*)$ is a characteristic luminosity(magnitude) where the LF exhibits a rapid change in its slope in the $(\log_{10}\phi, \log_{10} L)$ plane and a is the slope of the

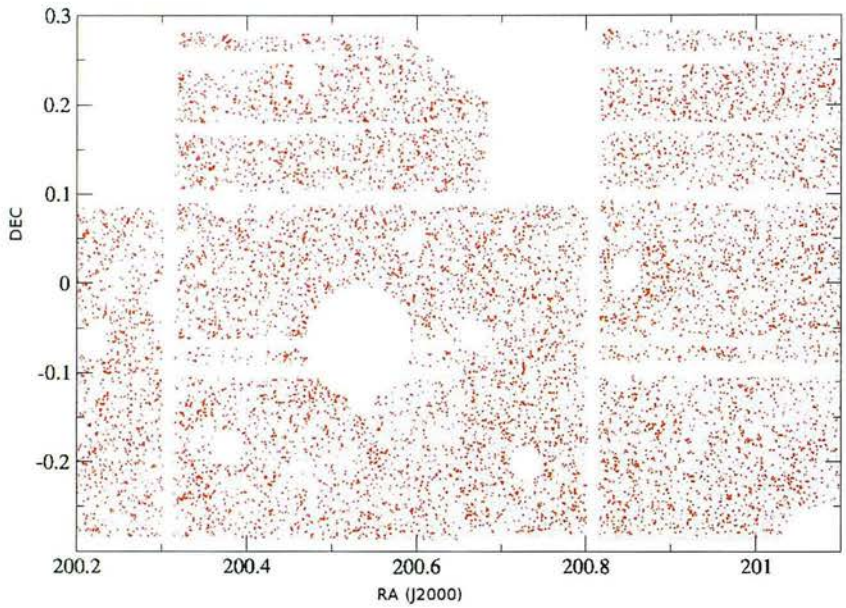

Figure 2.6: A small area of the MGC survey (red dots), superimposed upon a grid (gray area) of the same area that has been processed with the MGC mask algorithm. The holes in the survey area are due to CCD separation, bad pixels, overexposed stars, bad fields and cosmic rays (Liske *et al.*, 2003).

LF for values $L \leq L^*$ (faint end). ϕ^* is a constant with units of number density and is used in the normalisation of the LF.

The LF of galaxies is probably the most useful tool in use for statistical properties of galaxies. It has been studied extensively for many years and although it is well understood for a wide range of luminosities and galaxy types (Loveday *et al.*, 1992; Zucca *et al.*, 1997; Croton *et al.*, 2005a) the lack of very deep surveys that have accurate spectroscopic redshift information has hindered the accurate determination of the faint end (Trentham & Tully, 2002). There are various methods for the determination of the luminosity function. The choice is often dictated by the galaxy sample to be used or the problem parameters. Reviews on the various aspects of the luminosity function can be found in Binggeli *et al.* (1988) and Efstathiou *et al.* (1988). In this chapter, the luminosity function of faint galaxies will be determined using the method outlined in Phillipps & Shanks (1987) and Loveday (1997).

2.3.2 The correlation function of galaxies

Identifying structure is alone not enough. The presence of structure must be translated in a statistical quantity and a mathematical tool developed so various workers in the field can use these measurements to compare between various surveys. One way to do so is to compare the observed galaxy distribution with a distribution that is *de facto* random. In a given distribution, the probability of finding a galaxy occupying an infinitesimal volume element δV is:

$$\delta P = n\delta V \ , \tag{2.4}$$

where n is the mean number density and is independent of the position. The joint probability of finding an object in two volume elements $\delta V_1, \delta V_2$ at separation r_{12} is

$$\delta P = n^2 \delta V_1 \delta V_2 [1 + \xi(r_{12})] \ , \tag{2.5}$$

where $\xi(r_{12})$ is the two-point correlation function. Defined in an identical way, is the cross-correlation function between two different distributions of objects, with densities n_A and n_B respectively. The probability of two objects of type A and B being in volume elements δV_A and δV_B is given by:

$$\delta P = n_A n_B \delta V_1 \delta V_2 [1 + \xi(r_{12})] \ . \tag{2.6}$$

In a uniform Poisson distribution the probabilities of finding an object in δV_1 and δV_2 are independent so the joint probability is simply

$$\delta P = n^2 \delta V_1 \delta V_2 \ . \tag{2.7}$$

The probability of a galaxy having a neighbour within a distance r is,

$$\delta P = n\delta V[1 + \xi(r)] \ . \tag{2.8}$$

It follows that the average number of neighbours within a distance r is the integral of that equation and therefore

$$\langle N \rangle = \frac{4}{3}\pi r^3 n + n \int_0^r \xi(r)\delta V \ . \tag{2.9}$$

The correlation function $\xi(r)$ is therefore a measure of the clustering of galaxies. If $\xi(r) > 0$ then the galaxies are clustered together whereas $\xi < 0$ indicates anti-clustering and in that case galaxies are avoiding one another. In the case of $\xi = 0$ the distribution is random.

In order to calculate the probability faction for a given sample of galaxies, the number of pairs between galaxies must be retrieved. The expected number of galaxies for a given volume V is $N = nV\delta V(1 + \xi(r))$, therefore the number of distinct pairs in that volume would be $N_{\rm DD} = \frac{1}{2}n_D^2 V\delta V(1 + \xi(r))$. If the data are cross correlated with a random sample, then the number of pairs would be $N_{\rm DR} = n_R n_D V\delta V$. Solving for $\xi(r)$, the equation becomes:

$$\xi(r) = \frac{2N_{\rm DD}}{N_{\rm DR}}\frac{n_r}{n_d} - 1 \ . \tag{2.10}$$

There are other estimators for the correlation function that are more robust in certain cases. The estimator 2.10 was proposed by Davis & Peebles (1983), but was later shown to be biased for certain cases and have considerable larger variance that the estimator proposed by Landy & Szalay (1993)

$$\xi(r) = \frac{a_1 N_{\rm DD} + a_2 N_{\rm DR} + a_3 N_{\rm RR}}{N_{\rm RR}} - 1 \ , \tag{2.11}$$

with $a_1 = \frac{n_r(n_r - 1.0)}{n_d(n_d - 1.0)}$, $a_2 = -\frac{n_r - 1.0}{n_d}$ and $a_3 = 1$. This estimator was originally proposed as an angular correlation function estimator but it is applicable as a galaxy correlation function as well. Finally, Hamilton (1993) proposed a third estimator that has the form

$$\xi(r) = \frac{4n_d n_r N_{\rm DD} N_{\rm RR}}{(n_r - 1)(n_d - 1)N_{\rm DR}^2} \ , \tag{2.12}$$

that again exhibits better variance and is unbiased. The use of these estimators is somewhat complimentary and similar results from all the estimators is a good test to root out any systematic mistake. The estimator used for the calculation of any correlation function or angular correlation is 2.12

Estimating the correlation function is sometimes more complicated than it seems. The sample of galaxies is usually incomplete, since most surveys are magnitude limited. The survey covers a limited area of the sky and also has a specific magnitude range. To avoid errors arising from this incompleteness, our random sample must have the same characteristics. In most cases this is achieved by creating a random catalogue that covers the exact same area on the sky and has the same selection function for the galaxies and their magnitudes but it is unclustered, to compare against

2.3.2.1 Projected Correlation Function

Even when information about the redshift of a galaxy exists, this does not necessarily mean that an accurate three dimensional map can be constructed. Redshift information (as an indicator of the cosmological distance) is distorted by the galaxy's peculiar velocity. This can result in an incorrect estimation of the true distance and thus a miscalculation of the true spatial correlation function. One way of working around that effect is working with the projected correlation function and then inverting it to get the spatial correlation function.

Given two galaxies with redshifts z_1 and z_2 and with an angular separation θ_{12} in the sky, their separation parallel to the line of sight, π, and their separation perpendicular to the line of sight, r_p, can be calculated:

$$\pi = z_1 - z_2 \ , \tag{2.13}$$

$$r_p = \frac{z_1 + z_2}{H_0} \tan\left(\frac{\theta}{2}\right) \ . \tag{2.14}$$

The projected correlation function $\xi(\pi, r_p)$ is defined again by the probability of finding a galaxy at separations π and r_p, $\delta P = n\delta V(1 + \xi(\pi, r_p))$. As before, by calculating the number of pairs around each galaxy in the data sample and between the data and a random catalogue, the correlation function in bins of parallel and perpendicular in the line of sight separation can be calculated,

$$\xi(r_p, \pi) = \frac{n_r}{n_d} \frac{2N_{\mathrm{DD}}(r_p, \pi)}{N_{\mathrm{DR}}(r_p, \pi)} - 1 \ . \tag{2.15}$$

At small separations, $\xi(r_p, \pi)$ may differ from the space correlation function due to the peculiar velocity of each galaxy. In order to avoid that effect, $\xi(r_p, \pi)$ is integrated over the redshift difference π. In this way the projected correlation function $\Xi(r_p)$ is obtained. To get the spatial correlation function $\Xi(r_p)$ is solved for $\xi(r)$

$$\Xi(r_p) = \frac{1}{H_0} \int_{z_{\min}}^{z_{\max}} d\pi \xi(r_p, \pi) \ . \tag{2.16}$$

For appropriate values for the integral limits, in order to include all the galaxy pairs and peculiar velocities and change variables, equation 2.16 can be rewritten as follows,

$$\Xi(\sigma) = 2\int_0^\infty dx\xi(\sqrt{\sigma^2+x^2}) \quad (2.17)$$

$$= 2\int_\sigma^\infty rdr\xi(r)(r^2-\sigma^2)^{\frac{1}{2}} \ . \quad (2.18)$$

If the space correlation function is modelled as a power law of the form $\xi(r) = (r/r_0)^\gamma$ then

$$\frac{\Xi(\sigma)}{\sigma} = \left(\frac{r_0}{\sigma}\right)^\gamma \frac{\Gamma(1/2)\Gamma(\frac{\gamma-1}{2})}{\Gamma(\frac{\gamma}{2})} = \left(\frac{r_0}{\sigma}\right)^\gamma A(\gamma) \ . \quad (2.19)$$

2.3.2.2 Angular correlation function

In many cases information about a galaxy's distance is absent, yet its position is known. There are many catalogues with galaxy positions but without containing the redshift of the galaxies, since the acquisition of a redshift measurement was too time consuming or too difficult or even unnecessary when that particular survey was under way. In that situation the angular correlation function $w(\theta)$ can be used instead, which has a similar definition to the correlation function with the replacement of the volume element with a solid angle element and the physical separation between two galaxies with their angular separation. Therefore, in the same manner as before, the possibility of finding an object in a solid angle element Ω_1 and Ω_2 is defined as

$$\delta P = \bar{n}\delta\Omega_1\delta\Omega_2[1+w(\theta_{12})] \ , \quad (2.20)$$

so it follows that

$$w(\theta) = \frac{\bar{n}_R}{\bar{n}}\frac{2N_{\rm DD}}{N_{\rm DR}} - 1 \ , \quad (2.21)$$

where $\bar{n}$ indicates the surface density.

Inverting the angular correlation function $w(\theta)$, in order to get $\xi(r)$ is more complicated than inverting the projected correlation function. One has to solve for $\xi(r)$ from Limbers equation

$$w(\theta) = \frac{\int_0^\infty dx x^4\phi^2(x)\int_{-\infty}^\infty dy\xi[(x^2\theta^2+y^2)^{\frac{1}{2}}]}{[\int_0^\infty dy y^2\phi^2(y)]^2} \ , \quad (2.22)$$

where the selection function $\phi(x)$ is defined as the probability per unit volume of a galaxy at distance x to be included in the sample. As in the case of the projected correlation function, if $\xi(r) \propto r^{-\gamma}$ then $w(\theta) \propto \theta^{1-\gamma}$. This is an important result because it can help us estimate the value of γ for a given galaxy sample in a time efficient way (since the estimation of $w(\theta)$ is quite simple).

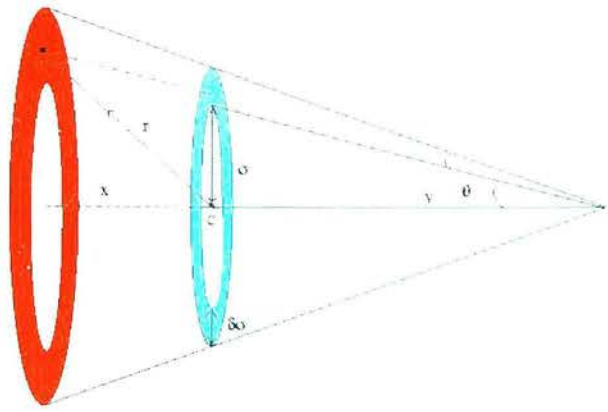

Figure 2.7: A centre galaxy at distance y and a galaxy at distance x viewed in projection, in a ring with radius σ around the centre

2.3.3 Measuring the luminosity function using galaxies seen in projection

The use of galaxies seen in projection to calculate the luminosity function was carried out by Loveday (1997). The method is based on the assumption that smaller galaxies will be clustered around bigger ones. Following Loveday (1997), consider a galaxy at known distance y. The mean number $\langle n \rangle$ of galaxies that are seen in projection to be clustered around it with magnitude m and are in projected separation σ, assuming a luminosity function $\phi(M)$ and a spatial correlation function $\xi(r)$ for the galaxy distribution, would then be

$$\langle n \rangle = \int_0^\infty \phi[M(x,m)]V(x)(1+\xi(r))\,dm\,dV \quad , \tag{2.23}$$

where $r = \sqrt{x^2+y^2-2xy\cos\theta}$, is the physical separation between the galaxy centre at distance y and a galaxy at distance x, with an angular separation $\theta = \sigma/y$. If the angle θ remains constant, then the volume of the cone defined by the observer and a ring around the centre at distance y of Figure 2.7 is given by

$$\begin{aligned} dV &= \textstyle\int_0^{2\pi}\int_0^\infty r^2 \sin\theta\, dr\, d\theta\, d\phi \Rightarrow \\ dV &= (2\pi \sin\theta\, d\sigma/y)\textstyle\int_0^\infty x^2\, dx \end{aligned} \quad , \tag{2.24}$$

since $\theta = \sigma/y \Rightarrow d\theta = d\sigma/y$.

The expected number of galaxies around the centre at distance y would then become

$$\langle n \rangle = \frac{2\pi\alpha \sin\theta\delta\sigma}{y}\int_0^\infty \phi(M(m,x))\,\delta m x^2(1+\xi(r))\,\delta x \quad , \tag{2.25}$$

where α defines the percentage of the projected ring that is included in the survey region and it is defined by the survey mask. Noting that the integral in the

equation can be broken in two parts

$$\int_0^\infty x^2\phi(M,x)\,dm\,dx + \int_0^\infty x^2\xi(r)\phi(M,x)\,dm\,dx \ . \tag{2.26}$$

Following Davis & Peebles (1983) and Norberg *et al.* (2002) the projected correlation function $\Xi(\sigma)$ (or w_P as it is sometimes known) is defined as

$$\Xi(\sigma) = \int_{-\infty}^{\infty} \xi(\sigma,\pi)d\pi \ , \tag{2.27}$$

where π and σ is the separation of 2 galaxies parallel and perpendicular to the line of sight. Equation 2.27 can be rewritten using the real space correlation function $\xi(r)$ as

$$\Xi(\sigma) = \int_{-\infty}^{+\infty} \xi(\sqrt{\Delta y^2+\sigma^2})\,d\Delta y \ , \tag{2.28}$$

where Δy is the parallel to the line of sight distance to the galaxy used as centre at distance y. If $y \gg \sigma$ and $\xi(y) \ll 1$. Taking into account that for a sphere of radius x

$$\int_0^\infty \phi\left[M(x,m)\right] x^2 dmdx = \left\{\frac{1}{4\pi}\int_S\int_0^\infty \phi\left[M(x,m)\right] x^2 dxd\Omega\right\} dm = \bar{N}(m)dm \ , \tag{2.29}$$

equation 2.26 is simplified into

$$\langle n\rangle \approx \frac{2a\pi\sin\theta\delta\sigma}{y}[\bar{N}(m)\delta m + \phi(M)y^2\Xi(\sigma)\delta m] \ , \tag{2.30}$$

where $\bar{N}(m)\delta m$ is the surface density of the faint survey.

Following the same procedure for a randomly generated catalogue, inside the geometrical limits of the faint survey, of galaxies that have the same luminosity function $\phi(M)$ but do not display any clustering, equation 2.30 follows the form

$$\langle n_r\rangle \approx \frac{2a\pi\sin\theta\delta\sigma}{y}\bar{N}_r(m)\delta m \ , \tag{2.31}$$

where $\langle n_r\rangle$ is the number of random galaxies observed around the centre galaxy and $\bar{N}_r$ is the surface density of the random catalogue. From equations 2.30 and 2.26 follows that

$$\frac{n}{n_r} = \frac{\bar{N}(m)+\phi(m)\Xi(\sigma)y^2}{\bar{N}_r(m)} \ . \tag{2.32}$$

Rearranging 2.32

$$\frac{\bar{N}_r(m)}{\bar{N}(m)}\frac{n}{n_r} = 1+\phi(m)\Xi(\sigma)y^2/\bar{N}(m) \ , \tag{2.33}$$

and defining the relative excess estimator $X(M,\sigma) = \phi(M)\Xi(\sigma)$ it follows ,

$$X(M,\sigma) = \frac{1}{p(m,\sigma,y)}\left[\frac{N_r(m)}{N(m)}\frac{n}{n_r} - 1\right] \quad , \tag{2.34}$$

with

$$p(m,\sigma,y) = \frac{1}{N(m)}k(m,\sigma,y)y^2 \quad , \tag{2.35}$$

where $k(m,\sigma,y)$ is a factor of order unity that is used to correct for the biases caused by the approximation in equation 2.30.

To make $X(M,\sigma)$ an unbiased estimator of $\phi(M)\Xi(\sigma)$, $k(m,\sigma,y)$ is taken to be

$$k(m,\sigma,y) = \frac{\int_0^\infty \phi(M(m,x))x^2\xi(r)\delta x}{y^2\Xi(\sigma)\phi(M(m,y))} \quad . \tag{2.36}$$

If the form of the solution for $\phi(M)$ is denoted by ϕ_i, it is obvious that a solution for ϕ_i depends of ϕ_{i-1}, making this calculation an iterative procedure. Choosing ϕ_0 as the luminosity function of the 2dFGRS survey, the solution converges for $i < 10$.

2.3.3.1 Optimal weights and variance

The relative excess estimator $X_i(M,\sigma)$ is calculated for each centre galaxy and gives a noisy estimation of the luminosity $\phi(m)$. In order to reduce the noise, all X_i estimators need to be combined in an optimal way. If each centre galaxy i with X_i, is assigned a weight b_i, then the final form of the excess estimator would be

$$X_{\text{final}} = \left(\sum_{i=0}^{N} b_i X_i\right) / \sum_i b_i \quad . \tag{2.37}$$

The expected variance in n_i is

$$\Delta n^i \approx n_r^i[1 + p(m,\sigma,y)\phi(m)\Xi(\sigma)][1 + \bar{N}(m)J_2(\theta)][1 + f\phi(M)J_3(\sigma)] \quad , \tag{2.38}$$

where f is the fraction of galaxies with measured redshifts and the quantities $J_2(\theta)$ and $J_3(\theta)$ are defined as

$$J_2(\theta) = 2\pi\int_0^\theta \theta' w(\theta')d\theta' \quad , \tag{2.39}$$

and

$$J_3(\sigma) = 4\pi\int_0^{\sigma'} \sigma^2\xi(\sigma)d\sigma \quad . \tag{2.40}$$

During the summation over all centre galaxies, each measurement is weighted by

$$b_i = \frac{[\Xi(\sigma)]^2}{\Delta(X_i)} \tag{2.41}$$

hence

$$\phi(M) = \frac{\sum_i b_i X_i / \Xi(\sigma)}{\sum_i b_i} \quad , \tag{2.42}$$

where

$$\frac{1}{b_i} = \frac{[1 + p(m, \sigma, y)\phi(m)\Xi(\sigma)][1 + N(m)J_2(\theta)][1 + \phi(M)J_3(\sigma)]}{n_i'[p(m, \sigma, y)\Xi(\sigma)]^2} \quad , \tag{2.43}$$

the estimated error in the final $\phi(m)$ is

$$\Delta\phi(m) = \frac{1}{\sum_i b_i} \quad . \tag{2.44}$$

2.4 Applying the method to redshift data

2.4.1 Direct estimation of the luminosity function

The measurement of the luminosity function using the satellite galaxies method is not a direct measurement nor is it the simplest way to calculate it. A much simpler and direct method to retrieve a luminosity function from a survey with distance information is by using the $1/V_{\rm max}$ method, assuming of course that a sufficient deep survey exists.

Consider a survey of N galaxies, covering a solid angle of Ω in the sky, down to magnitude $m_{\rm lim}$ and redshift range from $z_{\rm min}$ to $z_{\rm max}$. If the galaxies are binned according to absolute magnitude M, in bins with width ΔM, then the number of objects in a given bin is from the definition of the luminosity function

$$N_{\rm bin} = \int_{M1}^{M2} \phi(M) dM V_{lim} = \Phi(M) V_{\rm lim} \ , \tag{2.45}$$

where $V_{\rm lim}$ is defined by the maximum distance a galaxy with absolute magnitude M can have and still be included in the survey. For small ΔM the result is $\phi(M) = \Phi(M)/(\Delta M V_{\rm lim})$.

This estimator is seriously flawed. The assumption this method makes is that the galaxies populate the sky uniformly without taking in to account any inhomogeneities in the sample, especially if the sample is flux limited and not volume limited. Faint galaxies cease to be present in the sample but that does not mean that they do not exist but simply that they are not detected. Additionally, information on the exact position of the galaxies in the absolute magnitude bin is lost, since the exact information as to where the galaxy lies in the ΔM magnitude bin is omitted. To correct for the loss of information due to the binning and try to correct for the bias in the galaxy sample one may sum over all galaxies in an absolute magnitude bin using the maximum volume as a weighting function, as first proposed by Felten (1976)

$$\Delta M \phi(M) = \sum^{N} \frac{1}{V_{\rm max}} \ , \tag{2.46}$$

where $V_{\rm max}$ is the minimum value of $V_{\rm max}(z), V(z_{\rm max})$ where $V_{\rm max}(z)$ is the maximum volume defined by the maximum redshift a galaxy can have and still be included in the sample and $V(z_{\rm max})$ is the maximum volume the survey probes with a redshift limit $z_{\rm max}$.

This is the $1/V_{\rm max}$ estimator of the luminosity function. It is perhaps the simplest method for the calculation of the LF. This estimator is not very robust

and is biased in cluster environments or void regions but in a well defined sample like the 2dFGRS, it can be used to accurately retrieve the luminosity function (Takeuchi *et al.*, 2000).

2.4.2 The luminosity function of the 2dFGRS

As seen from equation 2.36 an initial luminosity function for the sample is needed as well as the angular correlation function and the spatial and projected correlation functions.

The luminosity function for the galaxies in the 2dFGRS has been accurately calculated for various galaxy types (Madgwick *et al.*, 2002) according to their η parameter. The luminosity function for different spectral types and the association of the η parameter with galaxy type and colour is a subject of discussion in the next chapter. In the present calculation, the published luminosity function for all the galaxies in the 2dFGRS is used as a reference function. This involves some extrapolation of the LF fit to faint magnitudes where the 2dFGRS results are noisy; the aim of the present work is to improve this solution. As initial $\phi(M)$ the luminosity function of the 2dFGRS Madgwick *et al.* (2002) for all spectral types was used together with the residual fit for the faint end. The luminosity function is plotted in figure 2.8. The luminosity function has the form

$$\phi(M) = \phi_{\rm Sch}(M, \alpha, M^*, \phi^*) + \phi_{\rm res}(M, a, b) \ , \tag{2.47}$$

where $\phi_{\rm Sch}$ is a Schechter function and $\phi_{\rm res}$ is a function of the form 10^{a+bM} with $a = 4.7$ and $b = 0.5$.

For each iteration, a Schechter function is fitted to the data until the solution converges (see figure 2.9). This happens after 5 iterations in most cases since the solution around $M = M^*$ is quite stable and well defined. A simple Schechter fit is not able to fit the whole range of data, therefore the final solution is divided in bright and faint end and is fitted with a second Schechter function as well.

2.4.3 The mock MGC survey

In order to test the method, a fake survey was created by John Peacock, from the galaxy simulation of Cole *et al.* (2000). The simulation is a semi-analytical model of galaxy evolution in Cold Dark Matter cosmologies. It has an arbitrary dark matter mass resolution and it successfully follows the formation of galaxies from the gas that resides in the DM haloes. The shape, size and colours of the galaxies that formed are calculated as well.

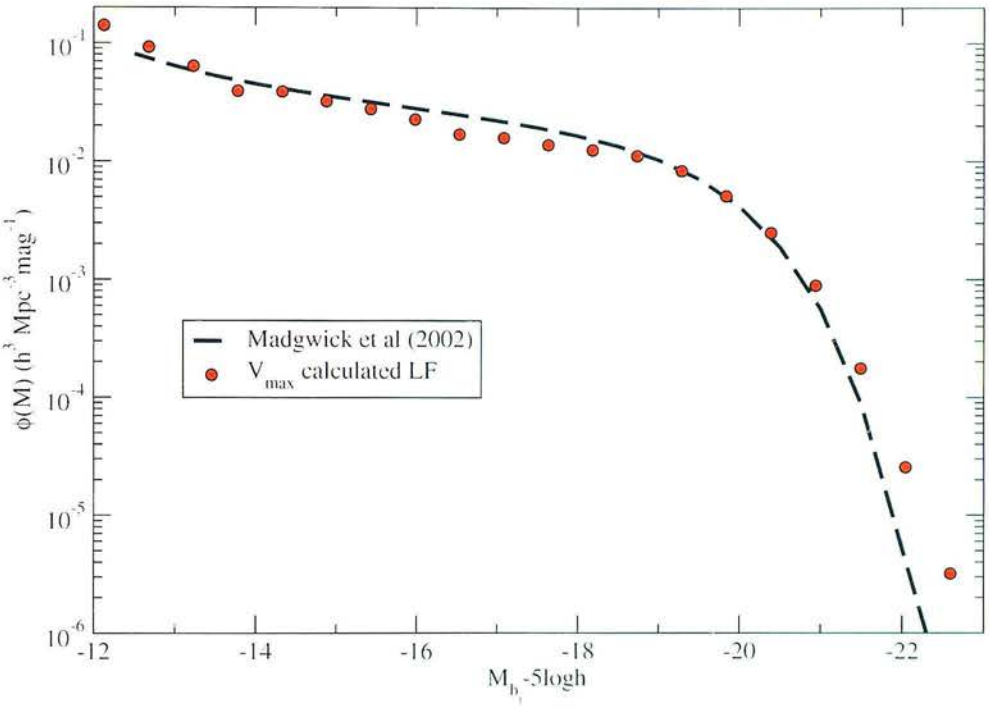

Figure 2.8: The luminosity function of the 2dFGRS that was used as initial function. The dashed line is the fit to the luminosity function as given by Madgwick *et al.* (2002), whereas circles indicate a $V_{\rm max}$ calculation on the 2dFGRS galaxies of the NGP. The LF stops around $M_{b_j} = -13$, although the fit is extrapolated to fainter absolute magnitudes when needed.

Schechter parameters	ϕ_*	α	M_*
Mock survey LF	0.015	-0.96	-19.38
result LF using $0 \leq \sigma \leq 5$Mpc	0.014	-0.95	-19.23
result LF using $2 \leq \sigma \leq 5$Mpc	0.014	-1.02	-19.19

Table 2.1: The fitted values for the mock survey. The luminosity function parameters for the simulation are taken from Madgwick *et al.* (2002). There are two different set of parameters for the result LF of the simulation. The first, using $\sigma \leq 5$Mpc as the projected distance length and the second using $2 \leq \sigma \leq 5$Mpc. The two results agree well.

The simulation occupies a cube with a side of $250\,h^{-1}$ Mpc and has a luminosity function that resembles the 2dFGRS luminosity function. A larger volume can be simulated by periodic replication of this fundamental cube if necessary. A thin slice was selected from this box, that would yield a strip of galaxies similar to the MGC strip, with $-45° \leq$ RA $\leq 45°$ and $0° \leq$ DEC $\leq 1°$. All galaxies that have an apparent magnitude less that 19.5 were grouped together to compile the catalogue of the centre galaxies, whereas the fainter galaxies were treated as a faint survey that resembles the MGC catalogue in the magnitude ranges. The 2-point correlation function of the simulation is similar to the correlation function of the 2dFGR survey (Madgwick *et al.*, 2003) for passive galaxies, with $\sigma_0 = 6.10\,h^{-1}$ Mpc and $\gamma = 1.95$. The simulation does not include galaxies with an absolute magnitude fainter than $M_B = -14$. The geometry of the simulation is quite simple, since there is no survey mask, therefore the creation of a random catalogue within the limits of the mock survey is straightforward. The random mock survey is created by redistributing the galaxy positions within the cube in a random way but not the magnitudes nor the redshift values of the galaxies, in order to preserve the luminosity function. The final random mock survey was constructed to be 5 times larger than the simulation.

The method works quite well for the simulation, as seen in figure 2.9. The resulting luminosity function is given in table 2.4.3. The fit is a non linear least squares fit to a Schechter function. After a few iterations the result converges and there is no change to the output. The luminosity function of the fake survey is a simple Schechter function with the parameters of the 2dFGRS luminosity function.

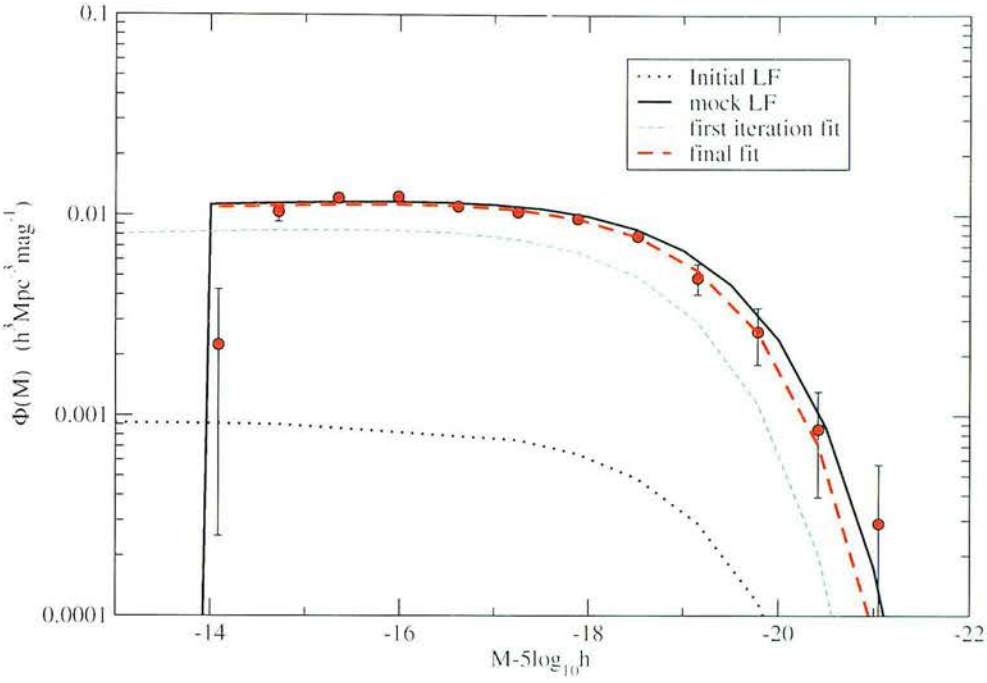

Figure 2.9: Contrast between the luminosity function of the simulation (solid black line) and the luminosity function recovered using the satellite galaxies method (circles). The simulation has a luminosity cutoff at $M = -14$. The bright end differs slightly, although it is well within the error. All galaxies that had an apparent magnitude of $m < 19.5$ were assigned as a simulated 2dFGR survey and the galaxies with $m > 19.5$ were used to calculate the LF. Also shown the initial luminosity function that was used to start the iterations. In order to test the adaptability of the method, a very different initial function was used than the luminosity function of the mock catalogue. The solution converged after only 3 iterations.

2.4.4 Galaxy correlation functions of the 2dFGRS and MGC surveys

The luminosity function of the 2dFGRS is used as the initial function for the method. The initial LF is not so important to be accurately calculated, since the method is iterative and will converge towards the best solution after time. One essential component of the satellite galaxies method is the accurate calculation of the correlation function of the survey. There is an extensive bibliography for the correlation function of the survey as seen in Hawkins *et al.* (2003) and Madgwick *et al.* (2003) and $\xi(r)$ for the 2dFGRS can be considered as well defined for the purpose of the present calculation.

According to Madgwick *et al.* (2003), the correlation length r_0 and slope γ for the faint galaxies in the 2dFGRS have the values $r_0 = 4.14\,h^{-1}$ Mpc and $\gamma = 1.78$. The correlation length does not change considerably for faint galaxies (figure 3 of aforementioned paper), so the use of these values should be accurate for the satellite galaxies. The correlation length value affects the normalisation of the luminosity function through equation 2.42 whereas the effect of the correlation length is not so pronounced.

There is a relationship between the strength of clustering and luminosity in galaxies, as was shown by Benoist *et al.* (1996). Bright galaxies were found to cluster more strongly than faint galaxies and the mathematical method for the measurement of this relationship has the form

$$\frac{b}{b^*} = 0.85 + 0.15\frac{L}{L^*} \ , \tag{2.48}$$

for the 2dFGRS galaxies, as quoted by Norberg *et al.* (2002). The quantity b/b^* is the relative bias and is measured against galaxies at L^*, which in the case of 2dFGRS is taken at $M^* = -19.7$ and equation 2.48 can be rewritten as

$$\frac{b}{b^*} = 0.85 + 0.15 \times 10^{0.4(M^* - M)} \ . \tag{2.49}$$

As was shown in Norberg *et al.* (2002) there is no evidence for clustering segregation according to luminosity for faint galaxies, so the bias correction is not so important for the faint end.

The projected correlation function is a derivative of the spatial correlation function, as seen in equation 2.19. If a power-law form is assumed for the spatial correlation function $\xi(r) = (r/r_0)^{-\gamma}$ then the projected correlation function takes the form

$$\Xi(\sigma) = \left(\frac{\sigma}{\sigma_0}\right)^{1-\gamma} \ , \tag{2.50}$$

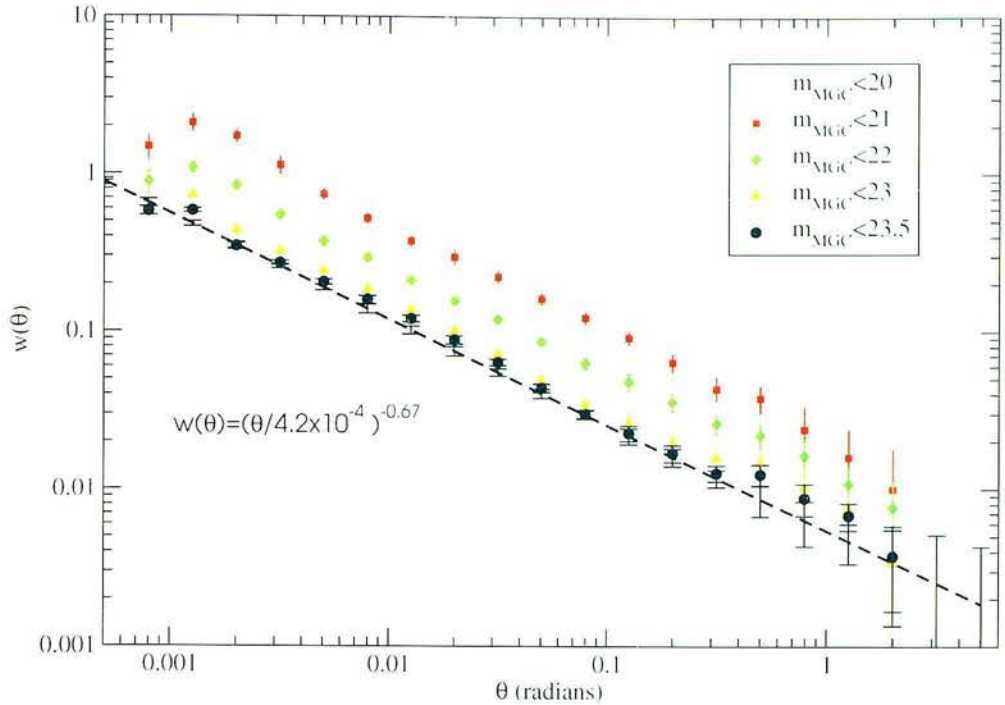

Figure 2.10: The angular correlation function for the MGC survey calculated for various magnitude ranges. The final angular correlation function ($m_{\rm MGC} < 23.5$) has been fitted with a power low of the form $w(\theta) = (\theta/\theta_0)^{-\alpha}$.

where

$$\sigma_0 = \left[r_0^{\gamma} \frac{\Gamma(\frac{\gamma-1}{2})}{\Gamma(\frac{\gamma}{2})} \right]^{\frac{1}{1-\gamma}} \quad . \tag{2.51}$$

The angular correlation function for the MGC catalogue $w(\theta)$ that was used is seen in figure 2.10. The function was calculated using equation 2.21 and computed for various magnitude ranges of the MGC catalogue. The fitted values to the function were computed from the angular correlation function of galaxies as faint as $m_{\rm MGC} = 23.5$. The function has the form $w(\theta) = (\theta/\theta_0)^{-\alpha}$ and the values of the parameters are $\theta_0 = (4.2 \pm 1.4) \times 10^{-3}$ radians and $\alpha = 0.67 \pm 0.3$.

Using the 2dFGRS galaxies as centres and the MGC catalogue, the application of the satellite galaxy method gives some interesting results. As seen in figure 2.11, the luminosity function resembles the 2dFGRS luminosity function for the most part, in the absolute magnitude ranges of $-19 \leq M \leq -15$ as expected. The purpose of this method is not to retrieve the luminosity function at those ranges, since the LF has been well established with more accurate and direct methods. The focus is on the faint end of the LF, where some interesting observations can be made. The luminosity function at the faint end differs significantly though. It appears that the number of faint galaxies is greater than the number inferred

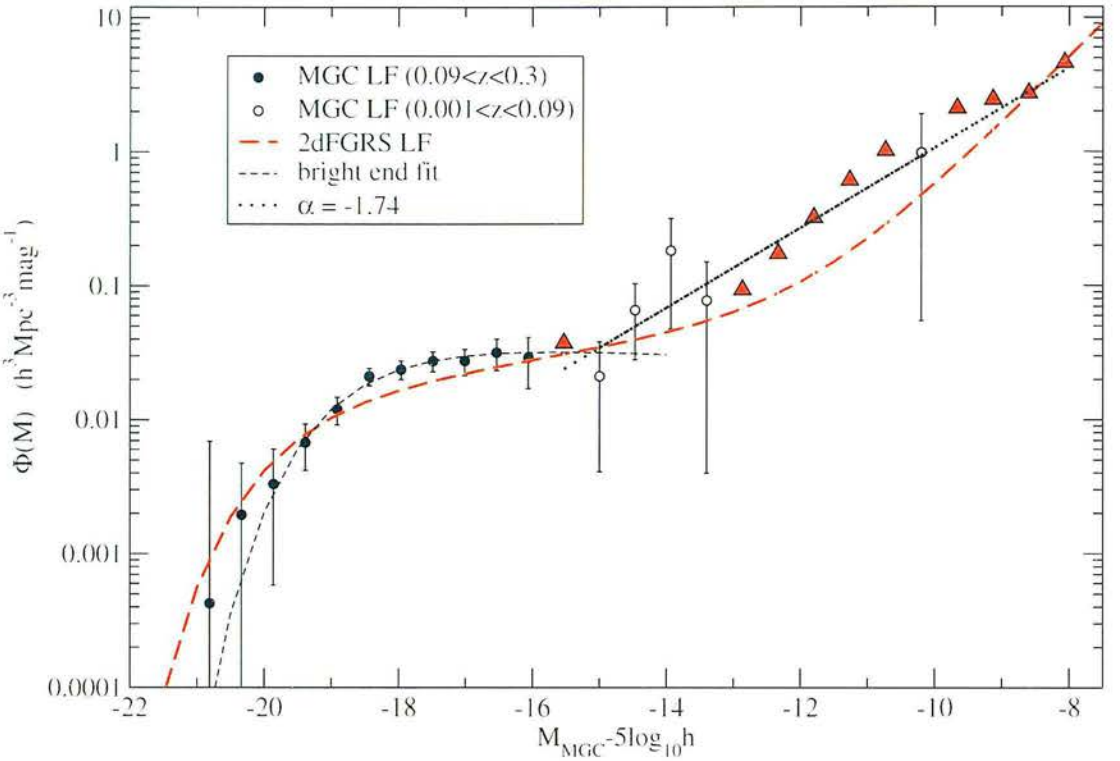

Figure 2.11: The luminosity function retrieved with the satellite method (black circles) compared against the 2dFGRS luminosity function (dashed line) for all galaxies. The luminosity function of the MGC was calculated in two separate redshift ranges as shown. Triangles with no error bars are an upper 1.8σ confidence limit to the function value at that point. The bright end of the luminosity function of the MGC resembles the 2dFGRS luminosity function. The faint end is not very well defined but there is indication that there are more galaxies that suggested by the faint end of the 2dFGRS luminosity function. The dotted line at the faint end indicates a slope of $\alpha = -1.75$.

from extrapolating the 2dFGRS luminosity in faint magnitudes. Unfortunately, the error in the estimation is quite large and the method yields only upper limits in most luminosity ranges. However, averaging over the measurements by fitting a power law appears to recover a steep faint slope as seen in figure 2.11.

The faint slope of the luminosity function has been reported before for dwarf galaxies residing in clusters. Sabatini *et al.* (2003) found a faint end slope of $\alpha = -1.7$ studying low surface brightness galaxies in the Virgo cluster. There are findings of even steeper slopes with $\alpha = -2.0$, as seen in the Fornax cluster (Kambas *et al.*, 2000). Not everyone agrees with such a steep slope though. Blanton *et al.* (2005) after conducting an analysis on extremely low luminosity field galaxies from the SDSS survey reported a faint end slope $\alpha \sim -1.3$, although their estimation is that if corrections for selection effects are applied, the slope will become steeper, around ~ -1.5. This is consistent with the value recovered in figure 2.11.

2.5 Conclusions

An attempt was made to retrieve the luminosity function of galaxies at the faint end by using the satellite galaxy method outlined in Loveday (1997). Even though the method works quite well for galaxies close to M_* luminosities, the resulting error in the estimation in the faint end does not allow a definitive outcome. The uncertainties in the calculation are due to the lack of a large number of center sources in such low redshift as to contribute to the faint end. In a statistical method such as the satellite galaxies method for the calculation of the luminosity function, this lack of objects generates a high level of noise. Another source of error is the fact that the center galaxies with low redshift have an angular search radius that is quick large. The high number of satellite galaxies associated with each center galaxy in this case would include a large number of galaxies that are not cluster around the center galaxy. Eventhough a correction factor is incorporated in the method to account for that bias, larger errorbars are unavoidable.

Despite the large errorbars at the faint end, there is strong indication that the number of dwarf galaxies is not as low as extrapolated from galaxy redshift surveys (Madgwick *et al.*, 2002). Especially important is the faint end slope of the luminosity function which appears to be steeper that the value reported for the 2dFGRS survey (~ -1.1). Eventhough the final result is not able to retrieve a faint end slope with good accuracy, it is able to place an upper limit to the faint end slope of the luminosity function. This is a very important result since

it allows the exclusion of models of galaxy formation within the cold dark matter theory that do not incorporate any mechanism to disrupt the creation of many dwarf galaxies and supports models that incorporate feedback in order to limit the number of low mass systems created (Efstathiou, 2000). The method itself can be used as an independent test for either direct calculations of the faint end of the luminosity function or another inderect method. Despite its complexity in the calculation of the luminosity function, the satellite galaxies method is easily applicable to faint samples with limited or no redshift information and as such it can be used until a very deep redshift survey becomes available.

The retrieved upper limit to the faint end slope agrees with values calculated from surveys of dwarf galaxies in clusters. Together, these results make the case that further investigation in to the faint end of the luminosity will provide valuable information for cosmology, although in order to do so in an accurate and definite way, the use of a large sample of dwarf galaxies with spectroscopic information is needed. The faint end of the luminosity funcion is a very important missing element of the CDM model of the universe. The accurate calculation of its slope will shed light in one of the major problem of cold dark matter theories and help solidify (or reject) the current paradigm.

Chapter 3

Black Hole Mass Function of the 2dFGRS

3.1 Introduction

Since the discovery of QSOs in the 1960s, it has been widely accepted that black holes were the driving force behind the massive energy output of quasars (Robinson *et al.*, 1965). Despite the success of gravity driven accretion for QSOs, the existence of supermassive black holes in the centre of normal galaxies was not subject to a similar reception until recent years.

Workers in the field noticed from early on that the observed quasars mostly exist in high redshift and are not present in the local universe. But clearly, their central engines, these massive black holes, had to be somewhere, if not necessarily active. One obvious place to look for these missing beasts was the centre of local massive galaxies (Soltan, 1982), and claims of discovering black holes in galaxies other than the Milky Way were made (Tonry, 1984), but skeptics persisted (Binney & Mamon, 1982). Models of quasar evolution backed this hypothesis though, and predicted that a large fraction of the massive galaxies should indeed contain a black hole in their centre (Chokshi & Turner, 1992; Cavaliere & Padovani, 1989). The observational constraint that prevented any undisputed discovery, was the limiting resolution of the telescopes of that time.

It was not until data from the HST became available, that the presence of black holes in normal galaxies was confirmed, ending the long standing debate (see Kormendy & Gebhardt (2001) and Ferrarese & Merritt (2000) for a review on black hole detection). Further studies showed that not only black holes existed as remnants of a troublesome past in normal galaxies, but they also played a very important role in galaxy evolution and formation (Silk & Rees, 1998; Kauffmann & Haehnelt, 2000).

The discovery of black holes in quiescent galaxies not only proved what people had been speculating for many years, but also provided the astronomical community with two unexpected (because no models predicted them yet) empirical relations between the black hole mass and the host galaxy characteristics. The first relation that linked the central black hole with the rest of the galaxy was noted by Richstone *et al.* (1998). The mass of the central black hole appeared to scale linearly with the luminosity of the spheroid component of the galaxy. That relation would have been an enormous boon, since the bulge luminosity is relatively easy to calculate, but for the great scatter ($\sim$ 0.5 dex) that it appear to have. Fortunately, a second, more accurate relation emerged, that between the mass of the central black hole and the luminosity weighted stellar velocity dispersions of the host bulge (Ferrarese & Merritt, 2000). This relation had a smaller scatter ($\sim$ 0.3 dex) and proved to be more effective in accurately determining the black hole mass that the previous one. The $M_{\rm bh} - \sigma$ relation holds true for all types of galaxies that exhibit a bulge component and it worked very well in retrieving the number density of the local black holes, which in turn verified the previous predictions that the central engines of QSOs lie dormant in the centre of massive galaxies in this cosmological epoch.

Unfortunately, velocity dispersions are hard to measure and in order to utilise the large samples of galaxies that were (and are) coming out of recent redshifts surveys, one would prefer to use the first relation between the black hole mass and the bulge luminosity. The difference in accuracy between the two relations was almost eliminated when McLure & Dunlop (2002) reported that the scatter in the $M_{\rm bh} - M_{\rm bulge}$ is not as large as previous results indicated. They found that the scatter around the relation was of the order of $\sim$ 0.39 dex for a sample of galaxies that consisted of AGN and quiescent galaxies. Furthermore, the relation exhibited much better behaviour ($\sim$ 0.33 dex) if only the elliptical galaxies of the sample were used. The same tight relation was reported by Erwin *et al.* (2004), after doing a careful bulge/disk decomposition of galaxies and correcting for cases where galaxies were miss-classified and the inner disk contaminated the bulge. They also noted a similar scatter (0.31-0.35 dex).

3.2 The Data

3.2.1 2dFGRS revisited

In this chapter the 2dFGRS survey will once more be the main galaxy catalogue. Both strips of the survey will be utilised, covering an area of 562.5 square degrees

for the NGP and 1125 square degrees for the SGP. Random fields were left out since they do not cover a continuous part of the sky. Almost all galaxies of the 2dFGRS have a spectroscopic redshift less that 0.3, with the median value being at $z_{\rm med} = 0.11$.

3.2.2 The SuperCosmos Sky Survey

The SuperCosmos Sky Survey is an ongoing project to digitise photographic plates taken with the UK Schmidt telescope (UKST), the ESO Schmidt, and the Palomar Schmidt, using the SuperCosmos plate scan facility, located in the Institute for Astronomy in Edinburgh. The aim of the project is to digitise the whole sky but it is not yet concluded. So far the survey has covered the whole of the southern sky and can provide B(UKJ) and R(UKF) band colours for that region (Hambly *et al.*, 2001). Since the 2dFGRS and SCSS survey both draw their galaxies from the same parent population (the APM survey), the final data release of the 2dFGRS survey include the b_j and r_f magnitudes from the plate scans of the SCSS . The plate magnitudes have been re-calibrated and are of high quality, with an rms of 0.13 in the $b_j - r_f$ colour. The measuring error, specifically for red galaxies, is even smaller in the range of ~ 0.08 (Peacock, 2003). One element that contributes to the scatter is that the colour equations in table 3.3 for the photographic magnitudes are imperfect. The colour transformations are based on SDSS photometry but the colours of the SDSS cannot predict the exact shape of the b_j and r_f magnitudes, since the passbands differ. Nevertheless, the scatter is still small and well within the required accuracy.

3.3 Elements of Galactic Morphology

3.3.1 Galactic Bulges

The objective of this chapter is to calculate the black hole mass function of the 2dFGRS galaxies and investigate its properties. For the calculation of the black hole mass of each galaxy, the relation between the absolute magnitude of the galactic bulge and the mass of the black hole will be used, as reported in McLure & Dunlop (2002).

The bulge is the central, amorphous, smooth stellar distribution of the galaxy and is defined relatively to the disk of the galaxy, from which it differs in shape and surface brightness. There are systems that have no bulge, either because there is no disk to compare to, and the galaxy is considered an elliptical or there is no central distinct feature and the galaxy has only a disk component.

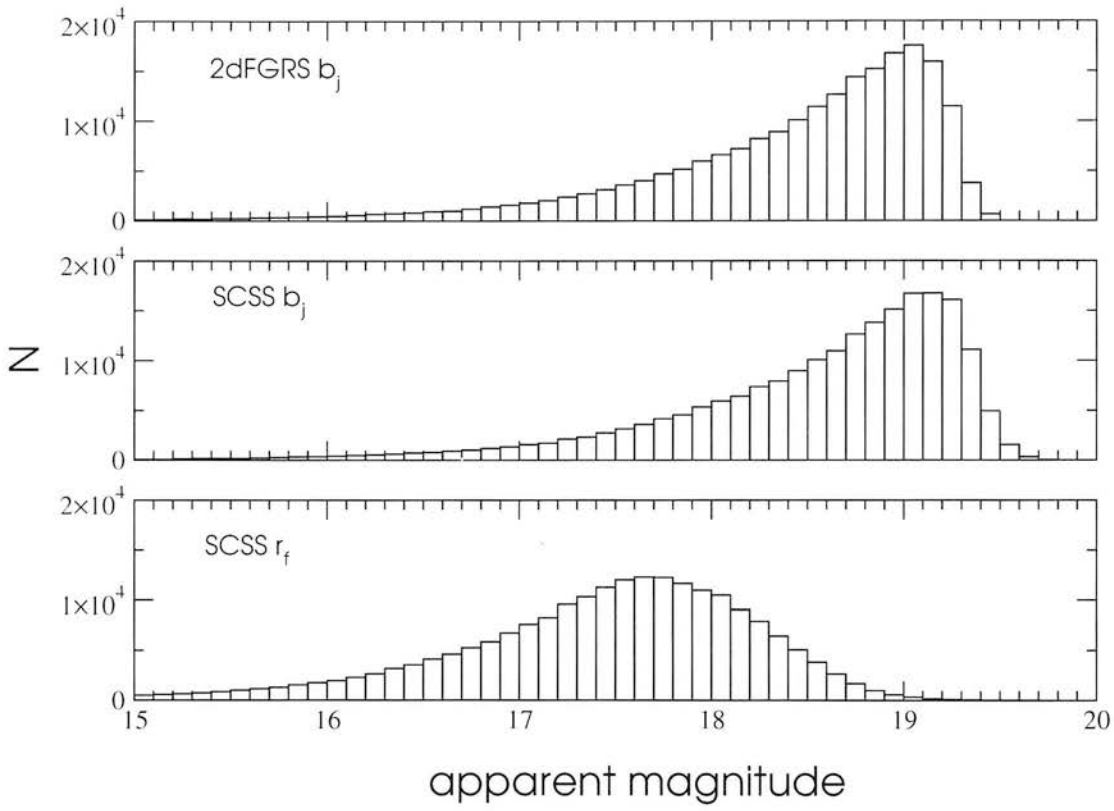

Figure 3.1: Apparent magnitude histograms for the final release of the 2dFGRS survey, displaying the 2dFGRS b_j magnitude (top) as well as the SCSS b_j (middle) and r_f (bottom) magnitudes.

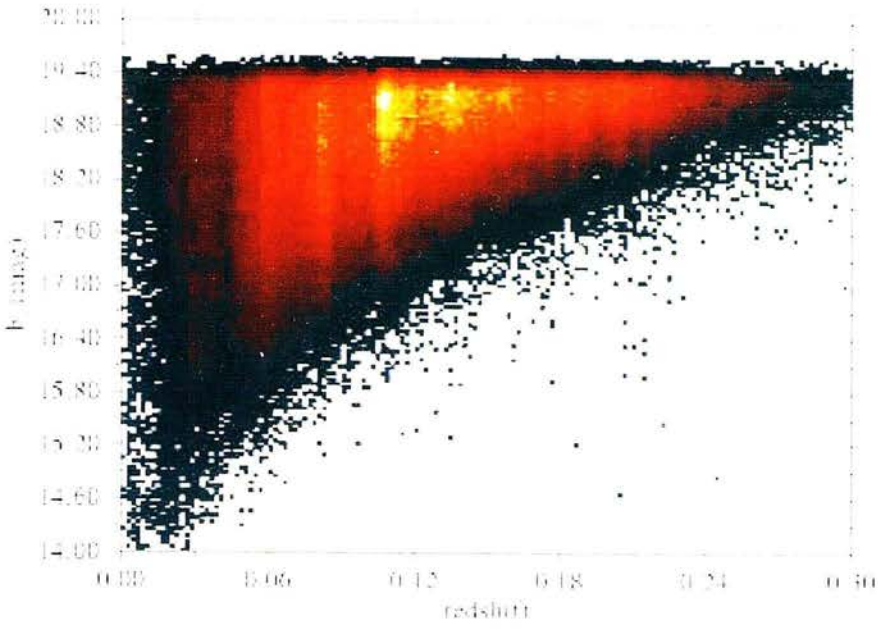

Figure 3.2: Apparent magnitude for the 2dFGRS survey plotted against redshift

This can be seen throughout the Hubble sequence of galaxies, which divides the galaxies in different categories according to their morphology. If the assumption that a galaxy consists of these two components, the bulge and the disk, then the Hubble sequence starts with systems that exhibit no disk structure (early types, ellipticals) and advances to systems that the disk component dominates until it reaches disk-only configurations and finally irregular galaxies. As mentioned before, the black hole evolution is closely linked with the nuclear part of the galaxy, therefore a way to separate the bulge from the disk must be developed.

Since there is no detailed CCD disk-bulge decomposition for the thousands of galaxies in the 2dFGRS sample, a statistical approach must be utilised in order to estimate the bulge component of a galaxy. It is believed that bulges are very similar to ellipticals in their properties of luminosity and colours and they are generally older than the disk. This is still a matter of debate though and may not be true in some cases. The exact nature of bulges is not a resolved issue and the debate is likely to continue (Wyse *et al.*, 1997) . Nevertheless, the similarity between bulges and ellipticals will be accepted as a given fact in the following analysis. Thus, working under the assumption that the bulge and the disk consist

of different stellar populations, the contribution of the bulge to the total galactic light will be calculated using the ratio of the different stellar populations as a measure. In order to do so, the colour $(b_j - r_f)$ information for the 2dFGRS sample will be utilised.

3.3.2 Galaxy colours

The colour index for two different bands A and B is defined as:

$$C_{AB} = -2.5 \log_{10} \left(\frac{\int_0^\infty f_\lambda S(A) d\lambda}{\int_0^\infty f_\lambda S(B) d\lambda} \right) \ , \tag{3.1}$$

where f_λ is the spectral flux of the galaxy and $S(X)$ the filter-telescope sensitivity.

Colours essentially measure the ratio of the fluxes near the effective wavelengths of the selected filters. The ratio therefore, holds information on the shape of the spectral energy distribution of the galaxy. In a galaxy dominated by old, cool, type II stars, the expected SED would tend to be more prominent in longer wavelengths, in contrast to the SED of a galaxy with ongoing star formation and a large population of young, hot, type I stars. In the latter case, the SED would be more dominant in shorter wavelengths.

The $(B - R)$ colour of an elliptical galaxy is expected to have a large value, since the galactic light would be mainly picked up in the band that measures longer wavelengths, which in this case would be the R band. Naturally, a disk galaxy, which has young stars and ongoing star formation, would have a small value of $(B - R)$. Unfortunately, since these particular filters are quite broad, the composition of the stellar populations is not the only influence to the SED, therefore a large scatter in the relation between colour index and galaxy type is expected.

3.3.3 The K-correction for 2dFGRS galaxies

Galaxies that have a cosmological redshift need a correction to their apparent magnitude, since the light that has been received in a given passband has actually been shifted from its original frame of reference due to the geometry of the universe. In order to acquire accurate colours, calculation of the the colour index at the frame of reference is necessary, therefore the appropriate k-correction must be calculated (Hogg *et al.*, 2002). The apparent magnitude for filter A will be using the k-correction:

$$m_A = M_A + 5 \log_{10} D_L + \mathrm{k(A, z)} \ , \tag{3.2}$$

where k(A, z) is a function of the given filter and redshift, M_A is the absolute magnitude of the galaxy which is the apparent magnitude the galaxy would have if it was at a distance of 10 parsec. D_L is the luminosity distance of the object. The luminosity distance is defined as $D_L = (1+z)r_{\text{comoving}}$, where r_{comoving} is the proper distance to an object with redshift z. In a flat model,

$$r_{\text{comoving}} = \frac{c}{H_0}\int_0^{z'} \frac{dz}{(\Omega_M(1+z)^3+\Omega_\Lambda)^{\frac{1}{2}}} \ . \tag{3.3}$$

The k corrections used for the SuperCosmos colours in the sample were calculated using the method of Blanton *et al.* (2003). This method was developed in order to calculate corrections for the colours of the Sloan Digital Sky Survey galaxies, but it is adaptable for other filters as well . The method is explained in detail in the aforementioned paper.

The basic idea behind the procedure is to generate artificial galaxies, by combining models of stellar populations, and observing them at various redshifts. These artificial galaxies (or Spectral Energy Distributions to be more precise) define a basis of orthogonal galaxy spectra that can be combined in linear combinations to produced any observed SED. Since the intrinsic properties of the galaxies are known a priori, one can calculate the k-corrections needed for each type of galaxy at given redshift, in order to retrieve the colour gradients of interest. The results of the above procedure for the SCSS colours can be fitted by the following equations:

$$K(B_J, z) = (4.53C - 1.63)y + (2.01C - 4.03)y^2 - \frac{z}{(1+(10z)^4)} \ , \tag{3.4}$$

$$K(R_J, z) = (1.45C - 0.08)y - (0.48C + 2.88)y^2 \ . \tag{3.5}$$

where $y = z/(1+z)$ and $C = (b_j - r_f)$. The error for the k correction estimated with the above equations is quite small. The uncertainty is of the order 0.01 mag throughout the colour index-redshift space, an order of magnitude more accurate than the colour uncertainty (Peacock, private communication).

The colour distribution of the 2dFGRS galaxies is a clear indicator that the $b_j - r_f$ rest frame colour value can be used as an estimator for the galaxy type. The colour-redshift plane is divided in two major populations as was expected. Elliptical galaxies, having no star formation and older stars than disk galaxies, appear quite red on that plot, whereas disk galaxies have a bluer colour.

This is clearly seen in figures 3.4 and 3.5, where the division in the two populations is very clear. Without the k corrections, the colour appeared to be heavily dependent on redshift (figure 3.5) and the population appeared homogeneous.

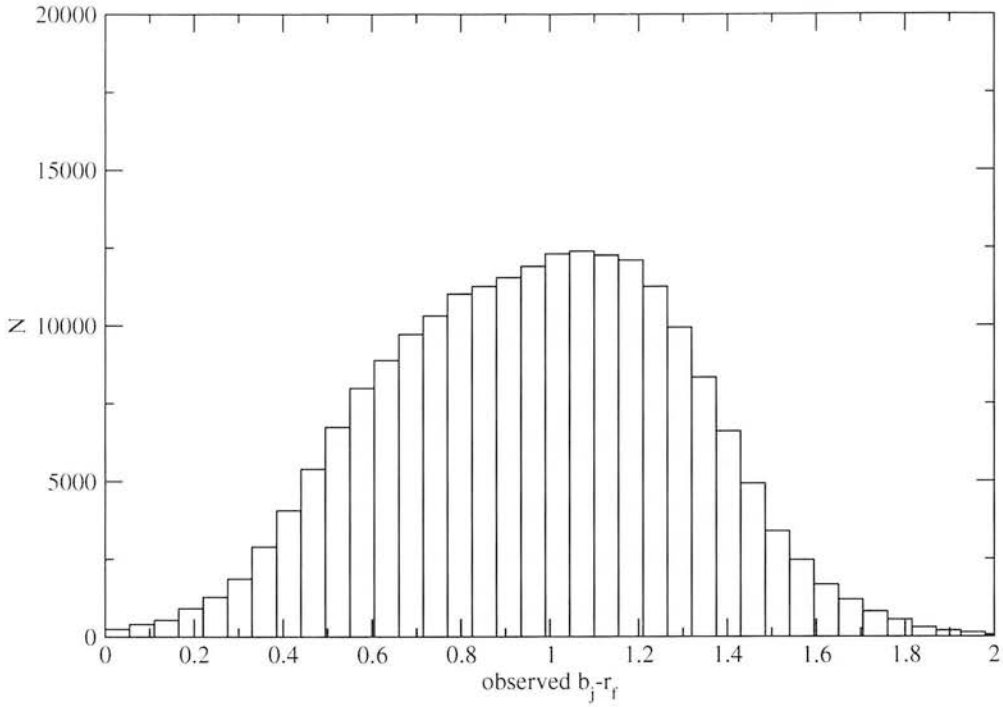

Figure 3.3: Observed $b_j - r_f$ colour for the galaxies in the sample. There is no visible separation of populations.

This is not true for the rest frame colour. There is a clear separation of the two populations as can be seen in figure 3.4 from the two peaks. Also any redshift dependence has been eliminated, especially for the red population (figure 3.5). In particular, the red galaxies appear to follow a very tight distribution, which is constant throughout the redshift range. The blue galaxy distribution, remains slightly redshift dependent, although not as strongly as before. The distribution is bimodal with a separation at around $(b_j - r_f)_0 \approx 1$.

The observed dichotomy in the galaxy population can be seen more clearly on the plot of the rest frame colour against the η parameter that is included in the 2dFGRS catalogue, for galaxies where its estimation was possible. The η parameter (Madgwick *et al.*, 2002) is the result of an effort to divide the 2dFGRS galaxies in categories, according to their spectral type. The method consists of projecting a galaxies spectrum onto different vector components, keeping information only for the most prominent spectral features. The η parameter is the sum of two of these components that was found to retain $\sim 70\%$ of the total variance across the entire sample. The parameter was shown to be very tightly correlated with galaxy morphology. The η parameter is not available for all the galaxies due to the absence of the Ha line from the spectrum at redshifts $z > 0.15$, where the line falls off the spectrum. The correlation between η and colour provides a

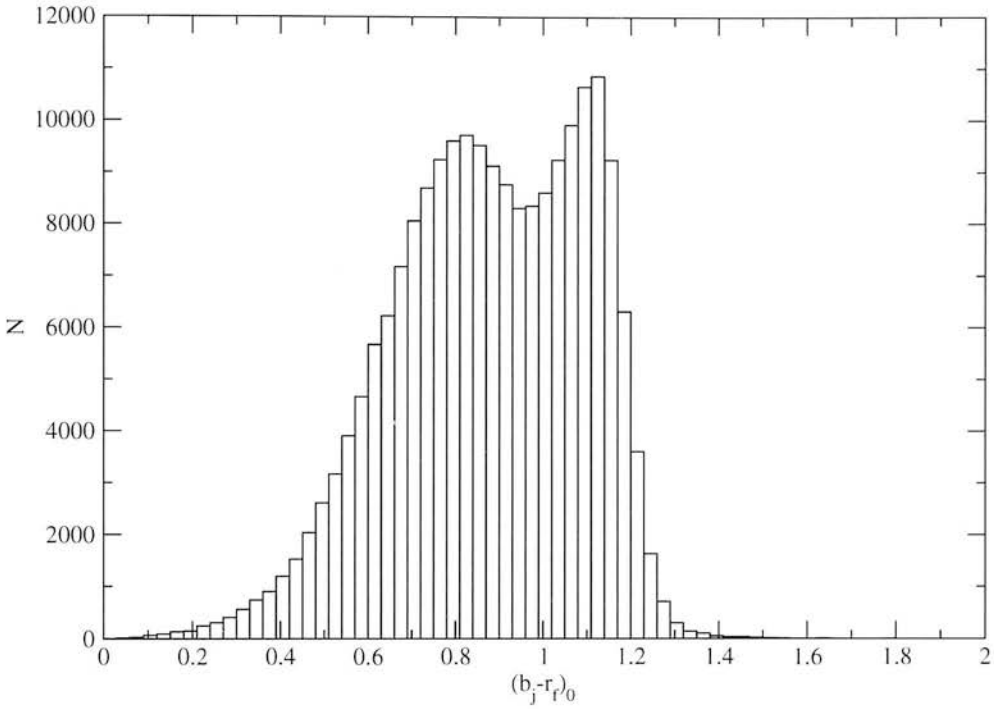

Figure 3.4: Rest frame colour $(b_j - r_f)_0$ using the k correction mentioned in equations 3.4 and 3.5. In contrast with figure 3.3, the separation in two populations can be seen after the k correction is applied and furthermore the red population exhibits a very small dispersion in colour. This pattern is an indication that the rms error of the red population is smaller than 0.13, as reported before.

Hubble	E	E/S0	S0	S0/Sa	Sa	Sab	Sb	Sbc	Sc	Irr
T	−5	−3	−2	0	1	2	3	4	5	10

Table 3.1: Galactic Hubble type and stage T adopted from Binney & Merrifield (1998)

	E	S0	Sab	Sbc	Scd
$B/T(r)$	1	0.75	0.40	0.24	0.10
$B/T(r_f)$	1	0.76	0.40	0.24	0.10

Table 3.2: Bulge to Total ratios taken from Kent (1985) using the median of the reported values and transformed to the SCSS r_f filter. The colour equations were taken from Fukugita *et al.* (1995) for the transformation between the Thuan-Gunn r filter of Kent and the SCSS r_f (Couch-Nowell filter of Fukugita). The colour equations are very similar for all galaxy types, which is why the ratios are almost identical.

confirmation that the split of the two populations is indeed physical in nature.

3.3.4 Correlation of colour and Hubble type

Galaxy colours have been found to correlate well with galaxy type as reviewed by Roberts & Haynes (1994), where the dependence of galaxy morphology to (B-V) colour index was given. If the colour transformations of table 3.3 are adopted, the (B-V) colour index can be transformed to a $(b_j - r_f)$ colour index, in accordance with the present galaxy sample. The subsequent plot is shown in figure 3.7.

3.3.5 Dependence of bulge to total ratio on colour index

Bulge to Total ratio is defined as the ratio between the luminosity of the bulge to the luminosity of the whole galaxy. It is a measure of Hubble type, since the hubble diagram is based upon that relation. Assuming a mass to light ratio for the galaxy, the B/T ratio is transformed to the ratio of the stellar masses in the bulge to the galaxy.

As the disk component and the bulge component of a galaxy differ in age and starformation rate, their observed colours differ, therefore the observed B/T ratio will be dependant on wavelength. For a specified set of filters, the bulge to total ratio could be specified by observing the colours. Kent (1985) has used CCD photometry of a volume limited sample of 105 luminous field galaxies of various types, to investigate the correlation between various parameters. His

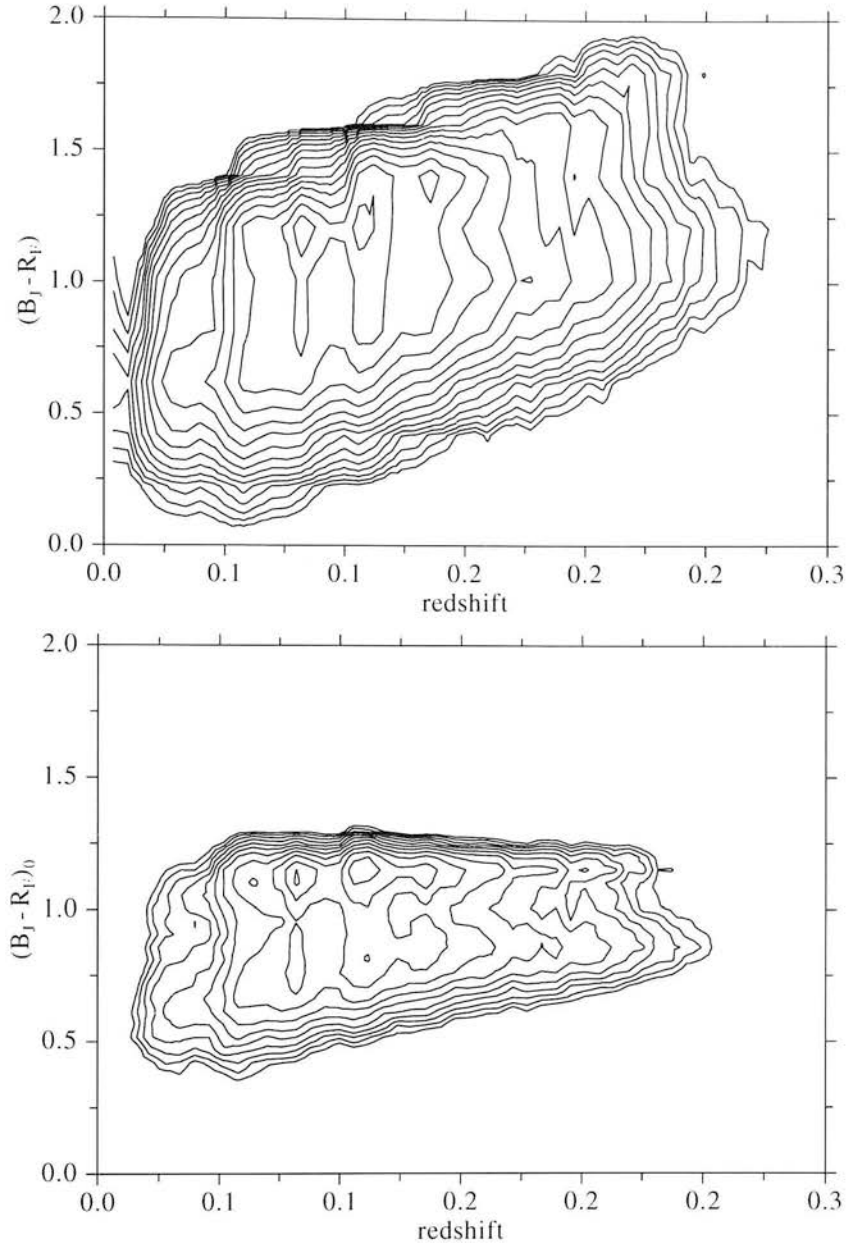

Figure 3.5: Contour plots of galaxy colours versus redshift. Top panel shows the observed colour whereas in the lower panel, the rest frame colour gradient is plotted. To calculate the rest frame colour, the k-corrections from equations 3.5 and 3.4 were used. It is apparent that the k corrections eliminate any redshift dependence the colour distribution had. Also noticeable in the rest frame colour plot is the indication of two separate populations. The red population exhibits a much tighter distribution throughout redshift space. The contours are logarithmically scaled.

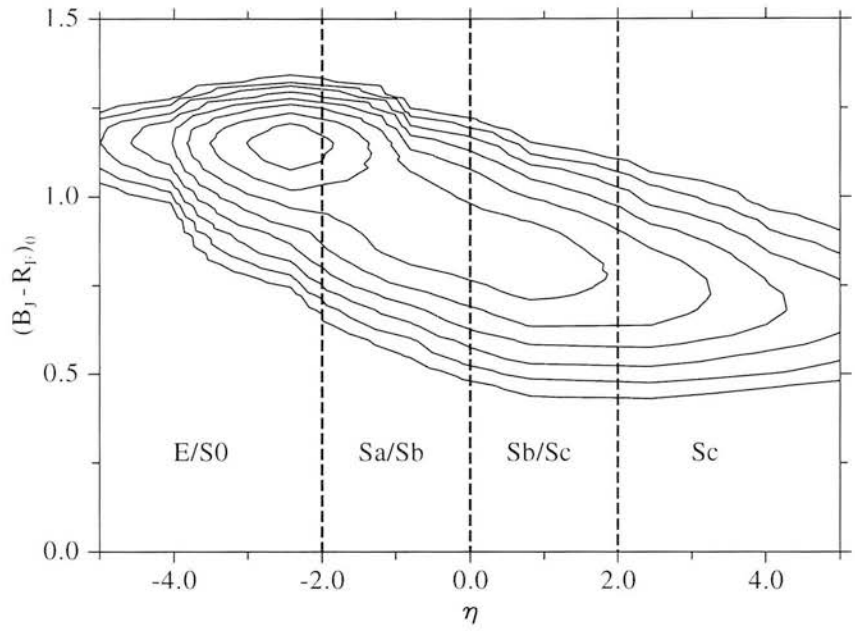

Figure 3.6: Correlation of rest frame colour with the η parameter of the 2dFGRS survey. The lines divide the plane in the categories of galaxies that the 2dFGRS survey was divided according to the η parametrisation. The contour lines depict number of objects in a two dimensional grid imposed on the two axis, and are scaled logarithmically. The outer contour line represents a number density of $10^{2.5}$ objects and the lines advance as $10^{0.2}$

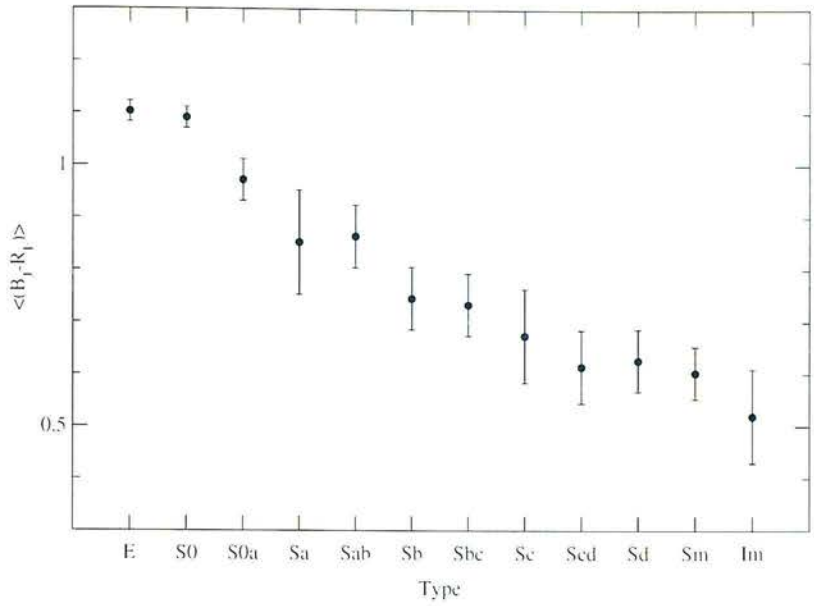

Figure 3.7: The correlation between morphology and mean galaxy colours. The values were taken from Roberts & Haynes (1994) and adopted for the SCSS photometric system, using the colour equation $b_j - r_f = 1.19(B - V) + 0.02$.

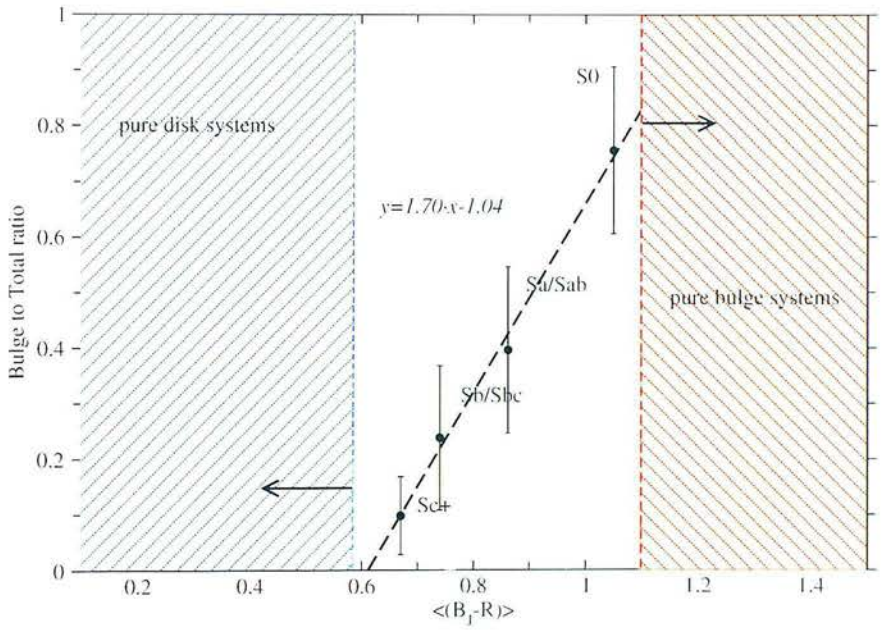

Figure 3.8: The relation used to retrieve the bulge to total ratio from the colours. Values are taken from Kent (1985) and Salucci *et al.* (1999). For objects with a colour value greater than $b_j - r_f = 1.1$, the B/T ratio is set at B/T=1, since those objects have no disc. Similarly, for objects that appear very blue ($b_j - r_f \leq 0.6$), there is no bulge component.

results indicate that galaxy type correlates well with colour gradient, although the dispersion is large. From these results, after adjusting for the filter system used, a simple linear fit between the galaxies $b_j - r_f$ colour and the bulge to total ratio was used to predict the B/T ratio of a galaxy from each colour:

$$B/T = 1.70(b_j - r_f)_0 - 1.04 \ . \tag{3.6}$$

The error bars in figure 3.8 are substantial. The inability to estimate a precise bulge to total ratio will contribute to a *systematic* error in the calculation of the black hole mass. This uncertainty represents the complexity of galaxies as entities when discussing physical parameters like size, composition and mass. Statistically speaking, red galaxies do have bigger bulges (Baldry *et al.*, 2004), but when one tries to apply relations like this to individual objects, the empirical relations break down. Galaxies are complex system and red disks or blue spheroids do exist. Using the equation 3.6 is not advisable for small samples, although it can be used to infer general characteristic of the total population. The contribution of this uncertainty to the accuracy of the calculation is investigated later in a Monte Carlo simulation.

mag/colour	transform
g'	$V + 0.54(B - V) - 0.07$
r'	$V - 0.44(B - V) + 0.12$
r'	$V - 0.81(V - R_C) + 0.13$
$g' - r'$	$0.98(B - V) - 0.19$
B	$g' + 0.47(g' - r') + 0.17$
V	$g' - 0.55(g' - r') - 0.03$
$B - V$	$1.02(g' - r') + 0.20$
$V - R_C$	$0.59(g' - r') + 0.11$
$b_j - r_f$	$1.13(g' - r') + 0.28$
R_F	$r' - 0.13$
$b_j - r_f$	$1.19(B - V) + 0.02$
$b_j - r_f$	$1.21(g - r) + 0.66$
R_C	$R_F + 0.75(b_j - r_f)$

Table 3.3: Colour transformations used in this chapter. Adopted from Smith *et al.* (2002); Windhorst *et al.* (1991); Fukugita *et al.* (1995).The filters are mentioned as follows: Johnson B, V, Gunn g, r, Photographic b_j, r_f, SDSS g', r', Cousins R_C.

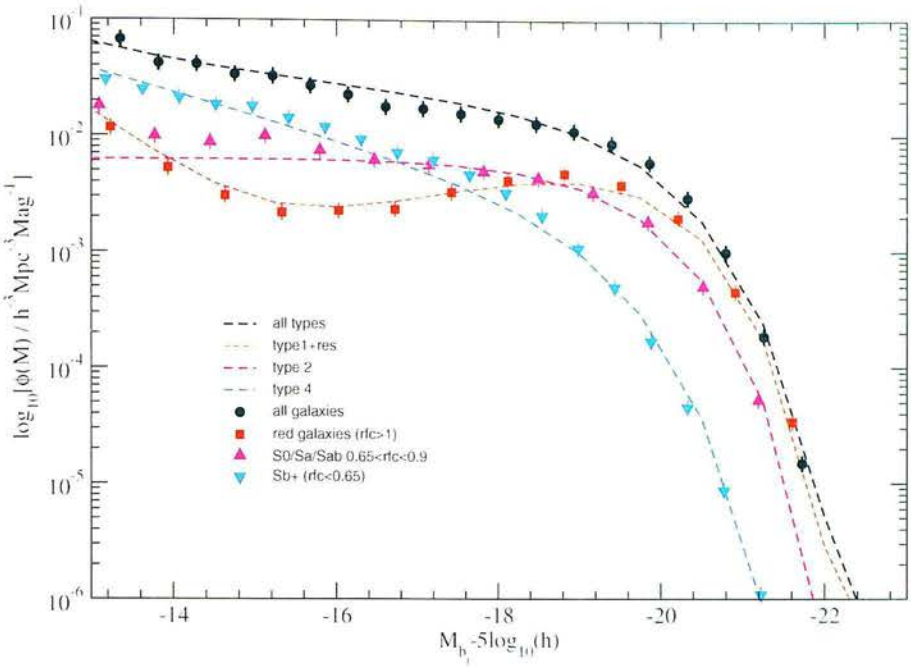

Figure 3.9: Luminosity functions for the 2dFGRS survey as reported in Madgwick *et al.* (2002), for all types and galaxy types 1, 2, 4 (ellipticals, S0/Sa/Sab and Sc+ morphological types respectively). The results are in good agreement with colour cuts of the survey. The colour cuts were based upon the Super Cosmos Sky Survey colours that are quoted for each 2dFGRS galaxy when available (Hambly *et al.*, 2001). The luminosity functions for the colour cuts were calculated with the $1/V_{\max}$ method.

Type	M^*	α	$\phi^*(10^{-3}h^3\mathrm{Mpc}^{-3})$
All	-19.79 ± 0.04	-1.19 ± 0.01	15.9 ± 1.0
1	-19.58 ± 0.05	-0.54 ± 0.02	9.9 ± 0.5
2	-19.53 ± 0.03	-0.99 ± 0.01	7.2 ± 0.4
4	-19.15 ± 0.05	-1.50 ± 0.03	2.4 ± 0.2

Table 3.4: Schechter parameters for the luminosity functions of the 2dFGRS survey as quoted by Madgwick *et al.* (2002). The cosmology that was used in that paper is $H_0 = 100\,\mathrm{km\,s^{-1}Mpc^{-1}}$, $\Omega_m = 0.3$ and $\Omega_\Lambda = 0.7$.

3.4 Black Hole Mass estimation

As mentioned before, recent studies have shown that there is a very tight correlation between the luminosity of the bulge and the black hole mass. One of the key points of this discovery was the fact that this relation holds true for active as well as inactive galaxies, therefore it can be used to calculate the BH mass of all the galaxies in the sample that have a bulge. This relation has the form (McLure & Dunlop, 2002)

$$\log_{10}(M_{\rm bh}/M_{\odot}) = -0.50(\pm 0.02)M_R - 2.96(\pm 0.48) \ , \tag{3.7}$$

where $M_{\odot}$ is the solar mass (1.98892×10^{30}kg) and M_R is the absolute magnitude of the galaxy in the R Cousins filter. The cosmology used by McLure & Dunlop is $H_0 = 50 kms^{-1}$, $\Omega_M = 1$ and $\Lambda = 0$.

For a galaxy with a bulge component of luminosity L_{bulge} and total luminosity L_T, the difference of the absolute magnitudes of the bulge and the galaxy is given by

$$M_{\rm bulge} - M_{\rm g} = -2.5 \log_{10} \left(\frac{L_{\rm bulge}}{L_{\rm total}} \right) \ , \tag{3.8}$$

therefore substituting for the absolute magnitude the equation for the bulge magnitude becomes:

$$M_{\rm bulge} = m - 5 \log_{10}(D_L) + 5 - k(z) - 2.5 \log_{10}(B/T) \ , \tag{3.9}$$

where D_L is the luminosity distance in parsecs and $k(z)$ is the k-correction used. When calculating black hole masses for very blue galaxies an upper limit was chosen based on the assumption that galaxies with no bulge (for a colour index less that 0.2) have an upper limit to their black hole mass, which is defined as the BH mass for a galaxy with the same absolute magnitude and a B/T ratio of 0.2.

3.4.1 Comparison with Estimated Black Hole masses

The scaling relation between the bulge luminosity and the black hole mass of the central region does not come from any theoretical models. It is an empirical relation that arose from analysing the relation of measured black holes masses and host galaxies properties. In order to confirm the validity of the mass estimation for the 2dFGRS galaxies, a comparison has been performed, between the original black hole mass (independent dynamical measurements) and a mass estimated in the same way as the previous analysis. The black hole masses were taken from

Name	B	V	R	A_R	R type	D (Mpc)	M (10^8M$_\odot$)
N4258	8.53	7.98	10.05	0.043	R_J	7.2	0.390 ± 0.034
N4486	9.49	8.56	8.62	0.060	R_J	16.7	35.7 ± 10.2
N3115	9.74	8.80	8.68	0.127	R_J	9.8	9.2 ± 3.0
N221	8.72	7.84	8.61	0.166	R_J	0.8	0.039 ± 0.009
N5128	7.30	6.42	6.35	0.307	R_C	4.2	$2.4^{3.4}_{-1.7}$
N4374	10.01	9.07	9.37	0.108	R_J	18.7	$17^{12}_{-6.7}$
N4697	10.07	9.18	9.03	0.081	R_J	11.9	$1.7^{0.2}_{-0.3}$
N4649	9.7	8.75	10.28	0.071	r	17.3	$20.6^{5.2}_{-10.2}$
N4261	11.39	10.39	10.21	0.048	R_J	33	5.4 ± 1.2
N4564	11.96	11.06	11.45	0.093	r	14.9	0.57 ± 0.15
N1459	10.83	9.88	9.43	0.042	R_C	30.3	4.6 ± 2.8
N3379	10.18	9.24	9.64	0.065	R_J	10.8	1.35 ± 0.73
N3245	11.65	10.76	10.76	0.067	R_J	20.9	2.1 ± 0.5
N4473	11.03	10.11	10.9	0.079	r	16.1	$0.8^{1.0}_{-0.4}$
N2787	11.61	10.59	10.46	0.36	r	7.5	0.41 ± 0.05
N3608	11.69	10.76	10.86	0.056	r	23.6	$1.1^{1.1}_{-0.3}$
N3384	10.75	9.8	10.51	0.071	r	11.9	0.14 ± 0.05
N4742	11.94	11.16	11.17	0.109	r	15.5	0.14 ± 0.05
N1023	11.76	10.93	12.16	0.139	r	10.7	0.44 ± 0.06
N4291	12.25	11.32	11.70	0.098	r	26.9	1.9 ± 1.2
N7457	11.76	10.93	12.16	0.139	r	13.5	0.036 ± 0.01
N821	11.72	10.79	11.11	0.294	r	24.7	0.39 ± 0.06
N3377	11.07	10.23	10.40	0.091	r	23.3	$0.13^{0.16}_{-0.08}$

Table 3.5: Values taken from Merritt & Ferrarese (2001)(black hole masses and distances) and the NASA/IPAC Extragalactic Database (magnitudes), for galaxies with measured black hole masses. The B, V magnitudes are taken from (Vaucouleurs *et al.*, 1991) and are k-corrected and galactic extinction corrected. Only galaxies that had a well defined magnitude ($\Delta m \leq 0.2$) were used. For the R magnitudes, the best defined was used and transformed in to R_C using the colour equations of table 3.3. R_J depicts Johnson's R magnitude, R_C Cousins R magnitude and r is used to indicate Thuan-Gunn r magnitude. Distances are given in Mpc and the mass is in units of 10^8 solar masses.

Merritt & Ferrarese (2001), where a summary for each individual detection is given. The colours and magnitudes, together with galactic absorption parameters, were taken from the NASA/IPAC Extragalactic Database. The details for each galaxy are included in table 3.5 and the comparison between estimated values and original values is plotted in figure 3.10.

3.5 Mass functions

3.5.1 The survey Black Hole Mass function

Although the luminosity function is an interesting result on its own, the main interest is the mass function of the survey, which is very easy to calculate in a similar fashion. The transformation of the luminosity function to a mass function is straightforward, given the assumption that $L = AM_{\rm bh}^{\beta}$. To avoid confusion the mass function in denoted with $\rho(M)$ and the luminosity function with $\phi(L)$. The symbol M here stands for the mass of the black hole and not of course for the absolute magnitude.

$$\phi(L)dL = \rho(M)dM \Rightarrow \rho(M) = \phi(L)\frac{dL}{dM} \quad . \tag{3.10}$$

Replacing the equation for the Schechter luminosity function with the mass of the black hole and $dL/dM = A\beta M^{\beta-1}$

$$\rho(M) = A\beta\phi_* \left(\frac{M}{M_*}\right)^{\beta\alpha} \exp\left[-\left(\frac{M}{M_*}\right)^{\beta}\right] M^{\beta-1} \quad . \tag{3.11}$$

For given values of A and β, a transformation of the optical luminosity function to a mass function can be performed.

A more direct method would be to use the $V_{\rm max}$ method directly to the galaxies with calculated black hole mass by replacing magnitude or luminosity bins with black hole mass bins. In essence it is the same procedure as transforming the luminosity function to a mass function, since the transformation is incorporated in the Magorrian relation. The mass functions for the 2dFGRS sample are shown in figures 3.11 and 3.12. The shape of the black hole mass functions suggests a parameterisation similar to the Schechter function

$$\rho(M)dM = \rho_* \left(\frac{M}{M_*}\right)^{\alpha} \exp\left(-\frac{M}{M_*}\right) \frac{dM}{M_*} \quad . \tag{3.12}$$

This form has the very useful behaviour of returning a very simple form when integrated over all masses in order to get the total density ρ_0:

$$\int_{M_{\rm min}}^{\infty} M\rho(M)dM = \int_{0}^{\infty} M\rho(M)dM \quad , \tag{3.13}$$

	ρ_* $(10^{-3}\mathrm{Mpc}^{-3})$	$\log_{10} M_*$	α	$\rho_0(\mathrm{h}^2 10^5 \mathrm{M}_\odot \mathrm{Mpc}^{-3})$
All types	(4.7 ± 0.3)	7.94 ± 0.26	-1.14 ± 0.02	4.6 ± 0.4
E	(3.4 ± 0.4)	7.92 ± 0.32	-0.77 ± 0.06	2.6 ± 0.6
S0,Sa,Sb	(4.2 ± 0.4)	7.62 ± 0.28	-1.00 ± 0.04	1.8 ± 0.4
Sc,Sc+	(1.5 ± 0.5)	6.91 ± 0.40	-1.30 ± 0.05	0.2 ± 0.8

Table 3.6: Schechter fit parameters for the mass functions shown in figures 3.11 and 3.12, together with the total black hole density value calculated for each population.The different populations are defined by their colour, as seen in figures 3.11 and 3.12. For comparison purposes with other density values in the literature, a minimum black hole mass of $M_{\mathrm{min}} = 10^6 M_\odot$ was assumed when calculating the total density.

$$\rho_0 = \rho_* \int_0^\infty \left(\frac{M}{M_*}\right)^{a+1} \exp\left(-\frac{M}{M_*}\right) dM \ , \tag{3.14}$$

and making the replacement $t = M/M_*$, equation 3.13 then takes the form

$$\rho_0 = \rho_* M_* \int_0^\infty t^{(a+1)} e^{-t} dt \ , \tag{3.15}$$

which leads to the simple form

$$\rho_0 = \rho_* M_* \Gamma(\alpha + 2) \ , \tag{3.16}$$

since the $\Gamma(x)$ function is defined as

$$\Gamma(x) = \int_0^\infty t^{x-1} e^{-t} dt \ . \tag{3.17}$$

The contribution of the low mass black holes is negligible, since they are orders of magnitude smaller than the majority of BH, which peaks around $M = 10^8 M_\odot$, therefore the lower limit can be pushed to zero in equation 3.16.

Another form of the black hole mass function is the $\log M$ form which has the same relation as the magnitude function $\phi(M)$ has with the luminosity function $\phi(L)$. There is no physical significance in using this particular form apart from the fact that it is much easier to fit a function to it. The equation is

$$\rho(M) dM = \log(10) \rho_* 10^{(w-w_*)(\alpha+1)} \exp\left(-10^{(w-w_*)}\right) \ , \tag{3.18}$$

where $w = \log_{10}(M_{\mathrm{bh}}/M_\odot)$. In figures 3.11 and 3.12 mass functions are plotted and fitted to the data. Fit values are given in table 3.6. The resulting total black hole mass density for the various galaxy population is also quoted.

3.5.2 Estimating the variance

The statistical error in the analysis is quite small (smaller that the size of the symbols in figures 3.11) and 3.12. To calculate the noise in the data, the usual error for statistical noise was used:

$$\frac{\delta\rho}{\rho} = \frac{(\sum 1/V_{\rm max}^2)^{1/2}}{\sum 1/V_{\rm max}} \ , \tag{3.19}$$

the same negligible error bars for the statistical noise resulted, when a jackknife analysis was performed on the data. The jackknife analysis consists of excluding a part of the data and doing the analysis again (Rodmann, 2004). Ultimately just one point of the data must be excluded, but for large samples the same results can be achieved by excluding a random sampling of points that represent a fraction of the data. The final error bars represent the variation from the mean for the calculated result values of each analysis.

The black hole mass estimation suffers from a large *systematic* error though, not due to noise. The 2dFGRS sample is large and well defined, but two assumptions were made, which are sources of uncertainty. The first assumption was that the different galaxy types have a well defined bulge to total ratio (equation 3.6) and the second was that the relation between the black hole mass and the luminosity of the bulge was well defined. In reality there is scatter in both equations as was mentioned in the previous sections. There is also some uncertainty concerning the colour gradients used and the some uncertainty in the colour transformations but its contribution to the overall error is negligible comparing to the previous two.

In order to include error bars that represent this systematic uncertainty in the calculation, a Monte Carlo simulation for the resulting black hole mass was performed. A Monte Carlo simulation is a statistical way to measure the uncertainty in a theoretical model. By producing a large amount of mock data points, an analysis can be repeated many times and a statistical error can be estimated for the resulting parameters. The data points are randomly generated by a convolution of the real data points and any error factor that needs to be investigated Rodmann (2004).

In the present application, the theoretical model was taken to be equation 3.7. For each iteration black hole masses were generated for all the galaxies in the sample, taking in to account the uncertainty of the bulge to total ratio (a scatter of ~ 0.2 for the quoted values was assumed) and the scatter of the mass luminosity relation in equation 3.7. The resulting mass functions for the 1000

source	method	value
(Aller & Richstone, 2002)	$M_{\rm bh} - \sigma$	$(4.8 \pm 1.6)10^5 M_\odot {\rm Mpc}^{-3}$
(Aller & Richstone, 2002)	$M_{\rm bh} - \sigma$	$(6.9 \pm 1.4)10^5 M_\odot {\rm Mpc}^{-3}$
(Marconi *et al.*, 2004)	$M_{\rm bh} - L_{\rm bulge}$	$(4.6 \pm 1.6)10^5 M_\odot {\rm Mpc}^{-3}$
(Yu & Tremaine, 2002)	$M_{\rm bh} - \sigma$	$(4.7 \pm 0.9)10^5 M_\odot {\rm Mpc}^{-3}$

Table 3.7: Reported results for total black hole mass density. The different estimates of Aller and Richstone were based on different luminosity functions.

realisations and the resulting 2σ confidence limits are shown in figure 3.14. The limits in figure 3.14 are not symmetrical, but there is a bias towards higher black hole masses. This is similar to the Malmquist bias (Butkevich *et al.*, 2005) and arises because the calculated black hole mass is in fact a measure of luminosity, since it is calculated using the Magorrian relation. As a result and since the luminosity function is calculated by using the maximum distance an object can be and still be included in a magnitude limited sample, brighter galaxies tend to be artificially boosted, since fainter magnitudes are not included at large distance. If the detected galaxies appear to increase in brightness with distance, then those galaxies will also appear to have a larger black hole mass. This is evidently at regions where the mass function is steep and a systematic change in shape is observed, with higher mass density being boosted. This is a inherit problem in luminosity like function calculations and should be taken into account when two different estimates are being compared.

3.5.3 The Black Hole Mass Functions in the literature

Results from the analysis of Aller and Richstone (Aller & Richstone, 2002) are used to compare with the mass function estimates. The results agree well with the published work, considering the scatter in the relations (values for the total mass density ρ are shown in table 3.6). Also, values of the total black hole mass density from other published papers are given. The results all agree at a value of $\rho_{\rm total} = 5 \pm 1.4$. Given the individual error bars, all methods give equivalent results for different surveys. These results give a total black hole mass density larger than previously reported (Franceschini *et al.*, 1998), which reflects the better calibration of the scaling relations used.

3.6 Conclusions

The summary of this chapter is as follows:

- Firstly, an overview of the 2dFGRS survey was given, together with an explanation of the colour b_j and r_f magnitude information included in the final release.

- Secondly, an accurate way of calculating k-corrections for the SCSS magnitudes was presented along with proof that the colours included in the 2dFGRS can be used as good indicators for galaxy types. A relation between galaxy type and bulge to total luminosity ratio was discussed in this context as well.

- Thirdly, the 2dFGRS luminosity and mass functions were calculated. The luminosity functions for various colour cuts was shown to be highly correlated to the 2dFGRS galaxy type luminosity functions. The mass functions for the survey were also computed, and an estimation for the total density of galaxies was given.

- Lastly, the previous results were compared to published values from the literature and shown to be well within the quoted error bars. Also, the ability of the scaling relation between the bulge luminosity and the black hole mass, to retrieve the accurate mass was discussed, using known masses from the literature.

In this chapter, the colour information included in the latest 2dFGRS release was shown to be a good statistical indicator of galaxy type. The b_j and r_f colours are well calibrated and accurate and thus are good additions to the 2dFGRS survey results. Furthermore, more accurate k-corrections were presented for the 2dFGRS survey than previous reported. Albeit the k-correction seldom takes the spot light in many project, it is essential and thus the new formulas will lead to better accuracy for future studies of the 2dFGRS.

This chapter serves the purpose of an introduction to the 2dFGRS black hole mass function. It is a necessary step, in order to continue to the next chapter, where the focus will shift to radio galaxies in the 2dFGRS. The colour information from the SCSS was shown that provides an accurate way to calculate black hole masses and also serves the role of an indicator to the galaxy type. The black hole mass function allowed the calculation of the black hole mass density for the local universe. The results agree well with previous work as seen in 3.7 and the size of the sample allows for good accuracy. This results also agree with the soltan argument and indicate that the quasars seen in higher redshifts are indeed present in the local universe and lie dormant in the centers of most galaxies (Soltan, 1982).

The scaling relation used for this analysis is found to be just as accurate as the velocity dispersions method of calculating black hole masses. There is a larger uncertainty when complex systems are considered (bulge and disk objects, due to the large scatter that the various galaxy types exhibit in the colours) but in the case of elliptical galaxies, the results are very accurate. This fact is vital for the next chapters, since the elliptical galaxies will be the centre of the analysis.

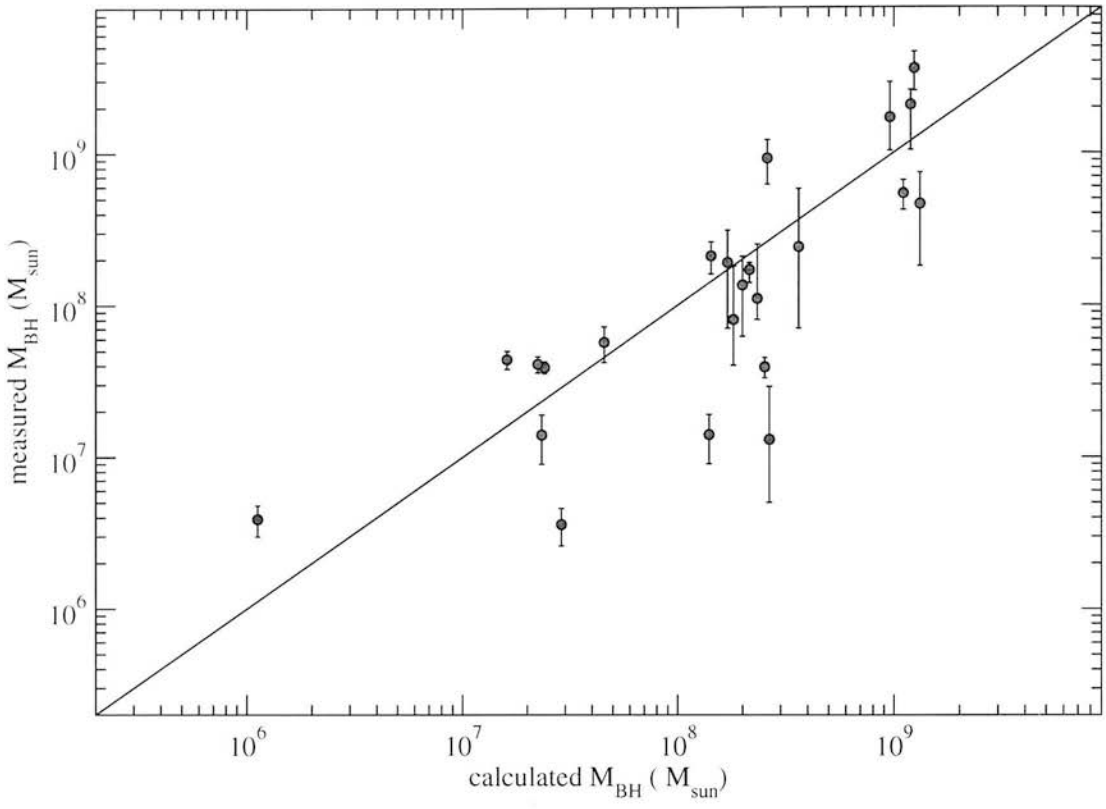

Figure 3.10: Comparison between the estimated black hole masses using 2dFGRS colours and the bulge luminosity - black hole mass relation from McLure & Dunlop (2002) and the quoted value for black hole masses from table 3.5. There is a good agreement for most values although there is a tendency to overestimate black hole masses using bulge luminosity. Nevertheless, considering that the scatter in the Magorrian relation is ≈ 0.39 dex, most calculated black hole masses do indeed coincide with the measured masses. Only 3 points differ from the expected relation by more than twice the reported scatter in the Magorrian relation. This shows that the simple $M_{\rm bh}$ estimation works as well as could be expected.

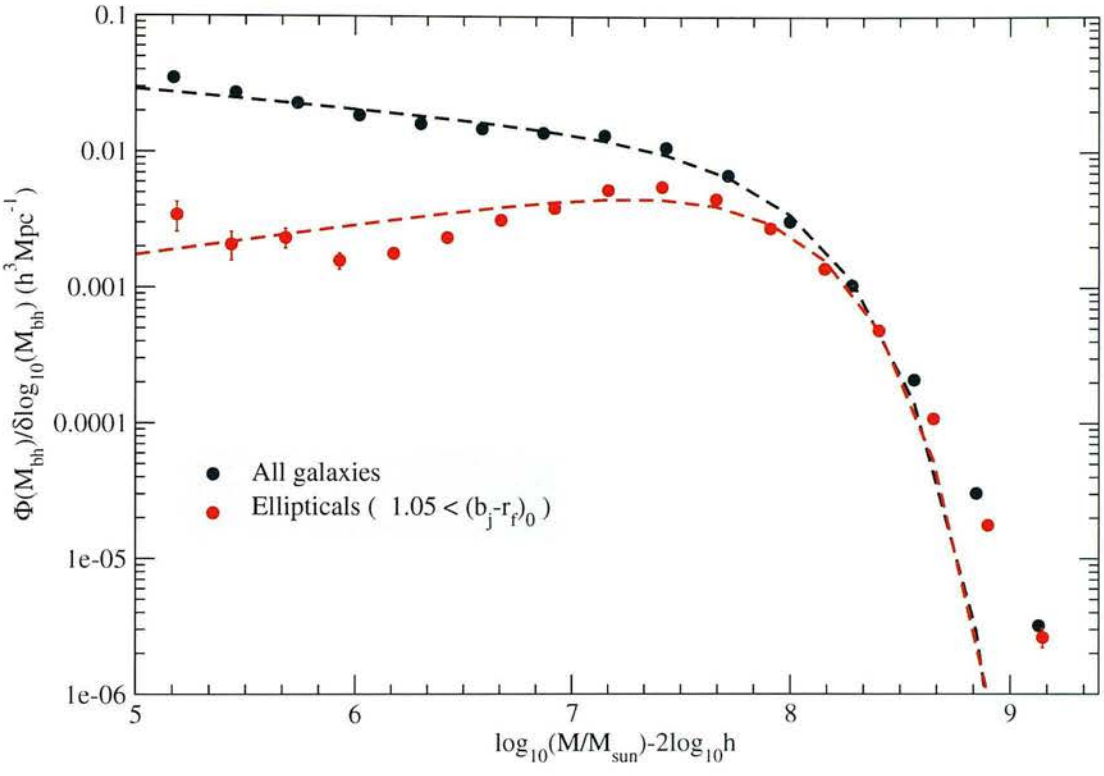

Figure 3.11: Black hole mass functions for the 2dFGRS total galaxy population (black circles) and the red galaxy population (red). The colour cuts are taken from figure 3.8. The high mass end of the total mass function is identical to the elliptical mass function. The fitted model was that of equation 3.18.

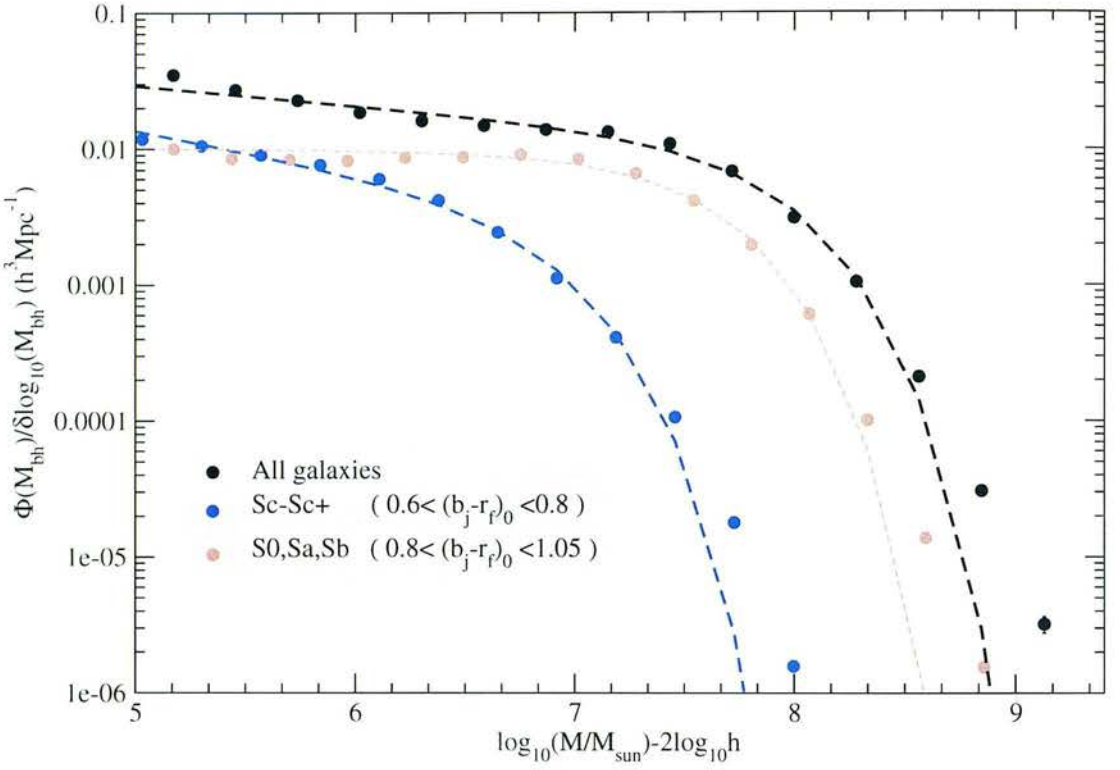

Figure 3.12: Black hole mass functions for the 2dFGRS total galaxy population (black circles) and disk system galaxies (blue and brown). The colour cuts are taken from figure 3.8. The fitted model was that of equation 3.18. The mass function of the Sc+ galaxies is restricted to very low masses and falls off quickly.

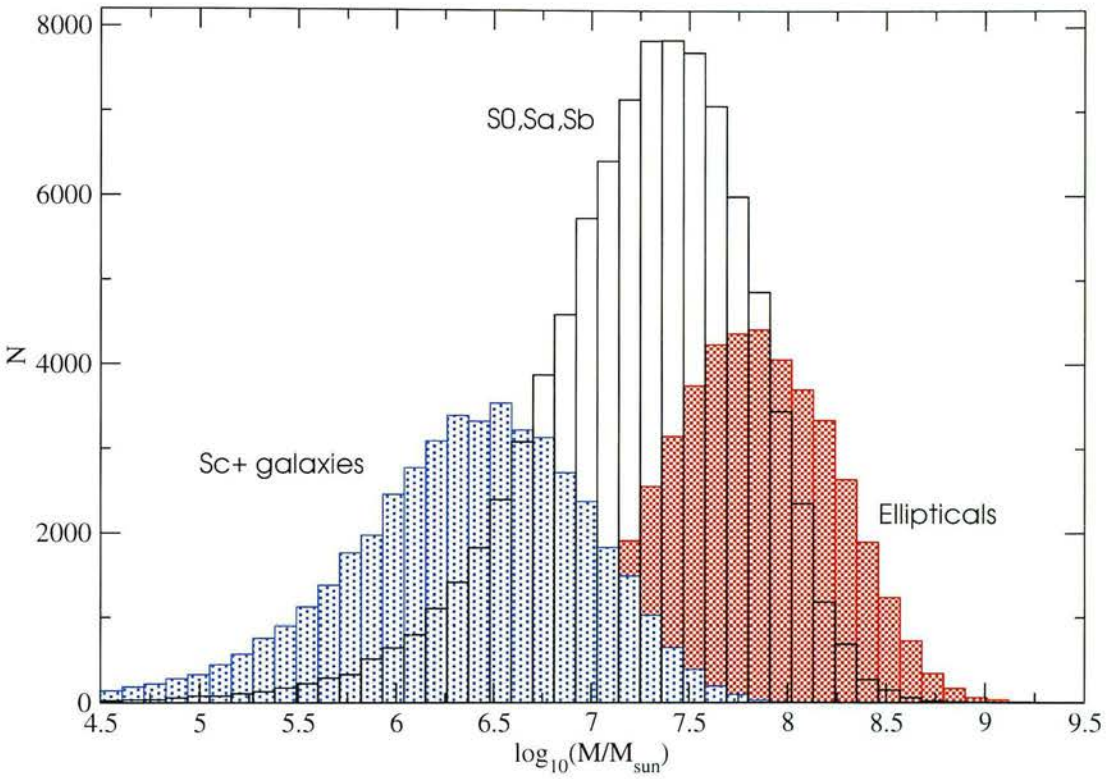

Figure 3.13: Histogram for the galaxies used in the calculation of the mass functions for the 2dFGRS survey. It is clear that galaxies with high BH mass are almost exclusively ellipticals, whereas S0/Sa galaxies dominate in the middle range. The contribution of Sc+ is restricted to very low black hole masses.

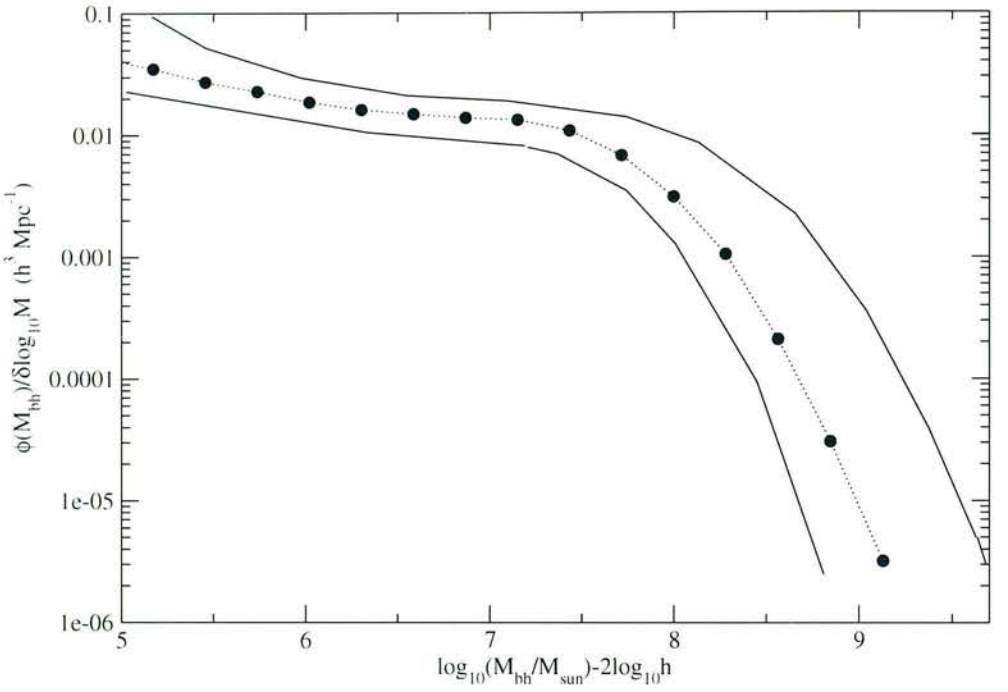

Figure 3.14: The mass function for all the galaxies in the sample. The solid lines indicate the 2σ in the scatter around the values after 1000 Monte Carlo simulations of the Magorrian relation convolved with the error in the bulge luminosity relation with the black hole mass (equation 3.7) and the error in the calculation of the bulge magnitude.

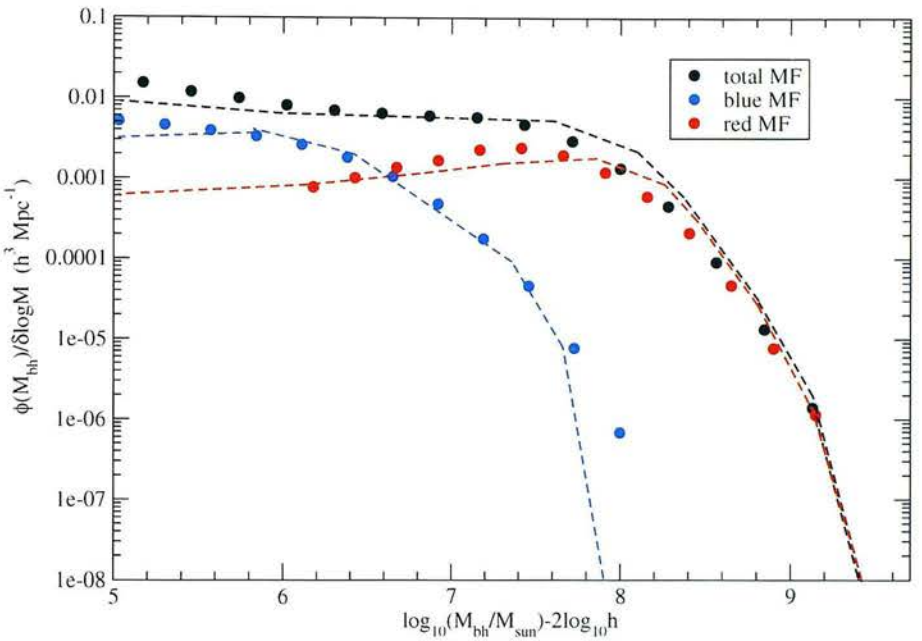

Figure 3.15: Comparison between the estimated black hole mass function (circles) for all galaxies, blue and red populations and the results from Aller & Richstone (2002) (dashed lines). The y axis has been modified to agree with figure 6 of Aller & Richstone (2002). The results agree reasonably well. The red galaxies mass function to small masses is an extrapolation in the aforementioned paper.

Chapter 4

Radio galaxies in the 2dFGRS

4.1 Introduction

The focus of the previous chapter was the central black hole of galaxies and the mass function. In the present chapter the focus will be the relationship between the central engine and one aspect of galactic activity, namely radio sources that are powered by AGN. Radio emission from galaxies is not only linked to the central engine but it is also observed in normal galaxies (Condon, 1992). When studying the properties of the central engines of radio galaxies, it is important to be able to distinguish between emission from the centre and emission from the galaxy. In the present analysis, the Hα line of the 2dFGRS spectra was used to gain an insight to the amount of radio power that was originating from the galaxy and not the AGN.

One other interesting aspect of radio galaxies, is the relation between the radio output and the mass of the black hole. There have been some conflicting results in the literature, with reports that a scaling relation of the form $P \sim M^{2.5}$ exists between the radio power and the black hole mass (Franceschini *et al.*, 1998) and claims that there is no such relation exists or at least it is not so straightforward (Ho, 2002).

4.2 The NVSS survey

The NVSS survey is a radio survey at the frequency of 1.4GHz, that covers almost all of the sky north of dec > -40 (J2000) covering 82% of the whole celestial sphere and overlaps with the 2dFGRS regions (excluding some random fields). It has a flux limit of 2.2 mJy and source density of 60 sources per sq.degree. It has an angular resolution of 45 arcsec FWHM and nearly uniform sensitivity. Positional uncertainties vary from $\sigma_{\mathrm{ra,dec}} \leq 1''$ for strong sources (displaying a flux greater than 15 mJy), to $\sigma_{\mathrm{ra,dec}} \simeq 7''$ at the survey flux limit. The survey has proved invaluable for the astronomical community, since its wide area coverage allows many surveys to add radio flux to their results by cross-matching with the NVSS. Further details describing the survey and its design can be found at Condon *et al.* (1998).

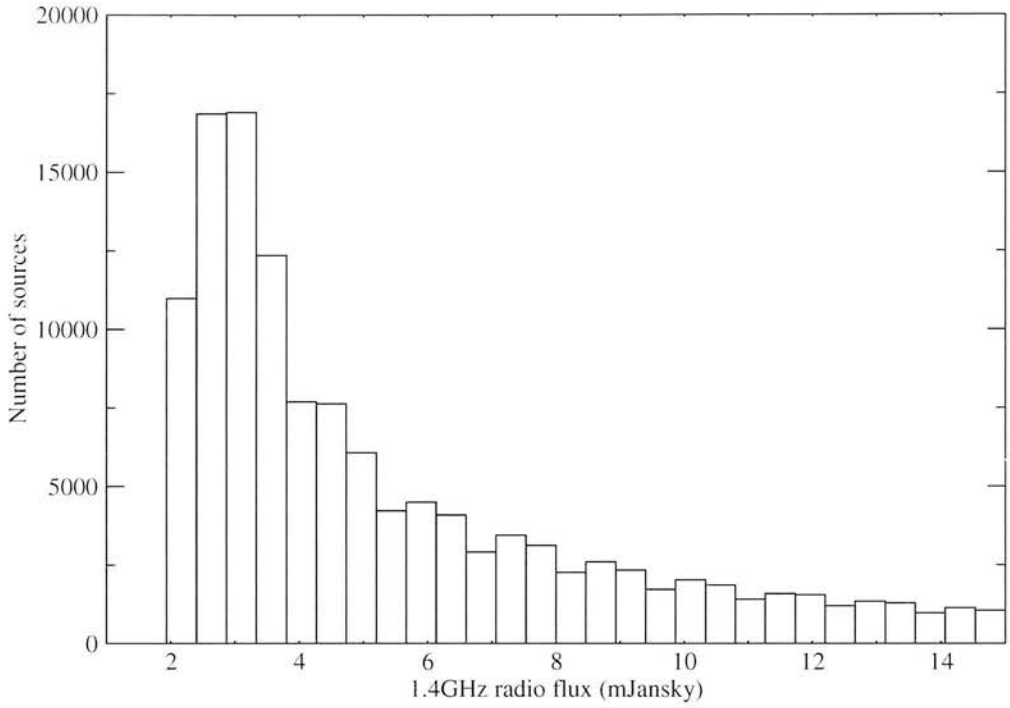

Figure 4.1: A numerical histogram for the sources in the NVSS survey that are contained within the limits of the 2dFGRS two main strips (NGP, SGP). Most of the sources have a radio flux at 1.4GHz very close to the NVSS limit (2.2 mJy). There are sources that have a radio flux of a few Jansky, although they are quite few. Of these sources, around 3500 were identified with optical galaxies selected from the 2dFGRS.

4.2.1 Matching radio sources with 2dFGRS galaxies

4.2.1.1 Binary tree search method

In order to identify the radio counterparts of the 2dFGRS galaxies, a nearest neighbour search in a binary tree approach was used. A search for nearest neighbours consists of identifying the nearest points of a data set to a query set of coordinates according to a distance modulus. The procedure is straightforward enough for small sets, were the distance to every point is calculated and subsequently compared with the distances to the rest of the set points, to form the group of nearest distances to the query point. In case of large databases though, this procedure is not time efficient, since for one set of query points N calculations have to be performed, where N is the number of elements in the database.

To achieve sufficient results in an acceptable time frame, manipulation of the database is needed. A common way to do so is to use a *search tree* configuration. The spatial coordinates of the set are arranged in a box or node, which is subsequently divided in two. The rules of the split depend on the method of search. The resulting nodes are themselves divided and the procedure continues, until the number of points in each node is equal to a predetermined small number (most usually one element per node). A binary search tree is a binary tree in which each internal node X stores an element such that the elements stored in the left subtree of X are less than or equal to X and elements stored in the right subtree of X are greater than or equal to X. By placing a query set of coordinates somewhere along the defined space, one can easily identify the node that the query point is part of. In this way, one can restrict the quantity of distance calculations measurements to only the points that are part of the same node, and if this is not adequate, to the neighbouring and parent nodes as well. In this way, the number of calculations is reduced to a worse case scenario of $\log_{10} N$ calculations.

4.2.1.2 The number of radio sources

The NVSS radio survey is very extensive, covering a large part of the sky and containing $\sim 2 * 10^6$ radio sources. It would be pointless to use all the survey, so it is better to apply the matching algorithm to the radio sources that are around the two large regions of the 2dFGRS field. Only the NGP and SGP region sources are used, whereas sources from the random fields are omitted. This is because the two regions have been studied extensively and the survey limits and masks are easier to use, unlike the limits and the mask of the random fields. There are 162754 radio sources in the region of the sky that the two main strips of the 2dFGRS are. The somewhat generous limits of this particular region of the NVSS are

$$\text{NGP} \begin{cases} \text{RA} \in [140, 230] \\ \text{DEC} \in [-10, 5] \end{cases} .$$

For the South Galactic Pole region, the coordinates are broken in two sets:

$$\text{SGP} \begin{cases} \text{RA} \in [0, 57.5] \\ \text{DEC} \in [-38, -22] \end{cases} \bigcap \begin{array}{c} \text{RA} \in [320, 360] \\ \text{DEC} \in [-21, -38.5] \end{array} .$$

4.2.1.3 Identifying double radio sources

During the procedure of identifying the radio counterparts of the 2dFGRS galaxies, a search for the ten nearest radio neighbours was performed. The number of nearest neighbours does not need to be very large since there are only a few possibilities.

- The first possibility is for the galaxy to have no radio counterpart. The resulting neighbours would then lie far away and the galaxy will be subsequently dropped from the final sample or there could be a random identification with a radio source. The way the search is performed is adjusted in such a way as to minimise the random encounters.

- A second possibility would be that the galaxy has a radio counterpart in a one to one match. Most identifications are realisations of this possibility.

- Not all radio sources in the NVSS are well defined and resolved. There are cases of extended sources that have been resolved in two or three individual sources. In this case, the search for an optical counterpart would take place in an area around the centre of the combination of the radio sources.

- Finally, an optical galaxy could lie in close proximity to more than one radio source. If the radio sources do not appear to be linked to each other (by being parts of an extended source), then the closest source to the optical galaxy is taken as the proper identification.

In order to investigate if a radio source is associated with another radio source, the semi empirical method of Magliocchetti *et al.* (1998) is used. Consider two radio sources with fluxes S_1 and S_2, separated by an angle θ. In order for the two sources to be linked, they have to fulfil two criteria. First of all the ratio of their fluxes should satisfy $0.25 < (S_1/S_2) < 4$ and secondly their projected separation should be less than their link length. The link length is defined as

$$r = (S_1 + S_2)^{\frac{1}{2}} \times 10 \ , \tag{4.1}$$

where the fluxes are in mJy and the link length is in seconds of arc. This empirical relation is a manifestation of the relation between the angular size of radio sources and their flux as seen in figure 4.2 (Oort, 1987) If two radio sources appear to be linked, then a new source is added to the catalogue, laying on the axis defined by the two linked sources and flux the sum of the two individual fluxes.

The optical galaxy sample consists of the public release of the 2dFGRS best spectroscopic observations in the redshift range $0.001 \leq z \leq 0.3$ and confined in the NGP and SGP strips. The result for a search in the 2dFGRS survey region for radio galaxies, using a maximum distance of 16 arcseconds, yields 3430 single sources and 21 sources associated with double radio sources. These galaxies make up a very large radio galaxy sample with accurate redshift and colour information.

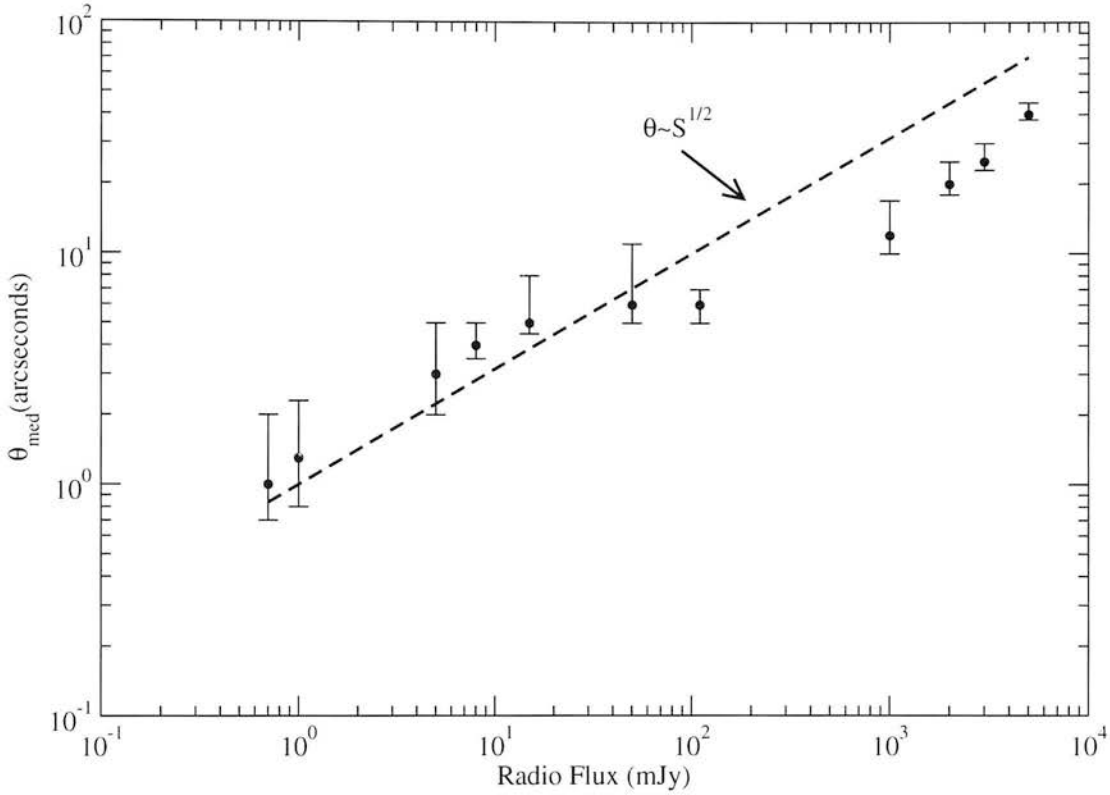

Figure 4.2: The relation between the median angular size of radio sources with the source flux. The graph was replicated from Oort (1987). Since the plot represents the median size of a source, a generous link length was used in the text, $r = 10 * \theta_{\text{med}}$, to include the large error bars.

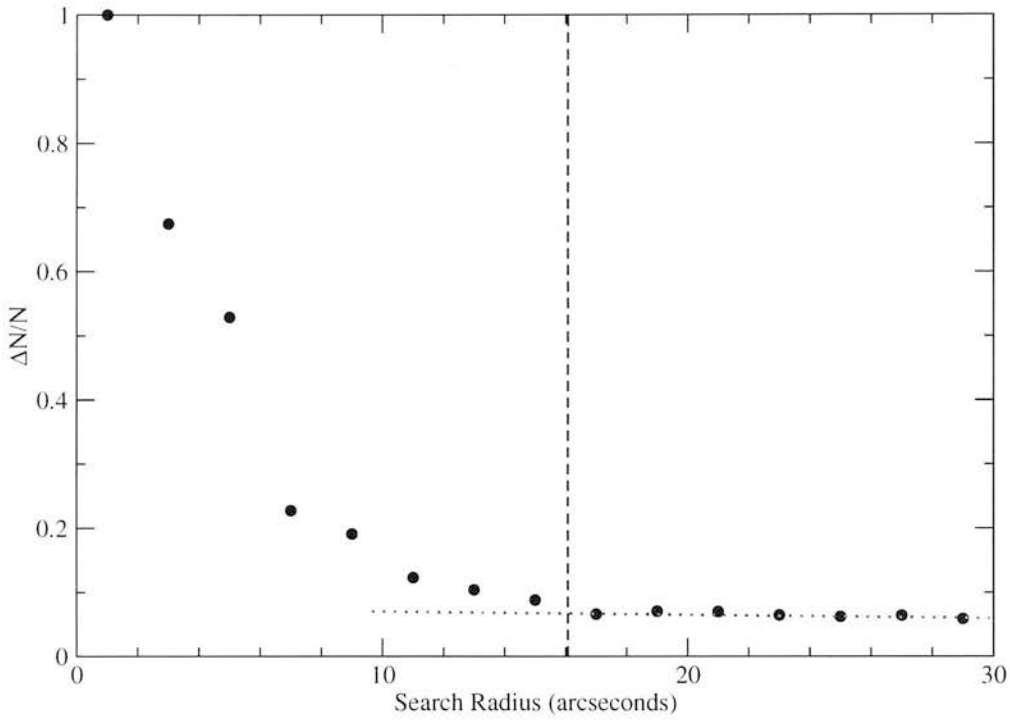

Figure 4.3: Of the 10 nearest radio survey neighbours reported for every 2dFGRS galaxy, only galaxies that have an angular distance of 16 arc seconds or less in the sky are kept. From this plot, it is obvious that for larger radii all the reported matches are probably due to random identifications. N on the plot depicts the number of matches and ΔN the increase in number of positive identifications from the previously used search radius. The dotted line represents the value $\Delta N/N$ expected from a random survey with surface density similar to the NVSS, namely 60 galaxies per square degree.

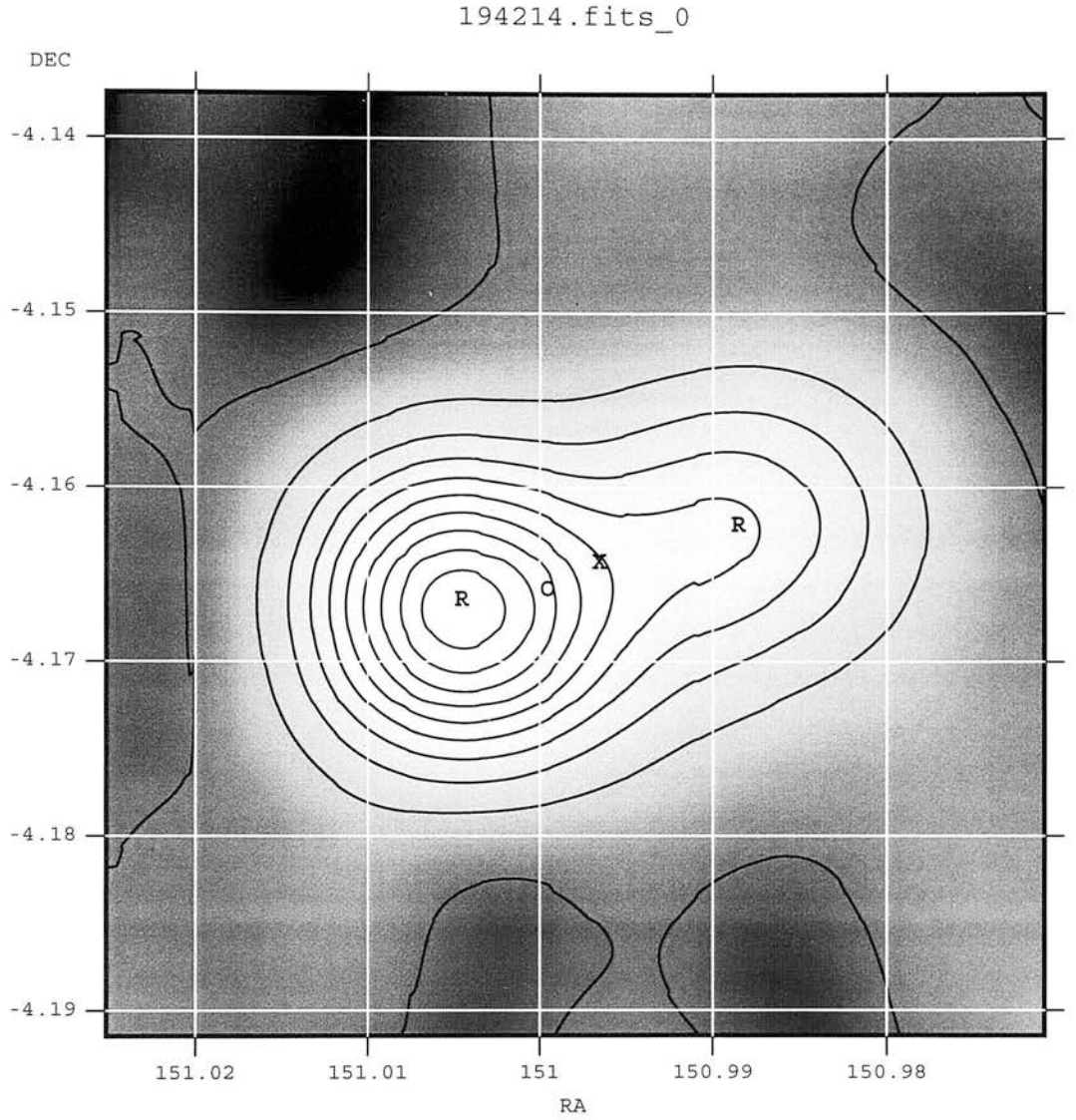

Figure 4.4: An example of a cross match between an optical source and two radio sources that appear to be connected and are replaced by a single radio source as described in the text. The markings are as follows: O marks the coordinates of the optical source ($z = 0.157$), R marks the coordinates of the two radio sources that were identified as connected with each other and X the computed centre of the new radio source. It is obvious from the contour plot of the NVSS fits file, that the galaxy is a radio source with lobes and the optical detection coincides with the central part of the galaxy.

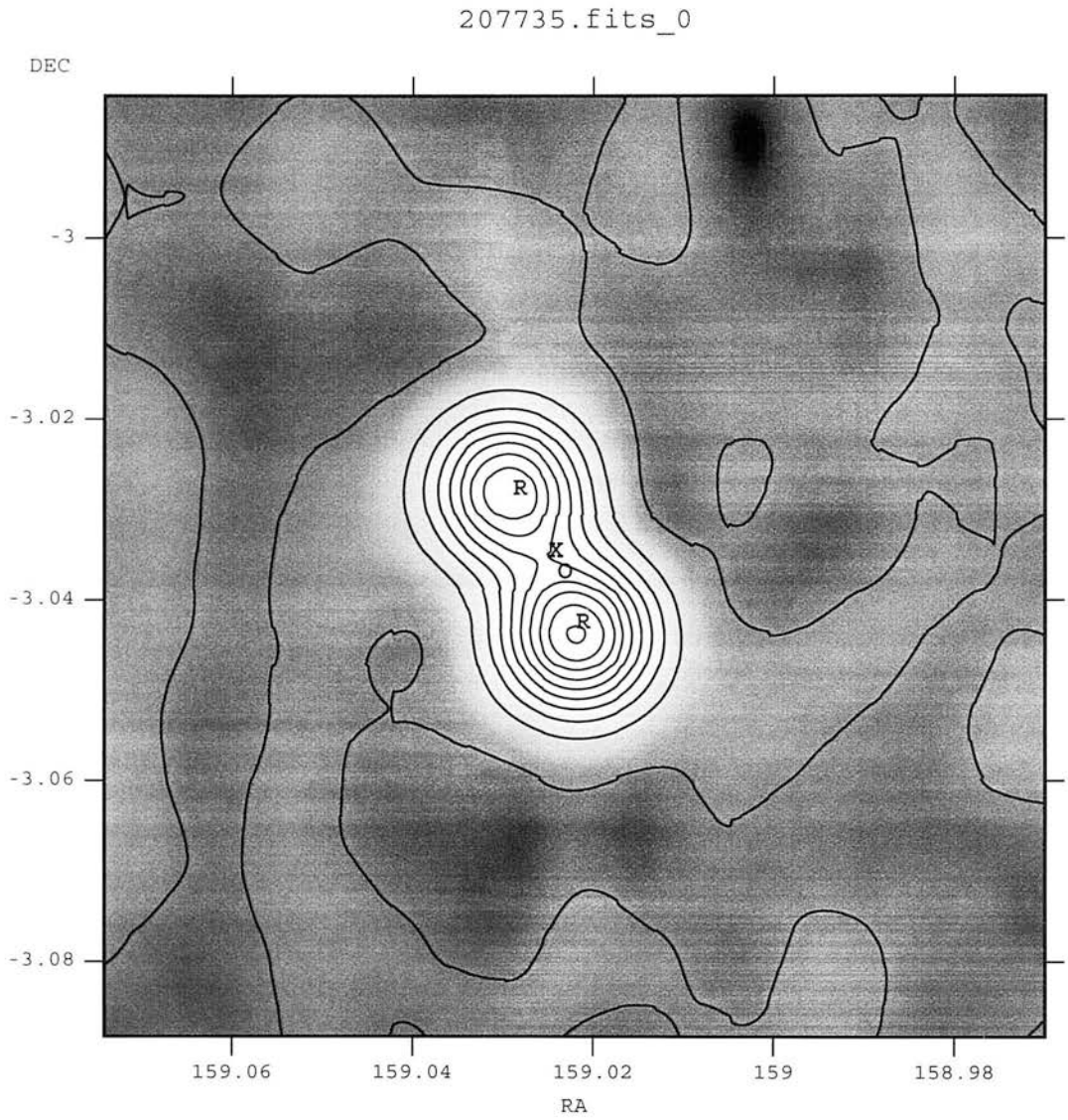

Figure 4.5: Another example that demonstrates more clearly how effective the empirical formula for identifying connected radio sources. The optical source lies at redshift $z = 0.0375$.

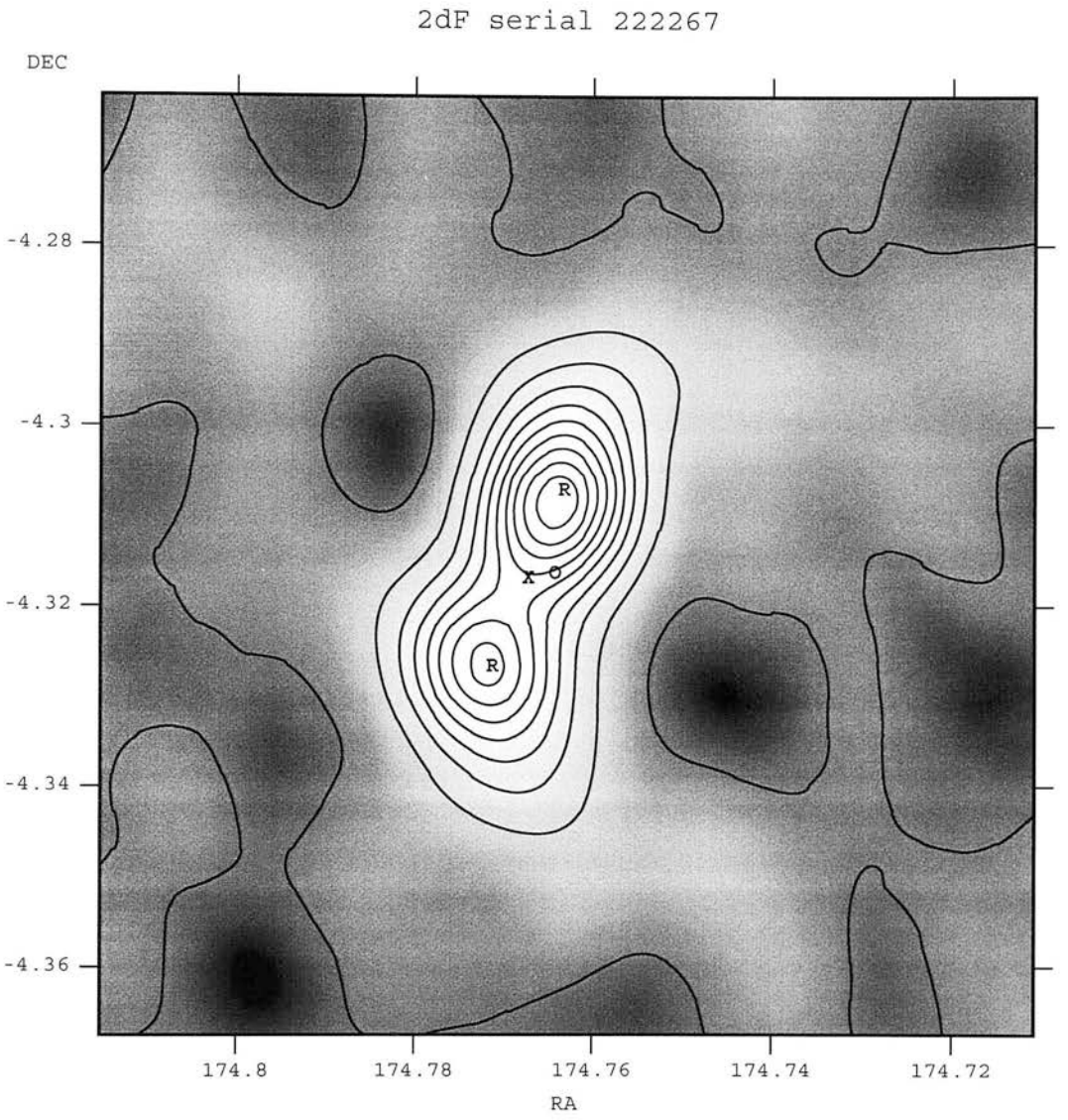

Figure 4.6: A double radio galaxy that was identified to have a redshift of $z = 0.0563$.

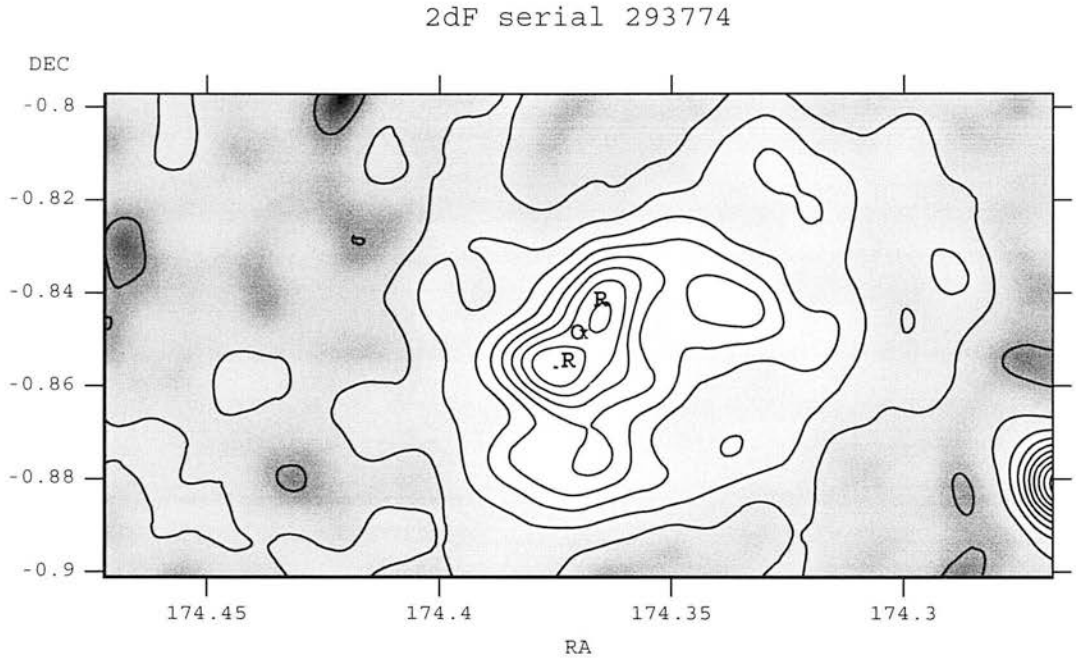

Figure 4.7: Even though the radio image appears to contain multiple radio sources, the computed centre of the radio galaxy again coincides well with the optical 2dFGRS identification. Galaxy at redshift $z = 0.0439$.

4.3 The radio luminosity function of the 2dFGRS

Following the same methodology as when calculating the optical luminosity function of the 2dFGRS, one can calculate the radio luminosity function for the selected radio galaxies in the database. The radio luminosity function has been accurately calculated for a number of surveys of radio galaxies, since radio observations of large samples have been around for a while and the results seen in figure 4.8 agree with previous publications. There is nothing new added in the calculation of the local radio luminosity function apart from perhaps slightly better accuracy, since most measurements were based on photometric redshifts that were not as good as the spectroscopic redshifts of the 2dFGRS and the samples used where smaller. Therefore, the chance to offer a slightly improved measurement of the radio luminosity function for the 2dFGRS area should not be overlooked.

The radio flux from the NVSS in combination with the redshift information from the 2dFGRS can be used to calculate the radio luminosity for every galaxy. The radio luminosity P is given by the formula

$$P = f_R D_A^2 (1+z)^{3+\alpha} \ , \tag{4.2}$$

where f_R is the observed radio flux at the given frequency (1.4 GHz for the NVSS), D_A is the angular diameter distance $D_A = R_{\text{comoving}}(1+z)^{-1}$ and in order to calculate k-corrections for the radio source, a power law spectrum was assumed ($f_R \propto \nu^{-\alpha}$ where ν the frequency of the radiation). The value used for α in this case was 0.8 (Peacock, 1999). The resulting quantity has S.I units of $\text{WHz}^{-1}\text{sr}^{-1}$.

The method for calculating the radio luminosity function is the $1/V_{\text{max}}$ estimator Felten (1976), although when calculating the maximum volume a galaxy can occupy and still be included in the survey, one has to take in to consideration the radio limit for the NVSS as well. Thus, the luminosity function estimator for galaxies with radio luminosity in the range $P - \frac{\Delta P}{2} \leq P \leq P + \frac{\Delta}{2}$ would take the form

$$\Phi(P) = \sum_i \frac{1}{V_{\text{max}}(i)} \ , \tag{4.3}$$

where $V_{\text{max}}(i)$ is defined as the least of the observed survey volumes V_{max}^{2dFGRS} and V_{max}^{NVSS} that the i-th galaxy can occupy and still be included in the final sample. The limit for the optical selection is $b_j = 19.45$ mag at the faint end and $b_j = 14$ at the bright end, whereas the flux limit for the NVSS is 2.2 mJy.

4.3.1 Isolating the core

4.3.1.1 Radio output due to star formation

Radio emission comes mainly from three categories of galaxies.

- Normal elliptical galaxies that exhibit a radio signature.
- Active galactic nuclei that are radio loud.

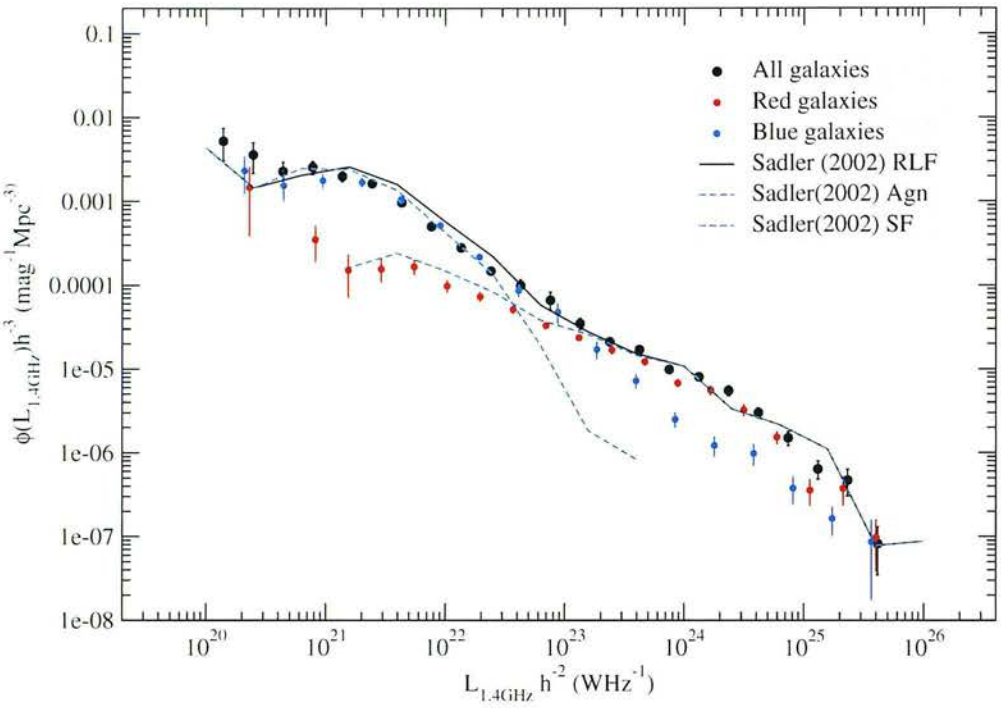

Figure 4.8: The local RLF for the joined 2dFGRS-NVSS sample, plotted with the radio luminosities published by Sadler *et al.* (2002). The local radio luminosity agrees very well with the published results. Similarly, the radio luminosity function for the AGN galaxies as published by Sadler *et al.* (2002) and the radio luminosity for the red galaxies in the sample are very similar. Blue galaxies dominate the faint end of the radio luminosity function and agree with the radio LF of the star forming galaxies. The differences in the radio LF appears at the point where the total RLF starts being dominated by AGN. Blue galaxies do not follow the fade out of the star forming galaxies but they are still present in the higher radio luminosities although their contribution to the total RLF is minimum. Colour alone is not enough to separate SF galaxies, thus the difference.

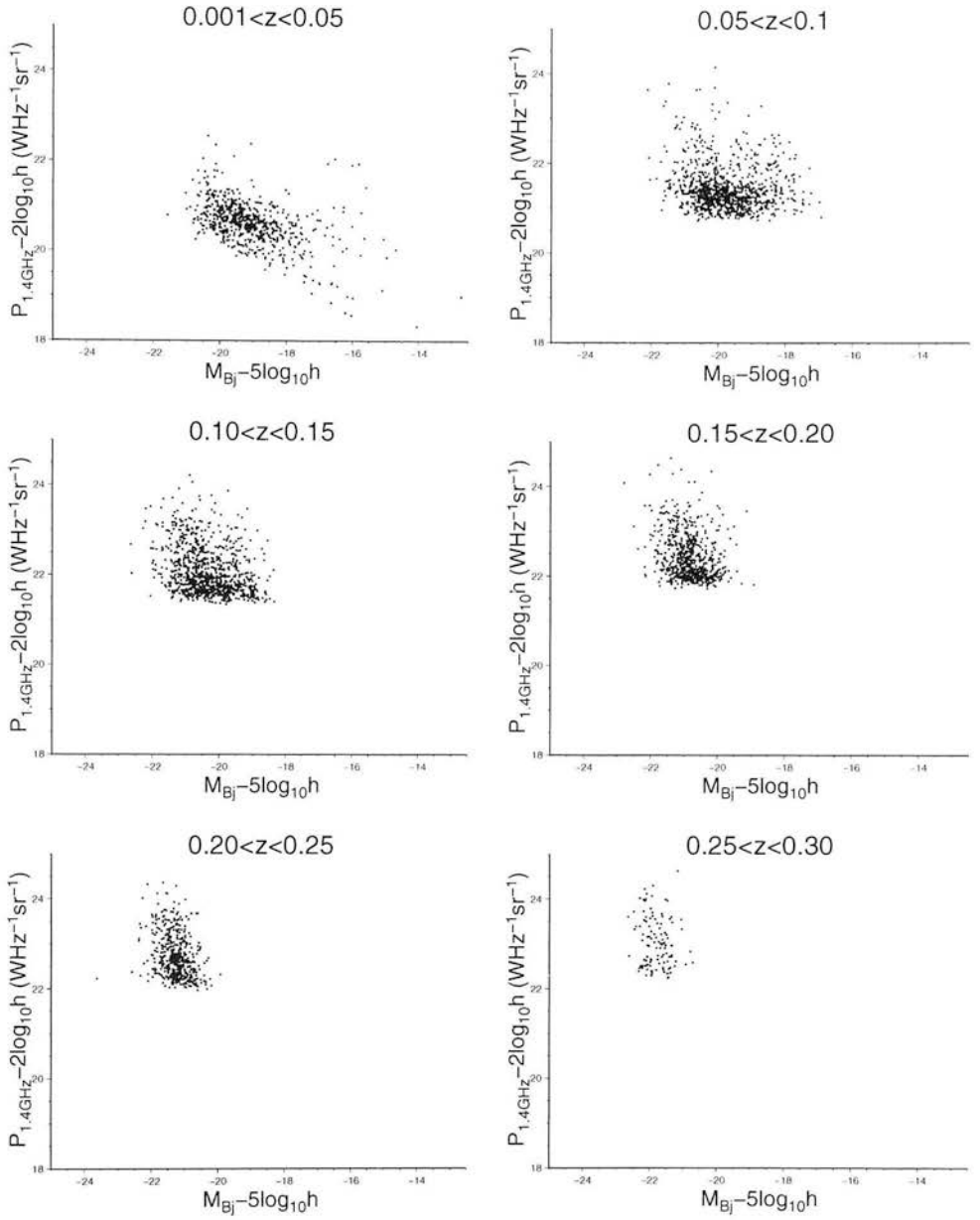

Figure 4.9: The absolute magnitude - radio luminosity plane for the radio selected 2dFGRS galaxies. There does not appear to be any correlation between the two quantities. The strong selection effect is due to the fact that most radio sources have radio fluxes close to the NVSS limit and inevitably the higher the redshift the more powerful the source needs to be to be included.

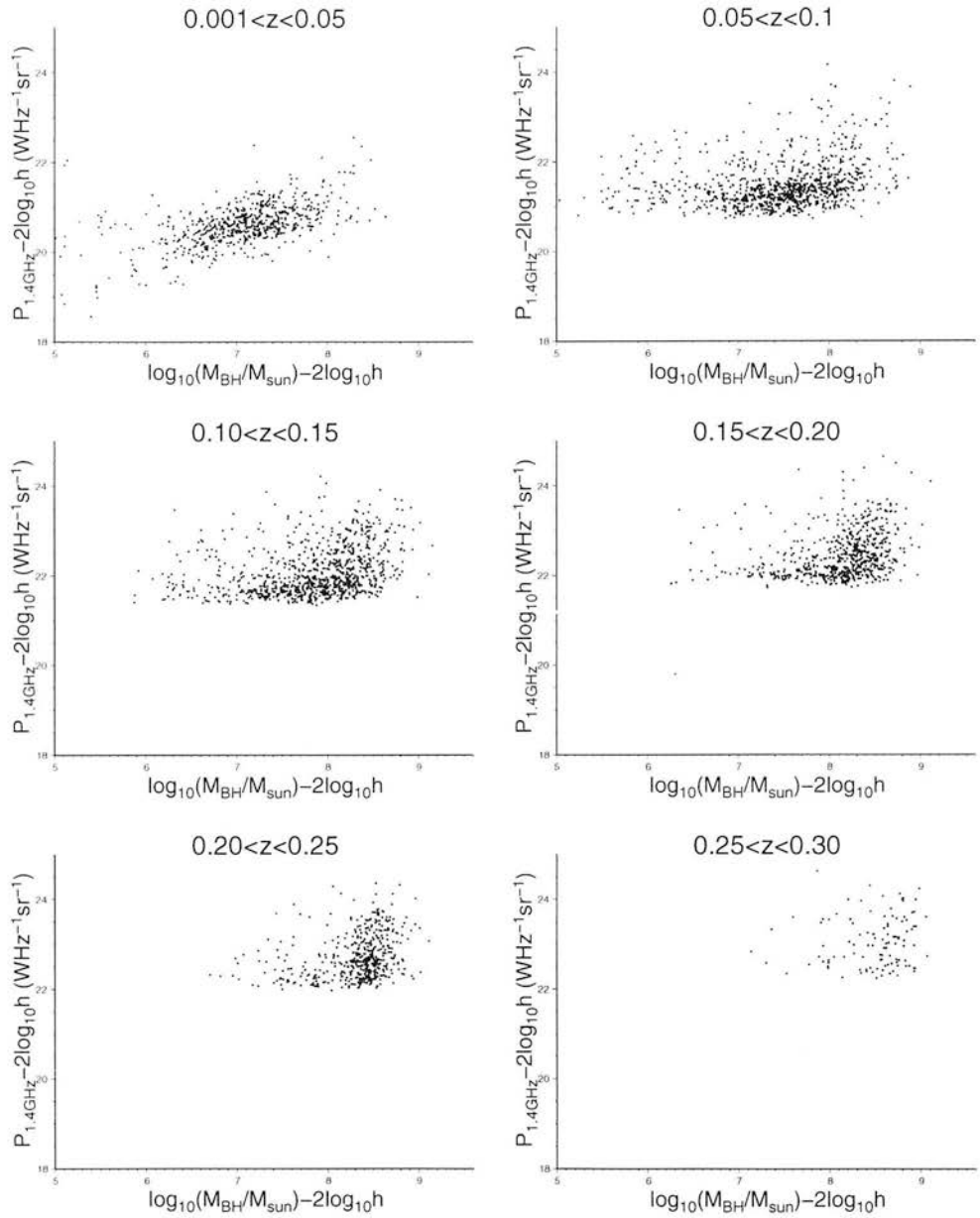

Figure 4.10: The black hole mass - radio luminosity plane for the radio selected 2dFGRS galaxies. Effects due to the flux limit of the NVSS survey are once again obvious. Despite that, hints of correlation between these two quantities are present, especially in the redshift bins $z \in [0.10, 0.15]$ and $z \in [0.15, 0.20]$.

- Star forming galaxies.

In the first two categories, the radio output comes mainly from the core of the galaxy and the central black hole is responsible for the radio output. In star forming galaxies the radio emission is due to supernovae bursts, which accelerate relativistic electrons that ionise HII regions at their outer shocks (Bell, 1978). The relativistic electrons emit synchrotron radiation that registers in the radio frequencies, together with the bremsstrahlung radiation from the ionised regions (at least for the 1.4GHz frequency of the NVSS, these are the main contributions to radio output that is not AGN originated. For higher frequencies, dust radiation prevails). At the same time such galaxies emit Hα recombination radiation due to the HII regions ionisation by radiation coming from massive stars.

Star formation is not present only in one particular type of galaxies, so in most systems the observed total radio power is the cumulative result of both nuclear activity and star forming activity. If any predictions are to be made about the core radio output, the contribution of the SF activity needs to be subtracted. For the largest percentage of complex galaxies (both AGN and star forming activity), this correction is very small and does not alter the total radio output in any significant way, since the radio output from the central engine outshines by order of magnitude the radio output due to star forming activity. This correction will effect weak radio sources that are present in mostly blue galaxies. Nevertheless, the correction is important in order to better understand the properties of weak radio galaxies and look for any correlation between radio activity and AGN properties such as central black hole mass..

4.3.1.2 Hα as a tracer of radio output due to star formation

The 2dFGRS spectra include information for the Hα emission from galaxies, since Hα lines fall inside the recorded spectrum limits. Since HII regions are a strong indicator for star formation, the power in the Hα emission line of the spectrum can be used as an indirect probe of the radio output due to SF activity. The calibration of the 2dFGRS spectra is troublesome, preventing any estimation for the Hα luminosity directly from the spectrum. Fortunately, the SCSS r_f magnitude can correct that.

Since the r_f magnitude covers the Hα line (Hα line is encountered at 656.3 nm, whereas the r_f filter is centred at 650 nm with $\Delta\lambda = 90$ nm) and in SF galaxies the line is very prominent, one can assume that the ratio of the equivalent width of the line to the $\Delta\lambda$ of the filter would be equal to the ratio of the Hα luminosity to the r_f luminosity.

Let r be the observed r_f magnitude of a galaxy. From the galaxy spectrum the equivalent width of the Hα line, $w_{\mathrm{H}\alpha}$, can be estimated. Therefore, the apparent magnitude due to the Hα line would be given by:

$$r_{\mathrm{H}\alpha} = r - 2.5 \log_{10} \left(\frac{w_{\mathrm{H}\alpha}}{\Delta\lambda} \right) \quad . \tag{4.4}$$

The apparent magnitude for a 1 Jy flux is $m(1\ \mathrm{Jy}) = 8.69$ (Peacock, 1999). Then the Hα flux of the galaxy will be given by:

$$f_{\mathrm{H}\alpha} = 10^{0.4(r_{\mathrm{H}\alpha} - 8.69)} \quad , \tag{4.5}$$

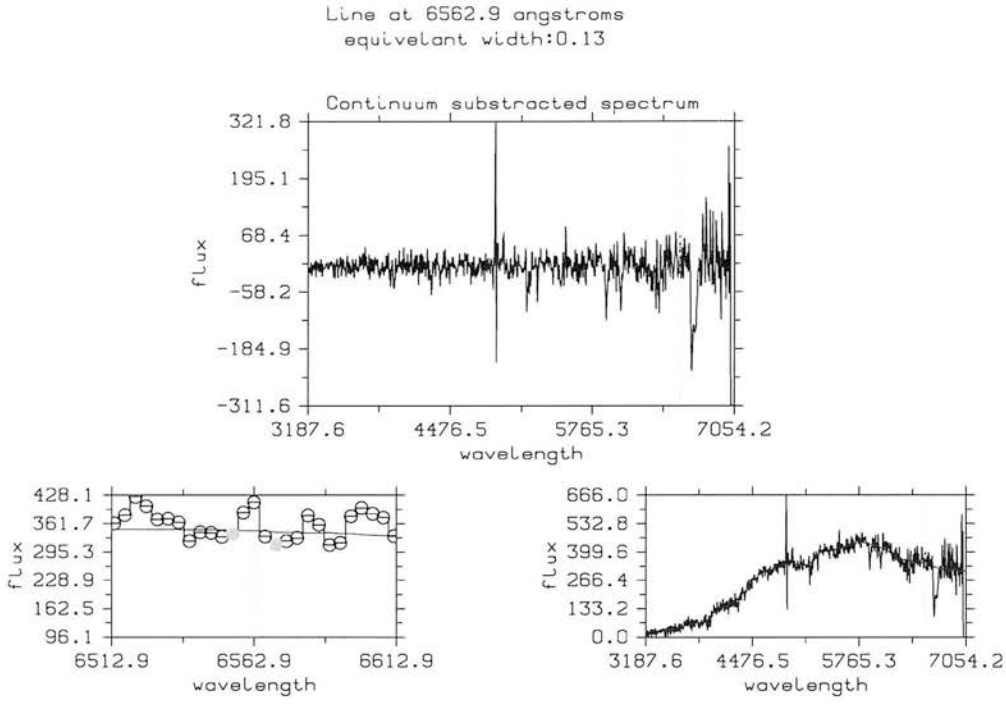

Figure 4.11: The spectrum of a galaxy (bottom right figure) at redshift $z = 0.14$, with negligible Hα emission. The spectrum has been shifted to the rest frame of the galaxy. The top panel, displays the spectrum after substacting the continuum. The continuum was calculated by taking the median of the values in regular, small parts of the spectrum.The bottom left panel display the values used to calculate the equivalent width of the line (circles indicate a flux point in the 2dFGRS spectrum file).

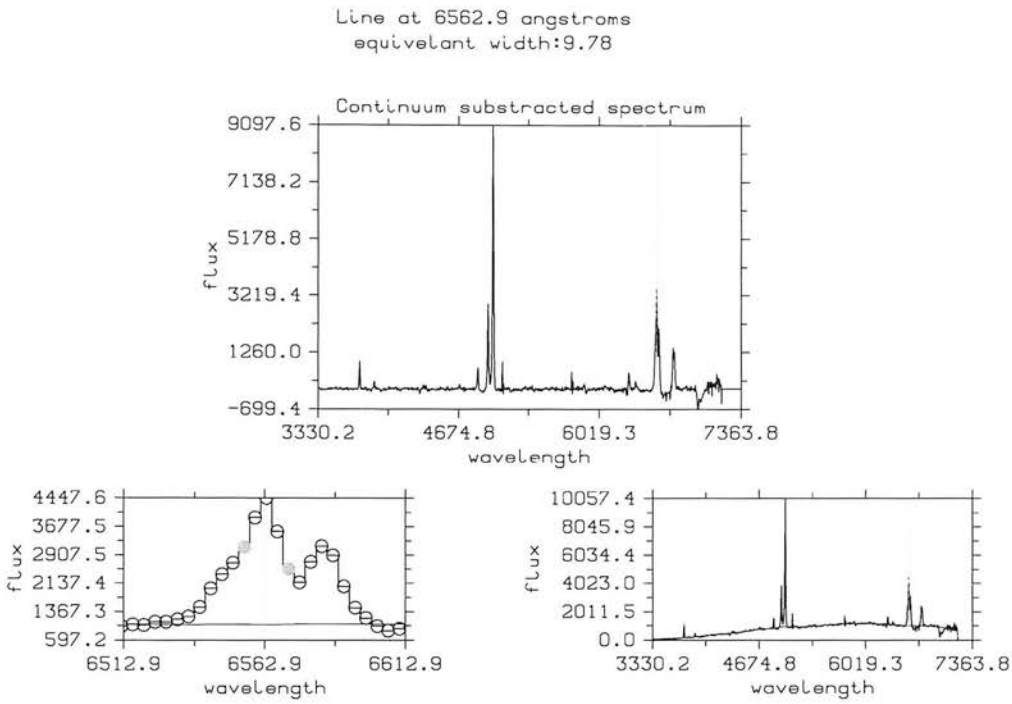

Figure 4.12: The spectrum of a galaxy (bottom right figure) at redshift z=0.09, with strong Hα emission. The spectrum has been shifted to the rest frame of the galaxy. Top panel, displays the spectrum after subtraction of the continuum. The continuum was calculated by taking the median of the values in regular, small parts of the spectrum. Bottom left panel display the values used to calculate the equivalent width of the line (circles indicate a flux "point" in the 2dFGRS spectrum file).

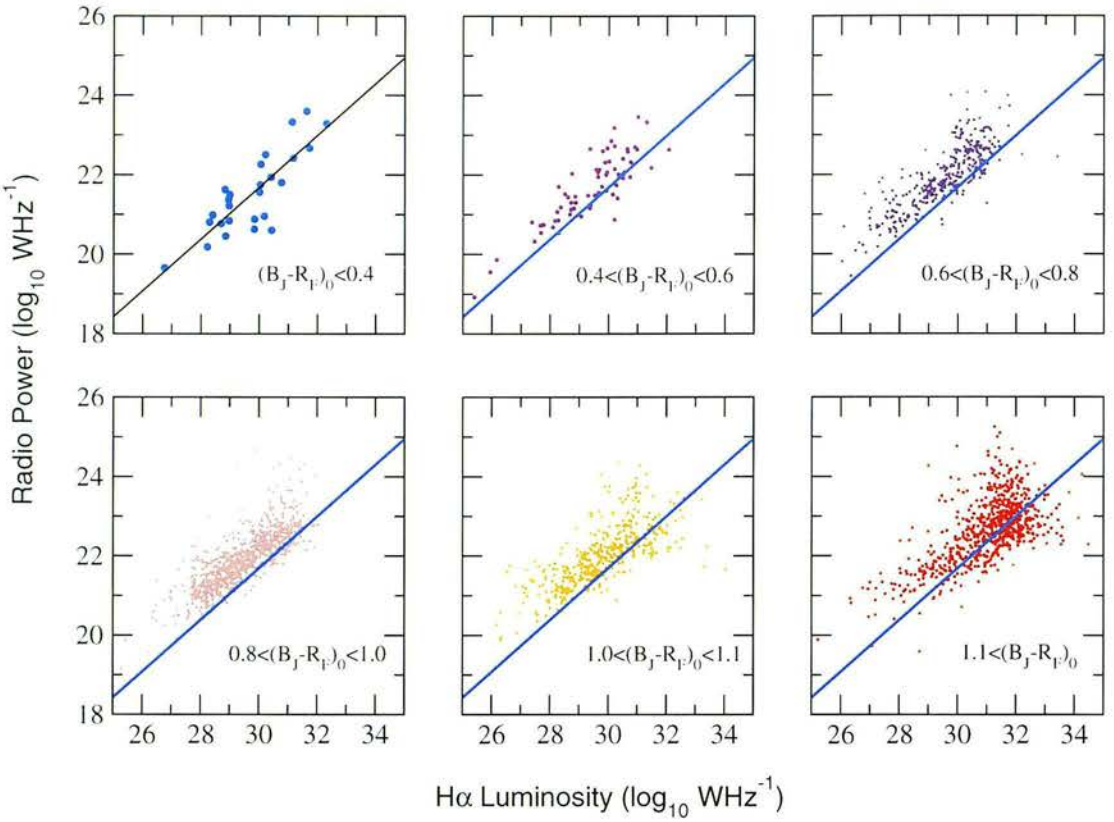

Figure 4.13: The Hα and $P_{1.4\mathrm{GHz}}$ relation for all the galaxies that have an Hα line. The galaxies are split according to rest frame $b_j - r_f$ colour from very blue (top left) to red objects (bottom right). The line in every plot indicates the linear fit between the optical and radio luminosity for the very blue galaxies. The assumption is that for these objects, most of the radio output comes from star forming activity and it is not due a central engine. For the rest of the galaxies, it can be seen that most objects exist above this line as expected.

and the monochromatic luminosity of the Hα line can be retrieved from 4.2 assuming a spectral index of $\alpha = 0.3$ for an optical source.

From the $L(\mathrm{H}\alpha) - \mathrm{P_R}$ relation, a lower limit of radio emission for galaxies with prominent H_α lines can be estimated, which will not be related to nuclear activity and then subtracted so the radio signal contains only core emission. Of course, for galaxies with powerful central engines, the radio emission from the AGN is order of magnitudes higher that any SF emission, so this correction effectively affects only low mass galaxies. The relation between the Hα luminosity and radio power at 1.4GHz for the very blue galaxies in figure 4.13 is

$$\log_{10} P_{1.4\mathrm{GHz}} = (0.65 \pm 0.09) * \log_{10} L_{\mathrm{H}\alpha} + (2.14 \pm 2.6) \ . \qquad (4.6)$$

The scatter in figure 4.14 has a large scatter which is a result of many factors. Since Hα is an indirect tracer of radio activity due to star formation, it is difficult to assure that the selection of the galaxies that define equation 4.6 is accurate. Complex galaxies also contribute to the scatter. It can be seen that

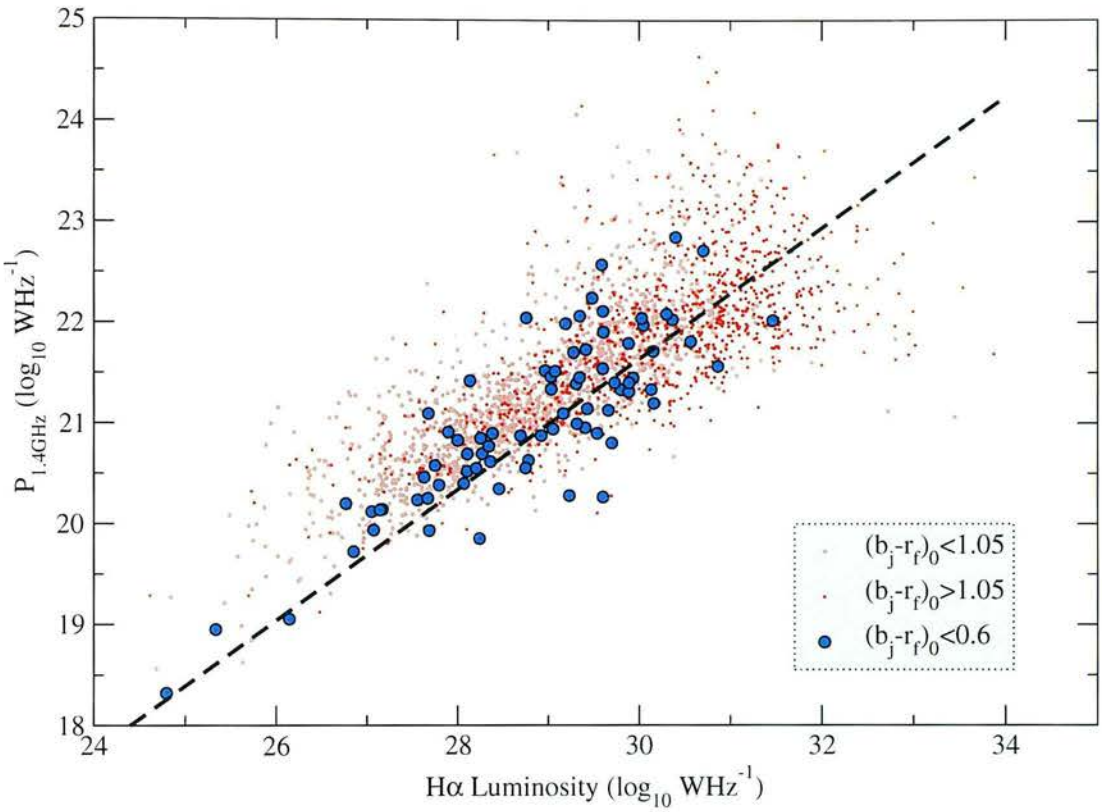

Figure 4.14: The Hα and $P_{1.4\mathrm{GHz}}$ relation for all the galaxies that have an Hα line. The galaxies are split according to rest frame $b_j - r_f$ colour. Very blue galaxies are plotted as blue circles, galaxies that are below the red galaxies split point ($(b_j - r_f)_0 < 1.05$) are plotted as brown circles, whereas red objects are plotted as red dots. The line indicates the fit from equation 4.6.

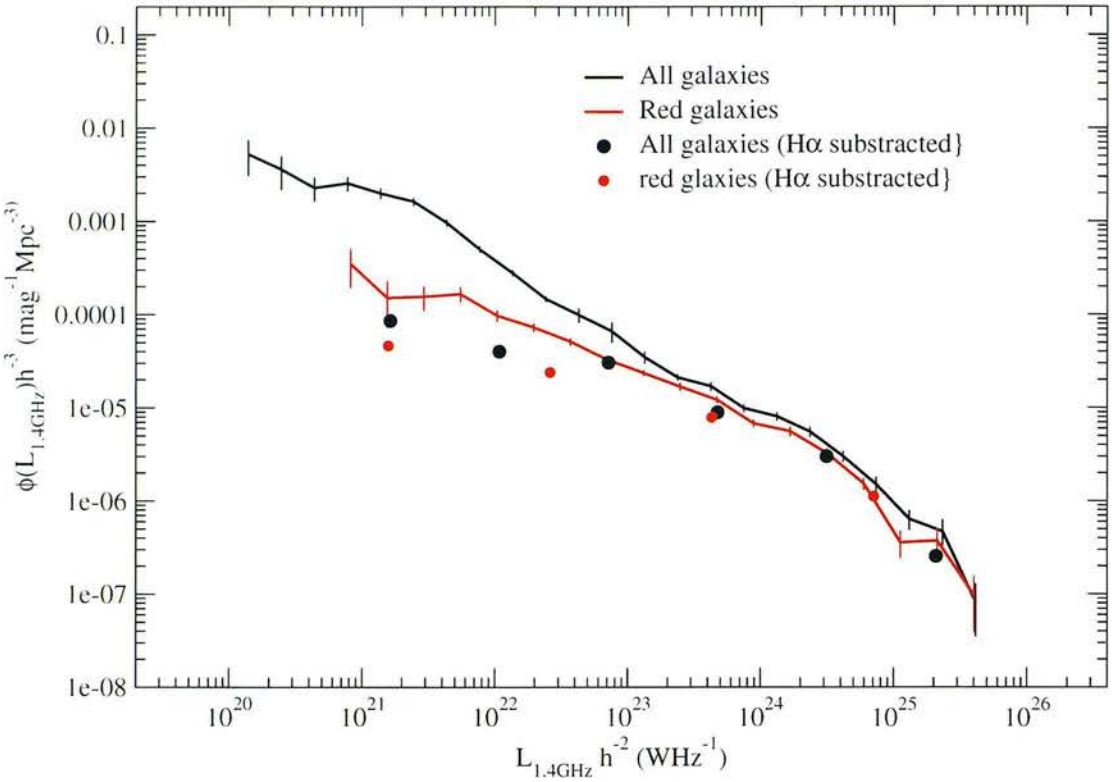

Figure 4.15: The RLF for all the sources before and after subtracting the radio output that is not caused by the central engine. The total radio luminosity function now is similar to the initial radio LF of the red galaxies. The red galaxy RLF has been slightly reduced as well. Blue galaxies have been eliminated. This is the radio luminosity function of the black holes without star formation contributions.

the galaxies with the most radio output in Hα luminosity are red galaxies that also are amongst the most powerful radio galaxies as well. Galaxies with a radio active AGN in the bulge component and a disk with ongoing star formation are common and cannot be identified by one spectral line only.

Dust also plays a role in the case of star forming galaxies. The presence of dust in a spiral will make this galaxy appear red, eventhough the radio output from the galaxy can be solely due to intense star formation. With only the $(b_j - r_f)_0$ colour and the Hα line as criteria these galaxies cannot be identified.

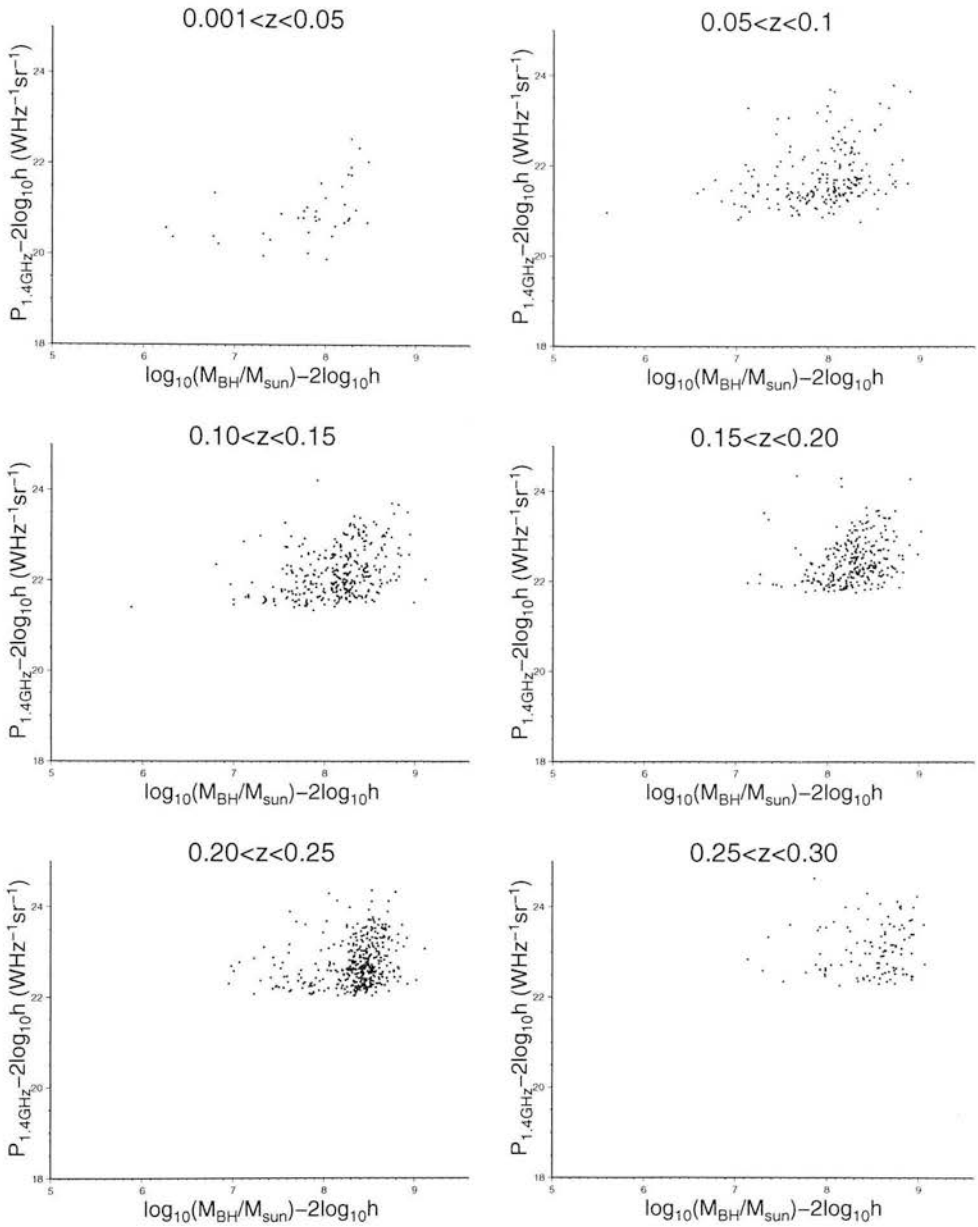

Figure 4.16: The black hole mass - radio luminosity plane for the radio selected 2dFGRS galaxies but with the radio output due to starformation subtracted. A weak correlation between these two quantities is more obvious, especially in the redshift bins $z \in [0.20, 0.25]$ and $z \in [0.15, 0.20]$.

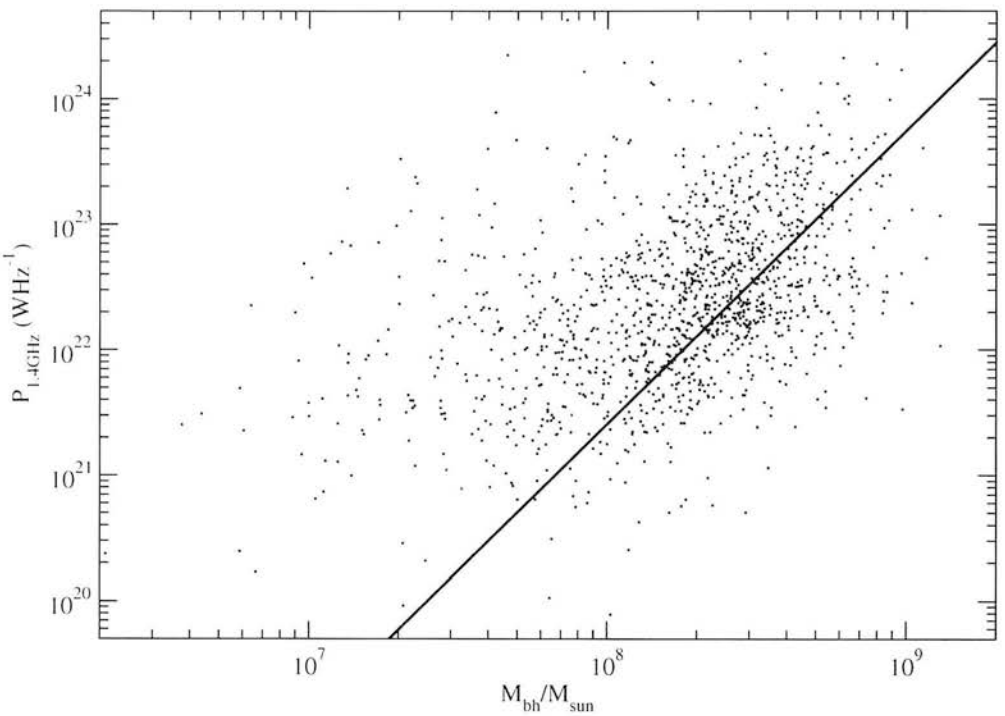

Figure 4.17: The black hole mass - radio luminosity plane for the radio selected 2dFGRS galaxies but with the radio output due to starformation subtracted. All the galaxies are plotted. The correlation has the form $P \sim {M_{\rm bh}}^{\alpha}$ with $\alpha = 2.4$.

4.4 The black-hole masses of radio galaxies

4.4.1 Relation between black hole mass and radio output

In figures 4.16 and 4.17 it can be observed that radio output scales with the mass of the black hole. The correlation is subject to discussion though, since the scatter is quite large even after subtraction of radio emission not coming from the core. The scaling relation of $P \sim M^{2.4}$ recovered agrees with previous results (Franceschini *et al.*, 1998) but a tighter correlation is necessary in order for this result to be considered accurate. Figure 4.16 shows that even if there is a correlation between black hole mass and radio output for galaxies with high black hole mass, the resulting relation is due to selection effects mainly. Especially for galaxies with a low radio flux, the combination of the NVSS flux limit with the 2dFGRS magnitude limit (since a low black hole mass indicates a low luminosity as well, as far as the Magorrian relation is concerned) will create an effect as seen in 4.16.

4.4.2 Black hole mass function of radio galaxies

It is expected that the mass function of the radio galaxies should follow the mass function of red galaxies, especially at the high end of the mass axis, where almost all ellipticals reside. The mass function of the radio sample was calculated in the same way as with the mass function for the whole of the 2dFGRS. As shown in the previous chapter, the colour information from the SCSS survey provides a fast yet accurate way to characterise galaxies according to their morphology. It is expected that the radio galaxy population will consist mostly from giant elliptical galaxies, therefore their mass function should coincide with the red galaxy mass function at the high end, as is the case as seen in figure 4.18.

4.4.3 Differential bivariate luminosity function

The mass function for the radio sample as well as the local radio luminosity function can be combined in such a way as to provide a bivariate luminosity function.

Let $\phi(\log_{10} P, \log_{10} M)$ be the number of galaxies per unit volume per $\log_{10}$ unit mass and per $\log_{10}$ unit radio power. This can be calculated using the same methodology as when calculating any luminosity function, but taking in to account the fact that there is a combination of surveys, thus when choosing the maximum volume a galaxy can inhabit, both survey limits must be taken in to consideration and the lower of the two $V_{\rm max}$ values used.

For all the black hole masses of the galaxies that have values in the range

$$M \in \left[M_{\rm bh} - \frac{\Delta M}{2} : M_{\rm bh} + \frac{\Delta M}{2} \right]$$

the radio luminosity function for that particular bin was calculated. (figure 4.19):

$$\phi(\log_{10} M, \log_{10} P) = \frac{N}{\Delta V \Delta \log_{10} P \Delta \log_{10} M} = \sum_{i}^{N} \frac{1}{V_{\rm max}}(i) \ , \qquad (4.7)$$

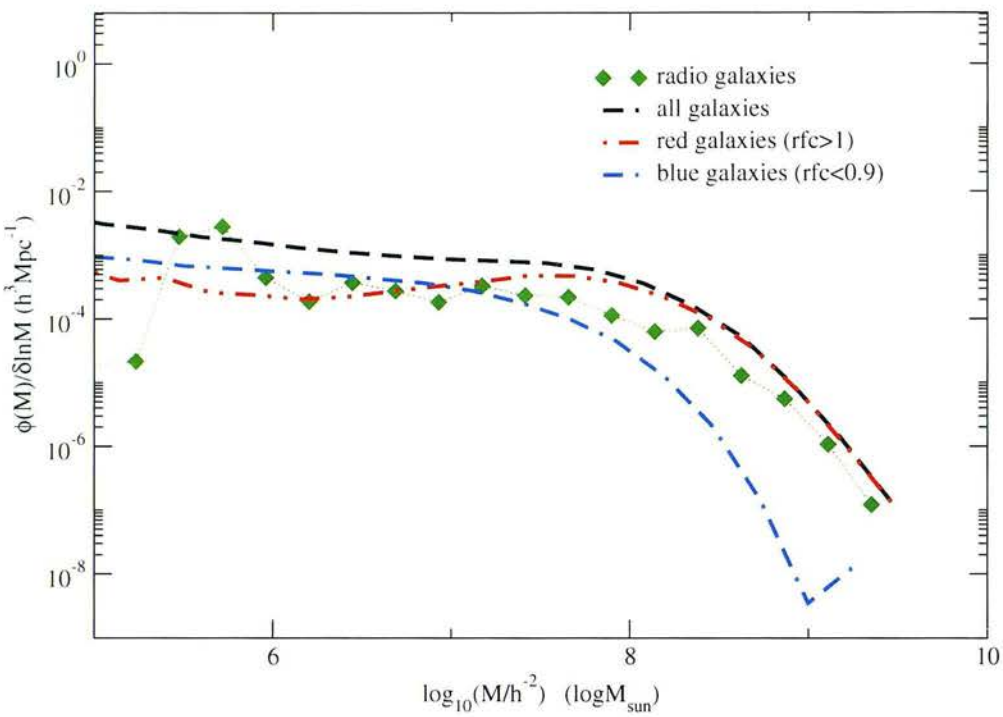

Figure 4.18: The mass function for radio galaxies and all the galaxies of the 2dFGRS with a rest frame colour larger that the reported values. It appears that the radio population does follow the mass function for all the red galaxies. The radio function begins to deviate as it approaches lower masses, since there exists a mix of populations and slowly the sample ellipticals cease to be included in the mass bins.

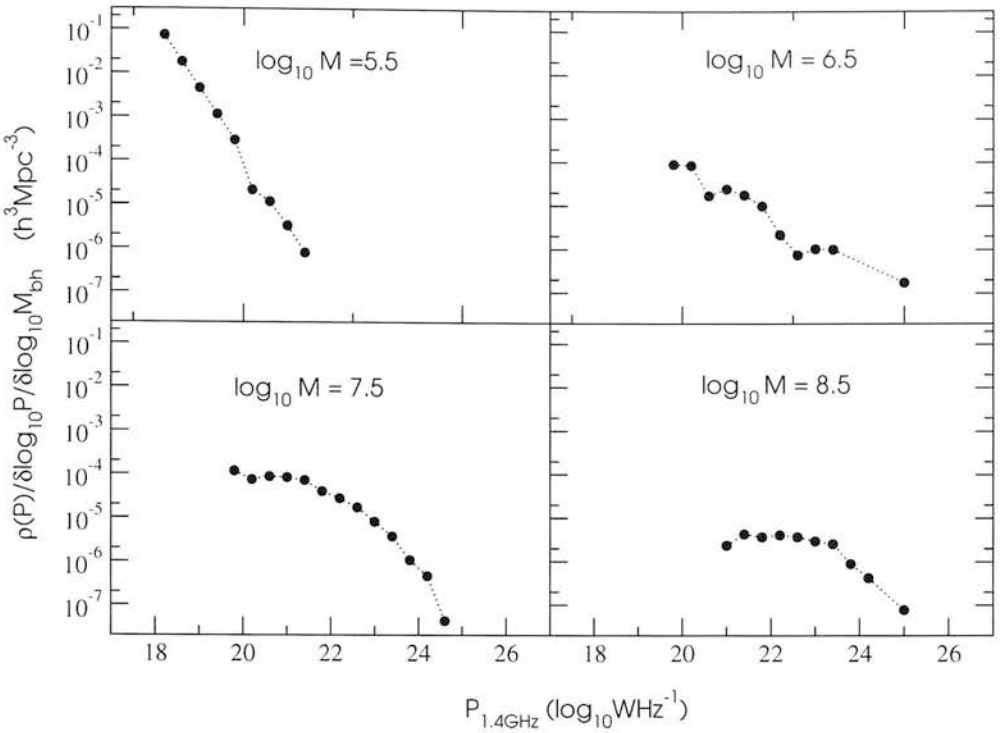

Figure 4.19: The bivariate luminosity function (radio power, black hole mass) for four black hole mass bins of size 1 dex. The panels are (top left, clockwise) for black hole mass bins centred at $\log_{10}(M_{\rm bh}/M_{\odot} = 6, 7, 8, 9$ respectively with $\Delta M = 1$.

where $V_{\rm max}(i)$ is the minimum volume for the ith galaxy.

4.4.4 Integral number counts

The number of galaxies that have radio output P greater than P_0 and their featured black hole has a mass in the range $[M - \frac{\Delta M}{2}, M + \frac{\Delta M}{2}]$ is given by

$$N(P > P_0) = \int_0^{P_0} \rho(\log_{10} M, \log_{10} P) d\log_{10} P \Delta \log_{10} M \ , \qquad (4.8)$$

where $\rho(\log_{10} M, \log 10P)$ is the differential bivariate luminosity function. The *total* number of galaxies with black hole mass in the same range will be given by

$$N_{\rm total} = \int_{M-\Delta \log_M /2}^{M+\Delta \log_{10} M/2} \phi(\log_{10} M) d\log_{10} M \ , \qquad (4.9)$$

where $\phi(\log_{10} M)$ is the mass function of the 2dFGRS survey. The ratio $\frac{N}{N_{\rm total}}$ is the probability $\Pi(> \log_{10} P | \log_{10} M)$ for a galaxy at that particular mass bin to have a radio output greater that $\log_{10} P$. The black hole mass function was calculated in the previous chapter and so the integral in equation 4.9 takes the form

$$N(M_{\rm bin}) = \ln 10 \int_{M-\Delta \log_M /2}^{M+\Delta \log_{10} M/2} 0.003410^{(M-7.92)(0.33)} \exp\left(-10^{M-7.92}\right) \ , \qquad (4.10)$$

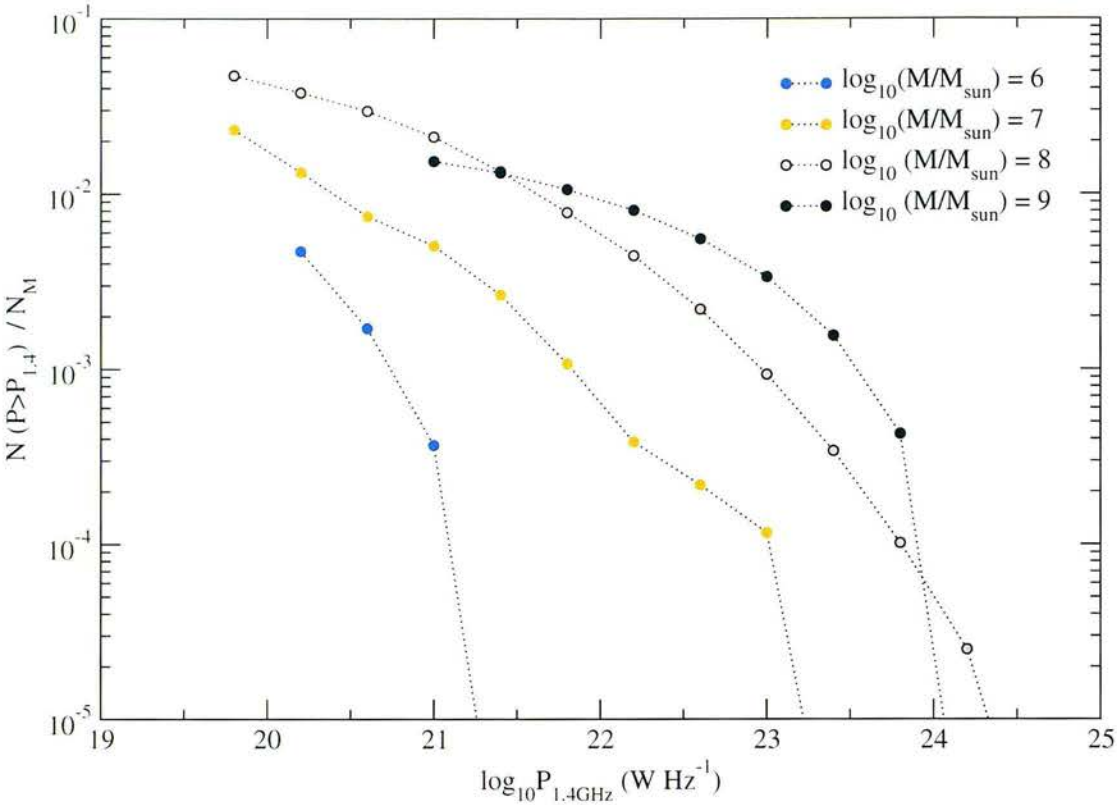

Figure 4.20: The normalised to the total black hole mass bin density probability for a galaxy to have a radio output greater than P, in four black hole mass bins with width $\Delta \log_{10} M = 1$, and centre at $\log_{10}(M/M_{\odot}) = 6, 7, 8, 9$ as indicated in the plot.

where the mass function was substituted with equation 3.18 and the values taken from table 3.6.

In figure 4.20 the points represent the normalised to the total black hole mass density probabilities for galaxies with a specific black hole mass to have radio output greater that the quoted radio luminosity. These results are similar to the results given in Best *et al.* (2005), from radio loud AGN in the SDSS survey.

4.5 Conclusions

In this chapter, the radio galaxies in the 2dFGRS sample were identified by combining the redshift survey with the NVSS radio survey. The resulting catalogue is a large radio catalogue with colour information and accurate redshift information. Using this sample, the local radio luminosity function of galaxies was calculated for the total as well as the red and blue populations in the 2dFGRS sample. The radio LF for the total population agrees very well with previous results. Also, the red population radio luminosity function is similar to the AGN radio luminosity function of Sadler *et al.* (2002), which confirms that the radio emission of red galaxies comes from the central region and shows that the use

of the $(b_j - r_f)_0$ colour to statistically select AGN is accurate. This is not the case with star forming galaxies where colour selection fails to strictly identify SF galaxies as can be seen in the resulting blue sample radio luminosity function in figure 4.8, where the radio LF for the blue galaxies does not display the observed cut-off of the optically selected SF galaxies.

An attempt was made to identify radio output due to star formation with the use of the 2dFGRS Hα line and the SCSS r_f magnitude, by retrieving the $L_{\mathrm{H}\alpha}$ luminosity and comparing with the radio output for blue galaxies. The relation is subject to large scatter but it can be used to provide lower limits for the AGN radio output. The use of the 2dFGRS spectra to retrieve the $L_{\mathrm{H}\alpha}$ line luminosities is a testament to the multiple uses the results from 2dFGRS can be put to.

A correlation between radio output and black hole mass was identified and fitted with a power law with index $\alpha = 2.4$ which is in agreement with previous results but the significance of this relation is not determined as it can be attributed to selection effects. This result is in agreement with the results of Ho (2002) and advocate the idea that radio emission from AGN is a complex procedure and not only a direct result of the black holes existance. The presence of selection effects casts doubts in previous results and the final conclution is that a direct scaling relationship does not exist.

By combining mass estimates with the radio LF, the bivariate radio luminosity function for different mass bins was retrieved. This function can in turn be used to retrieve the probability of a galaxy given each black hole mass to have a radio output greater than a given radio luminosity, The resulting functions have very similar shapes (apart from bins where there were very few galaxies and the result was skewed) which suggests that the distribution of radio luminosities is independent of black hole mass. This result confirms that there is no direct relationship between the black hole mass and the radio luminosity in AGN.

Chapter 5

The environment of radio galaxies

5.1 Introduction

The environmental dependence of galaxy properties was always a major issue in astrophysics. Almost every aspect of modern observational cosmology is influenced by the underlying density field in which the galaxy or galaxies in question are embedded. From cosmology models that predict the form of large scale structure to radiational properties of star forming galaxies, knowledge of the galactic environment plays an essential role.

The long established empirical observation was that spiral galaxies tend to prefer the lower density regions (field galaxies), whereas $S0$ galaxies and particularly elliptical galaxies had a preference for clusters (Spitzer & Baade, 1951; Melnick & Sargent, 1977). Dressler (1980) offered a mathematical relation for this behaviour and showed that the percentage of spirals decreases with increasing density whereas ellipticals and $S0$ tend to prefer high density regions. This was the first case where a mathematical relation was offered between the galaxy fraction and the local density. This result was expanded (Whitmore *et al.*, 1993) to include a description based on cluster radius as well as local density, which verified previous findings and showed that ellipticals tend to prefer the centre of clusters in particular, an area where spirals are absent. Using a much larger sample, Hogg *et al.* (2003) confirmed that red galaxies (ellipticals and lenticulars) have a preference for overdense regions but found that the dependence of blue galaxies on density is a weak function.

Models of galaxy formation within a Cold Dark Matter framework have allowed a theoretical approach to the problem. Benson *et al.* (2003) showed that the luminosity functions of galaxies residing in different mass haloes are expected theoretically to show major differences. They found that for galaxies in low mass haloes the luminosity function is quite steep at the faint end, having a power-law form, whereas the bright end is dominated by very few galaxies. Only high mass systems display a luminosity function that is similar to the traditional Schechter form. The global luminosity function, a combination of all the contributions from different sized haloes, does not reflect the significant differences though and fol-

lows the shape of the high mass systems. Mo *et al.* (2004) using a halo occupation model in which the only parameter that influences the luminosity distribution in a dark matter halo is the halo mass to predict that bright galaxies should exhibit a Schechter like luminosity function regardless of environment and only the characteristic luminosity L_* is affected by the environment. For late type galaxies, the slope of the luminosity function has very weak environmental dependencies whereas early type galaxies display a significant change in the slope of the function. The luminosity function for underdense regions was predicted to depart from the Schechter like model considerably.

In this chapter, the environmental dependency of the radio galaxies in the 2dFGRS sample will be considered. A numerical density map of the 2dFGRS sample will be constructed, using smooth particle hydrodynamics (SPH) techniques. The dependence of galactic populations on the local density will be investigated. The important question that needs to be answered is if radio emission depends on environment beyond any secondary correlations. The radio population is predominately red, so it is expected that radio galaxies will be display similar dependence to environment as red galaxies. It will be very interesting to see if there is any difference between the two populations.

5.2 Theory

The basis of the work done in this chapter is the calculation of a density map for the 2dFGRS survey. The goal is to add information about the density of the region each galaxy resides in and use to split the analysis according to this information. The calculation of the local density is very similar to the estimation of a fluid density in SPH. Of course, there is no motion nor time dependence in the calculation so there are no dynamics involved. The SPH name is still used though since the idea for an adaptive density calculation was inspired by previous work on astrophysical fluids and SPH code.

5.2.1 Smoothed Particle Hydrodynamics

The most common density estimator is to define an elementary volume element dV around a point of interest and count the number of objects N that are included in it. Assuming that each object has $m = 1$, then the density is simply $\rho = \frac{N}{dV}$. This method is quite straight forward and simple in its implementation but suffers from information loss at certain cases. The size of the volume element plays a critical role. If the volume element is too big there would be loss of information regarding any substructure within. If the volume element is too small, there would be loss of information regarding structure in the vicinity of the point (see figure 5.1 for a simple example). Another drawback of this method is that it defines a grid unto which all properties are calculated. The resolution of the grid will influence the speed of any computations considerably.

One solution to this problem is to use a different approach when defining the elementary volume, a technique that is encountered in smoothed particle

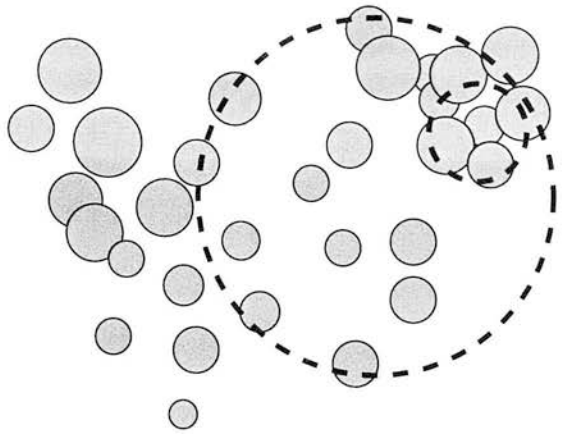

Figure 5.1: An example of information loss when using a fixed volume element. If the element is too small, highly overdense regions tend to be underestimated. In case of a large volume element, the information loss is positional. The dense region occupies only the upper part of the volume element.

hydrodynamics. Instead of a fixed radius imposed on a grid, the volume element can adapt to the presence of objects around it.

5.2.1.1 Smoothed Particle Hydrodynamics: Introduction

Smoothed Particle Hydrodynamics (SPH) is used to describe a assemblage of computational techniques that simulate or investigate very complex physical systems that consist of a very large number of particles. It is a tool that has been used extensively in astrophysics (see Monaghan (1992) for a review) and SPH code has been used as basis of various models. The applications of SPH are numerous and they are by no means restricted to astrophysics. Examples of the uses of SPH in astronomy can be found in Gingold & Monaghan (1977), Lia & Carraro (2001), Benson *et al.* (2001) and Marinho & Lépine (2000).

In SPH, the traditional approach of measuring the properties of particles (being gas molecules or stars or whatever the physical system consists of) on a grid, is replaced by assigning a zone of influence for each particle. Thus, when the need arises, retrieval of the properties in question, at a point in space, is done by calculating the influence at that point of the closest particles. This increases the speed of the code substantially, especially in environments where the system evolves with time, because it eliminates the need for continuous iterations over the grid. Evolution with time is easier to monitor, since the code can keep track of the closest particles to the point of interest and monitor their evolution, eliminating the need to perform calculations with particles that are not going to contribute to the result.

5.2.1.2 SPH basics: The kernel

The kernel $W(h, dr)$ (where h is the smoothing length of the kernel and dr the distance between the two points of interest, $dr = |r_1 - r_2|$) is the founding block of

the SPH methods because it represents the zone of influence of the SPH particle.

Consider a particle i, positioned at r_i. In order to measure a property $f(r)$ of the fluid (i.e the sum of all the particles) at a point r close to the particle, the contribution of particle f_i needs to be defined. Then $f(r) = \sum_i f_i$. The quantity f_i is dependent on the distance between the particle and the point of interest and the kernel function is a measurement of that dependence. Far away particles, will have very little or no contribution to the total sum whereas close by particles should heavily influence the value of $f(r)$. The form of the kernel is arbitrary and is chosen to correspond better to the physics of the problem.

A common example of a kernel function W is the Gaussian kernel,

$$W(h, dr) = \frac{e^{-dr^2/h^2}}{\pi^{3/2}h^3} \quad . \tag{5.1}$$

The kernel function is normalised is such a way that $\int_0^\infty W(h, dr)dV = 1$ over the volume of the system. Another kernel and the one that is used in the rest of the chapter is the spline kernel proposed by Monaghan (1992)

$$W(h, dr) = \frac{1}{\pi h^3} \begin{cases} 1 - \frac{3}{2}(dr/h)^2 + \frac{3}{4}(dr/h)^3, & 0 \leq dr/h \leq 1 \\ \frac{1}{4}(2 - dr/h)^3, & 1 < dr/h \leq 2 \\ 0, & 2 < dr/h \end{cases} \tag{5.2}$$

The reason for choosing a spline kernel instead of a Gaussian (the initial choice for most physical problems) was that the spline kernel has a point at which the influence falls to zero. For density calculations, it produced better results.

One advantage of smoothed particle hydrodynamics is that the kernel is very easy to change, so various configurations can be tried. If the need arises for a fixed volume element that the kernel can simply become

$$W(h, dr) = \begin{cases} 1 & dr \leq h \\ 0 & dr > h \end{cases} \quad . \tag{5.3}$$

5.2.1.3 SPH basics: Smoothing length h

The smoothing length can be chosen in various ways. It can either be a fixed length or be decided according to the particles that are in the vicinity of the point of interest. The second approach is preferable because it is able to give better results in extreme cases. This approach is sometimes termed Adaptive SPH. There are two different ways to choose a smoothing length:

- h is chosen so that $l * h \leq r_N$, where l is a number defined from the kernel. Usually $2 \leq l \leq 3$. For the spline kernel used, $l = 2$. r_N is the distance to the Nth neighbour. In this case, only the closest N particles influence the point of interest.

- h is chosen by averaging the distance of the N closest neighbours. The average can be a simple mean value (emphasising the more distant neighbours),

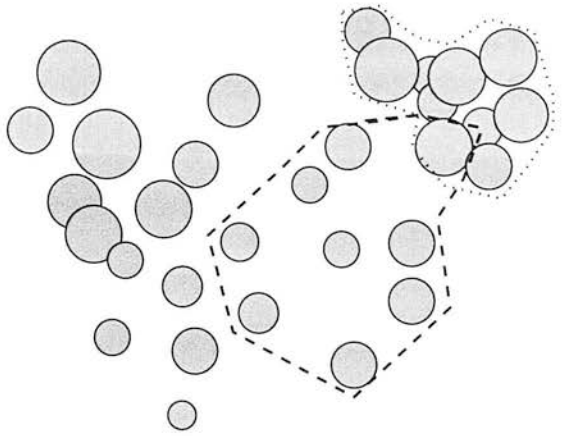

Figure 5.2: A simple drawing of an adaptive SPH volume element. The volume considered in each case is molded to fit the environment at each point.

the median value to avoid dominance of particles at great distance or even a sum of the form

$$h = \left(\frac{1}{N} \sum_{i}^{N} \left(\frac{1}{dr_i} \right)^m \right)^{-1} ,$$

where m is an integer, in order to emphasise the closest particles.

5.2.1.4 SPH basics: density

The density of a fluid at a particular point is one of the crucial properties of every physical problem. In SPH formalism, the calculation of the density becomes simply the sum of the influence of all the particles. Namely the density at particle i is given by

$$\rho(dr_k, h) = \sum_k m_k W(dr_k/h) \tag{5.4}$$

where dr_k is the distance between the points i and k , m_k being the mass of the k particle. If the calculation requires a simple numerical density then $m_k = 1$. Which smoothing length is used in 5.4 depends on the physics of the problem. The two most common approaches to assigning a smoothing length are:

- Scatter approach. $h = h_k$ in 5.4 and for every term in the sum a different smoothing radius is used. This is useful when the point at which the density is calculated is not a particle.

- Gather approach. $h = h_i$ in 5.4, where i is the particle that resides at the point the density is calculated at.

There is no difference in the results for these two methods at least for the present application of a simple density calculation and so a gather approach was used.

5.2.2 The coordinate system

The first step in retrieving the density at any point of the survey is to define a coordinate system. The distribution of galaxies in the 2dFGRS survey can be viewed as a 3-dimensional distribution in space. The right ascension and declination of a galaxy are the longitude and latitude of a spherical coordinate system. The redshift component z of the galaxy can in turn be transformed to a radial distance component, thus the triplet (ra, dec, R), where R is the distance that the redshift z corresponds to, will map the three dimensional distribution of the galaxies in the volume that has been observed with the 2dFGRS.

These coordinates are redshift space coordinates and not real space, since the redshift is the sum of the cosmological redshift and the redshift due to peculiar velocity, but nevertheless an overdensity estimator should not be heavily influenced by that effect.

To avoid large iterations over all galaxies a binary tree approach was used. Since the binary tree uses Cartesian coordinates to calculate distances, the transformation for each galaxy then takes the form

$$\begin{aligned} x &= R\cos\theta\sin\phi \\ y &= R\sin\theta\sin\phi \\ z &= R\cos\phi \end{aligned} \tag{5.5}$$

where R is the redshift of the galaxy, θ is the right ascension (in radians) and ϕ is defined as $\phi = \frac{\pi}{2} - dec$, where dec is the galactic declination.

5.2.2.1 The distance between galaxies

This change in coordinates only takes place so the closest neighbours can be identified. Having identified the closest N galaxies, the appropriate distances are calculated for each one as follows:

- For each galaxy in the survey, its comoving distance is calculated using the formula
$$R_{\text{comoving}} = \frac{c}{H_0}\frac{z}{1+0.24z} \tag{5.6}$$
This formula is a good approximation for the low redshifts the galaxy sample includes $z \in [0.001 : 0.25]$

- Following Yoshii *et al.* (1993) the distance between two objects is defined as
$$r^2 = \left(\frac{dx/dz}{\sqrt{1-kx^2}}\right)^2 u^2 + x^2\theta^2 \tag{5.7}$$
where $u = \Delta z$, $z = \frac{z_1+z_2}{2}$, $x = R_{\text{comoving}}(z)$, θ is the angular separation of the galaxies and
$$\frac{dx/dz}{\sqrt{1-kx^2}} = \frac{c/H_0}{(1+z)\sqrt{\Omega_0(1+z) - \kappa_0 + \lambda_0/(1+z)^2}} \ . \tag{5.8}$$

For the cosmology used with $\kappa_0 = \Omega_0 + \lambda_0 - 1 = 0$ and $\Omega_0 = 0.3$ and $\lambda = 0.7$ the above equation reduces to (Phillipps, 1994):

$$\frac{dx}{dz} = \frac{c/H_0}{\sqrt{\Omega_0(1+z)^3 + 1 - \Omega_0}} \quad . \tag{5.9}$$

5.3 The Data

Unfortunately estimating a number density in a magnitude limited survey is not as straightforward as one would like. A magnitude limited sample is defined as one that contains all galaxies in the area surveyed that are *brighter* than the limiting magnitude $m_{\rm lim}$. As a result, the farther a galaxy lies, the brighter it has to be in order to be included in the sample. Thus, as the redshift range shifts to higher values, the number of observed galaxies decreases since the limiting absolute magnitude decreases with distance.

There are three basic methods that can be used to correct for this effect.

- The most frequently used method is to define a volume limited sample. For a specific redshift range, that defines the volume of the sample, there are galaxies that belong to an absolute magnitude range that would have been observed regardless of their positioning in the effective volume. This cut in redshift and magnitude reduces the size of the sample, but given a large number of observed galaxies, the remaining subsample should be adequate for the calculation of wanting quantities with a small statistical error.

- A second method consists of applying a correction to the survey in order to account for the lack of dim sources, effectively weighting any computation according to a positional vector of the galaxy or elementary volume that is being considered at the time. One weighting scheme uses the selection function. In this case 5.4 becomes

$$\rho(dr_k, h) = \frac{\sum_k m_k W(dr_k/h)}{S(r_k)} \tag{5.10}$$

  where $S(r_k, M_k)$ is the survey selection function and is defined as

$$S(r_k) = \frac{\int_{-\infty}^{M_{min}(r)} \Phi(M) dM}{\int_{-\infty}^{\infty} \Phi(M) dM} \tag{5.11}$$

  and $M_{\rm min}(r)$ is the faintest absolute magnitude that a galaxy must have at a cosmological distance r in order to be included in the catalogue.

- The third approach and the one used in this chapter is to use a random survey which is subject to the same selection function for the galaxies. In this occasion an estimation of the overdensity is possible instead of the absolute density. The use of the random catalogue eliminates the problem of accounting for faint sources for an overdensity estimator.

5.3.1 Accounting for the survey mask

Using a random catalogue in the calculation of the local density has some advantages over the other methods mentioned. It eliminates the need to calculate weights for every point, which is an increase in speed, and makes it unnecessary to reduce the sample size to a volume limited sample. Finally, the use of a

random catalogue corrects for any effects the geometry of the survey contributes to the calculation and avoids complications in cases with complex mask like the 2dFGRS.

For samples that consist of a large number of telescope pointings and exposures, like a large redshift survey, the need for a survey mask is presented. There are fields in the 2dFGRS survey that have partial coverage or not at all. The 2dFGRS has a rather complicated mask so there are areas where there is a deficiency of galaxies not only due to the magnitude limits but also because the particular area was not completely covered. To avoid introducing complex geometrical transformations in order to correct for the mask it is much better to use already existing random 2dFGRS catalogues.

The random catalogues have the same luminosity function as the original and also have the same mask. The random catalogue is unclustered though. Therefore its density can be viewed as the mean density $\langle\rho\rangle$ and is a function of position r. The overdensity $\delta\rho$ at distance r will be:

$$\delta\rho(r) = \frac{\rho(r) - \langle\rho(r)\rangle}{\langle\rho(r)\rangle} \tag{5.12}$$

where $\langle\rho(r)\rangle$ is the mean density of the survey at position r. The mean density is taken to be the density at that point of the random survey.

region	$\delta_{\min}$	$\delta_{\max}$
void region 1	-1.00	-0.90
void region 2	-1.00	-0.75
void region 3	-0.75	-0.43
mean region 1	-0.43	$+0.32$
mean region 2	$+0.32$	$+2.10$
mean region 3	$+2.10$	$+6.00$
cluster region	$+6.00$	∞

Table 5.1: The definition of different regions in density space. The division of the density regions follows the division used in Croton *et al.* (2005a) for comparison purposes. The format of the table is region $\in [\delta_{\min}, \delta_{\max}]$

5.4 The numerical density field of the 2dFGRS

For each galaxy i, the $N = 40$ closest neighbours are retrieved from the binary tree into which the survey was decomposed. For each of these galaxies the real distance d is calculate as in equation 5.9. As a smoothing length the quantity

$$h_i = \frac{1}{N} \sum_{k=0}^{N} d_k \tag{5.13}$$

is used. A similar calculation for the smoothing length of the galaxies that belong to the random survey is performed.

The smoothing radius is calculated for every galaxy and stored. The next step is to reiterate through all the galaxies in the real survey and retrieve a higher number of closest neighbours (~ 500) and calculate the density at galaxy i, by summing over them. The density ρ_i is calculated for each galaxy using the gather approach for the smoothing length, as well as for calculating the $\langle\rho\rangle$ at the same position from the random catalogue. The gather approach was chosen in order to avoid calculating a smoothing length for the random catalogue, thus increasing the computational time needed. Then the resulting overdensity for galaxy i is

$$\delta_i = \frac{N_{\text{real}}}{N_{\text{fake}}} \frac{\rho_i}{\langle\rho_i\rangle} - 1 \tag{5.14}$$

where N_{real} and N_{fake} is the total number of galaxies in the real and random catalogue respectively.

Once the overdensity has been calculated, it is easy to separate the galaxies according to their environment. The values chosen for the various areas given in table 5.1.

5.4.1 The numerical density error

In order to get an understanding about the error in the calculation of the overdensity in equation 5.14, a density calculation was performed using two unclustered catalogues. The first catalogue of random galaxies had the size of the 2dFGRS

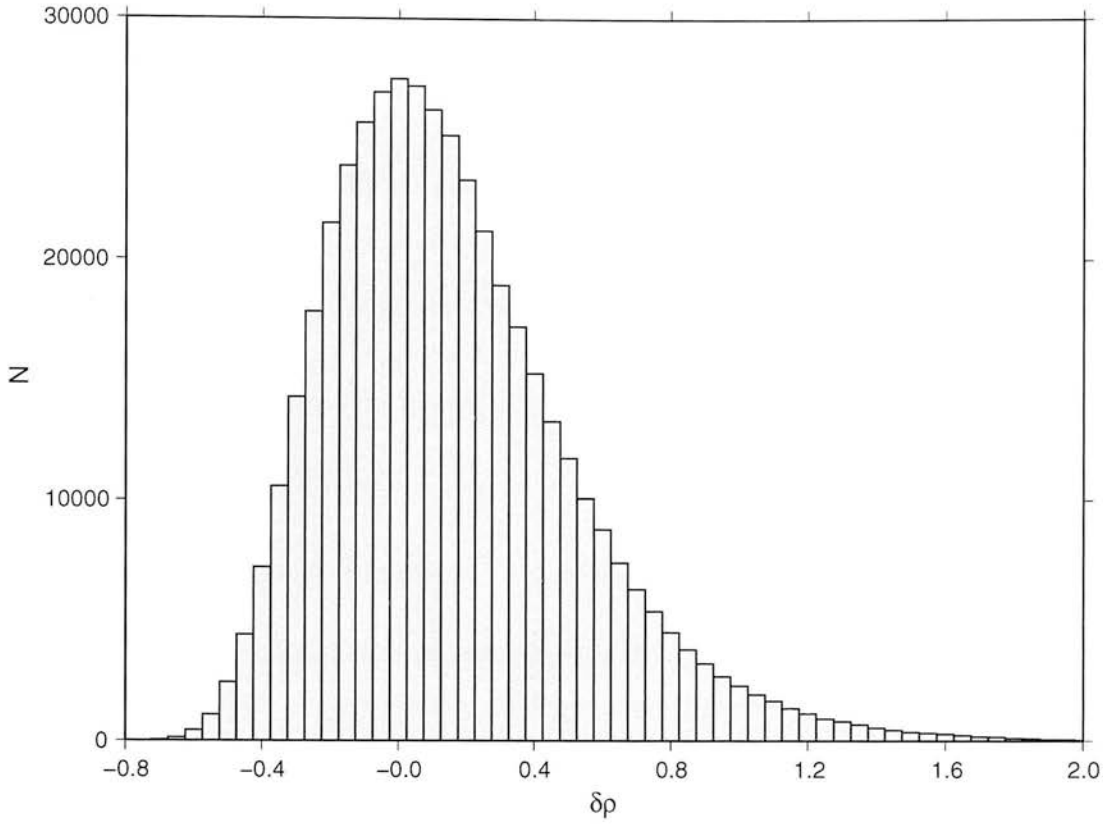

Figure 5.3: The distribution of the overdensity values using two unclustered random catalogues of the NGP strip as input and random catalogue. The distribution resembles a Gaussian but it is slightly tilted towards higher values. If it is treated as Gaussian with a full width at half maximum value of 0.8, then $\sigma_\delta = 0.34$

sample, whereas the second unclustered catalogue had the same size as the random catalogue that was used during the density estimation of the 2dFGRS sample. Since both catalogues are unclustered, the expected value of $\delta\rho$ is 0. The values deviate from the 0 value as seen in figure 5.3. This distribution of values around 0 can be used to estimate the error of the overdensity calculation. The calculated error for the distribution if $\sigma_\delta = 0.34$.

5.4.2 LFs in various density environments

Once the survey has been divided in various density regions, the retrieval of the luminosity function for each density region is possible. Unfortunately, the simple LF estimator that was used previously is not suitable for the task. There is difference when calculating the luminosity function of a subsample of galaxies in the survey that is characterised by galactic properties (*i.e* colour or mass) and a subsample that is characterised by environmental properties like the local density.

The difference is due to the fact that environmental dependencies exclude certain parts of the survey for the calculation, therefore the LF does not sample

the full volume. For example, when calculating the LF for the red galaxies in the 2dFGRS, the sample of red galaxies covers the whole volume of the survey. But when calculating the LF of the galaxies in very dense regions, in $\sum_i \frac{1}{V_{\max_i}}$ it is assumed that the full volume is sampled. That is not true because regions are excluded on their properties, so the total volume is less than the full sample. In order to correct for this bias it is necessary to consider a different LF estimator.

5.4.2.1 The Stepwise Maximum Likelihood estimator

One non parametric estimator of the luminosity function is the SWML estimator that was introduced by Efstathiou *et al.* (1988). Following the aforementioned paper, the luminosity function can be assumed as a function of N steps:

$$\phi(L) = \phi_k, \quad L \in (L_k - \Delta L/2, L_k + \Delta L/2), \quad k = 1, \ldots, N$$

The likelihood, then is:

$$\ln L = \sum_{i=1}^{N} W(L_i - L_k) \ln \phi_k - \sum_{i=1}^{N} \ln\{\sum_{j=1}^{N} \phi_j \Delta L H[L_j - L_{\min}(z_i)]\} + C$$

where C is a constant and the functions $W(x)$ and $H(x)$ are defined as

$$W(x) = \begin{cases} 1 & x - \frac{\Delta x}{2} \leq x \leq x + \frac{\Delta x}{2} \\ 0 & \text{everywhere else} \end{cases}$$

and

$$H(x) = \begin{cases} 0 & x \leq -\frac{\Delta L}{2} \\ \frac{x}{\Delta l} + \frac{1}{2} & x - \frac{\Delta x}{2} \leq x \leq x + \frac{\Delta x}{2} \\ 1 & x + \frac{\Delta l}{2} \end{cases}$$

The normalization constant resulting from this method is arbitrary, therefore it is important to impose some constraints in order to be able to directly compare results from different samples. The constraint adopted is of the form

$$g = \sum_k \phi_k \left(\frac{L_k}{L_f}\right)^{\beta} \Delta L - 1 = 0$$

where L_f is a fiducial luminosity and β is a constant. introducing the constraint to our estimator we have to maximise the quantity $\ln L' = \ln L + \lambda g(\phi_k)$ with respect to λ and ϕ_k Finally:

$$\phi_k \Delta L = \frac{\sum_i W\left(L_i - L_k\right)}{\sum_i \{H\left[L_k - L_{\min}(z_i)\right] / \sum_{j=1}^{N} \phi_j \Delta L H\left[L_j - L_{\min}(z_i)\right]\}} \tag{5.15}$$

from which we can calculate the ϕ_k parameters with iteration.

	void1	void2	void3	mean1	mean2	mean3	cluster
$V/V_{\rm total}$	0.09	0.11	0.19	0.30	0.24	0.07	0.01

Table 5.2: The fraction of the total volume $V_{\rm total}$ associated with each density region. The values are taken from Croton *et al.* (2005b).

5.4.2.2 Normalization of the LF

The SWML method recovers the shape but not the normalization of the luminosity function ϕ^*. To calculate ϕ_* independently, The estimator proposed by Efstathiou *et al.* (1988) for the normalisation of the luminosity function relies on the survey selection function. The probability that a galaxy at distance x is included in the catalogue is

$$S(x) = \frac{\int_{\rm min(L_{min}(x),L_{min})}^{L_{\rm max}} \phi(L)dL}{\int_{L_{\rm min}}^{L_{\rm max}} \phi(L)dL} \tag{5.16}$$

and for a Schechter function this gives for the estimate of ϕ:

$$\phi^* = \frac{\sum_i S^{-1}(x_i)/V}{\Gamma(a+1, L_{\rm min}/L^*) - \Gamma(a+1, L_{\rm max}/L^*)} \tag{5.17}$$

summing over all galaxies in the volume V.

This is the proper procedure for the normalisation of a luminosity function that includes all counts in the sample that is being considered. In the present application, when the survey volume is split into different density regions, this procedure fails because of the change in the selection function. By separating galaxies in different density bins, one has to account for the fact that the binned galaxies do not sample the same volume any more. In order to compare the different luminosity functions and normalise them to the same volume, the fraction of the volume that each density bin occupies must be calculated. The fraction of the total volume that each density bit occupies was taken from Croton *et al.* (2005b) (table 1). The values are reproduced in table 5.2.

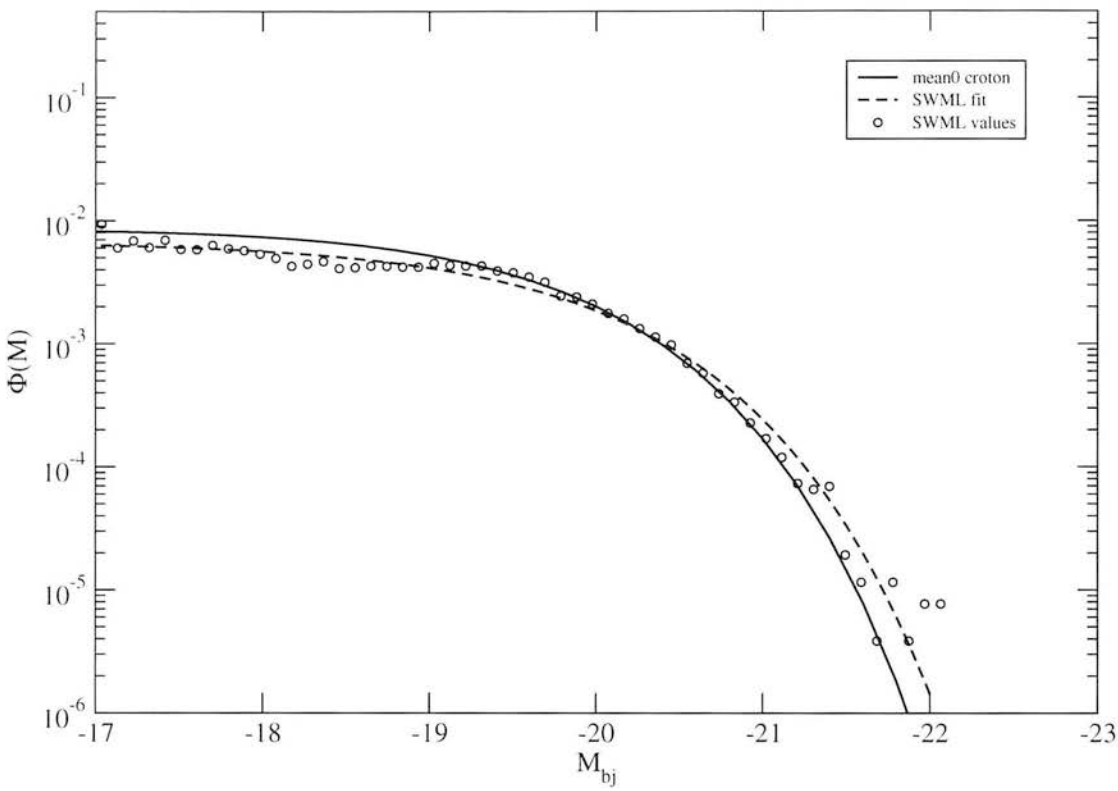

Figure 5.4: Comparison between the published results of Croton *et al.* (2005b) and the luminosity functions calculated using a combination of $V_{\rm max}$ and SWML estimators. The luminosity functions are for the first mean overdensity region (table 5.1).

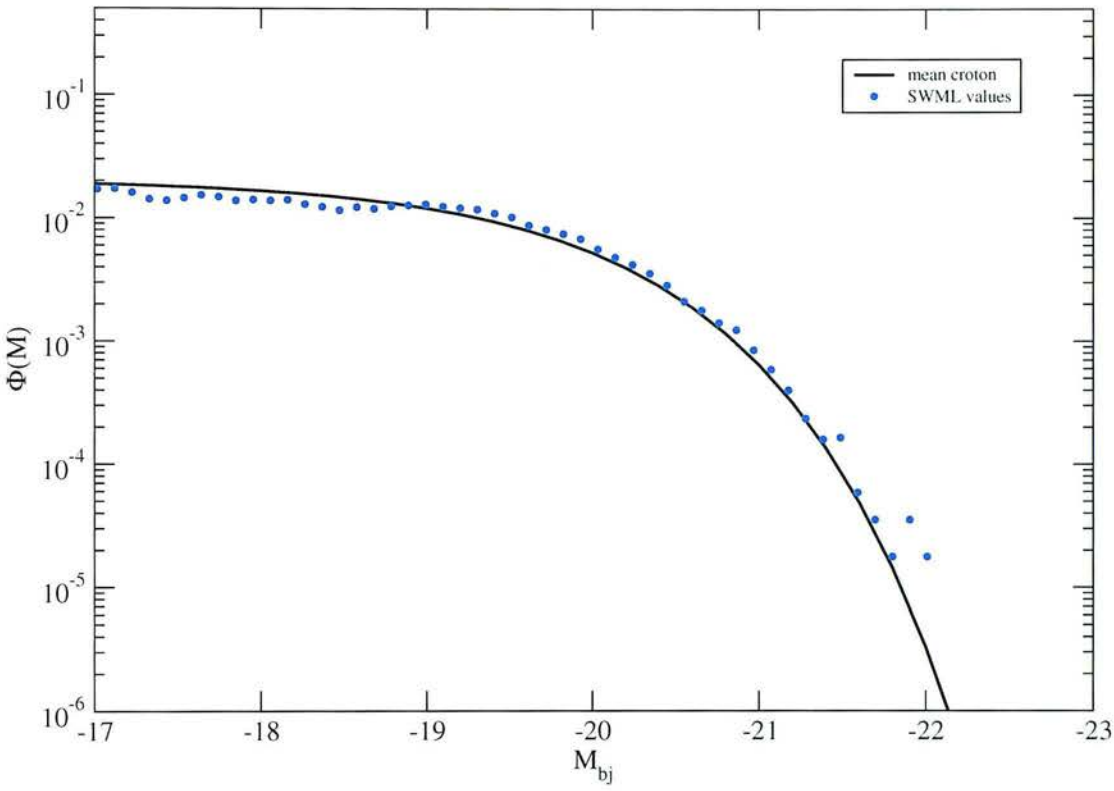

Figure 5.5: Comparison between the published results of Croton *et al.* (2005b) and the luminosity functions calculated using a combination of $V_{\rm max}$ and SWML estimators. The luminosity functions are for the second mean overdensity region (table 5.1).

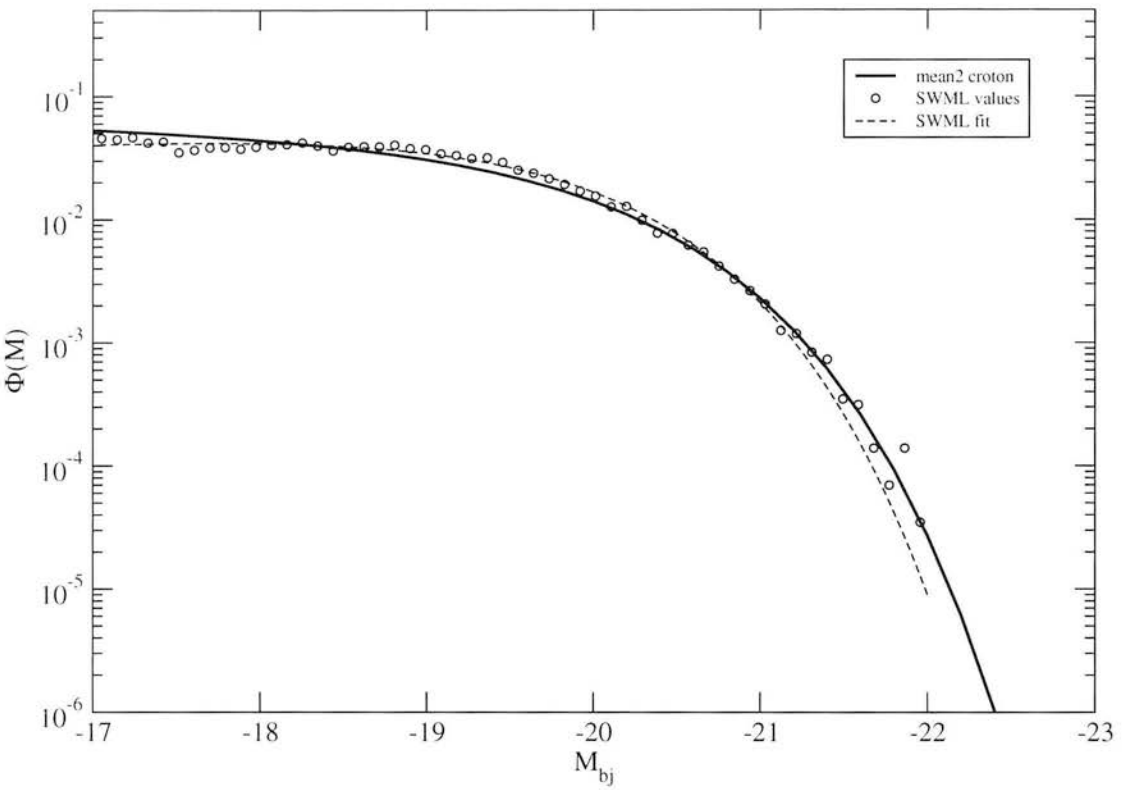

Figure 5.6: Comparison between the published results of Croton *et al.* (2005b) and the luminosity functions calculated using a combination of $V_{\rm max}$ and SWML estimators. The luminosity functions are for the third mean overdensity region (table 5.1).

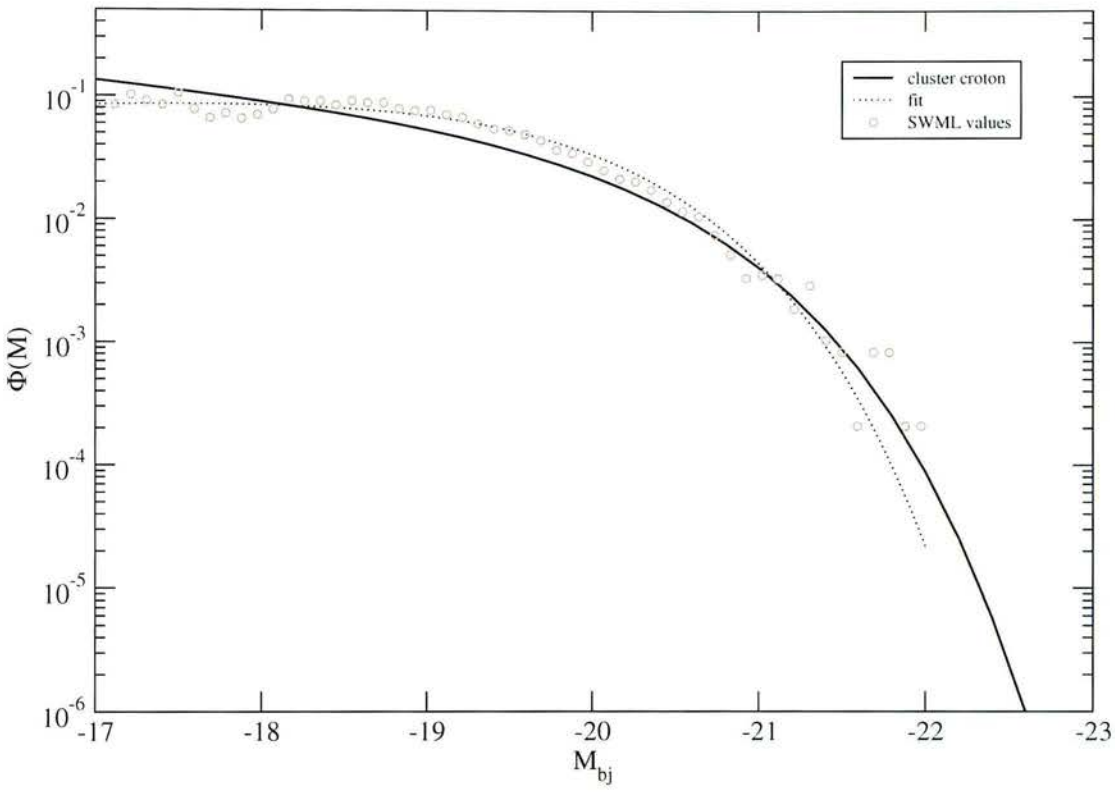

Figure 5.7: Comparison between the published results of Croton *et al.* (2005b) and the luminosity functions calculated using a combination of $V_{\max}$ and SWML estimators. The luminosity functions are for the cluster region (table 5.1).

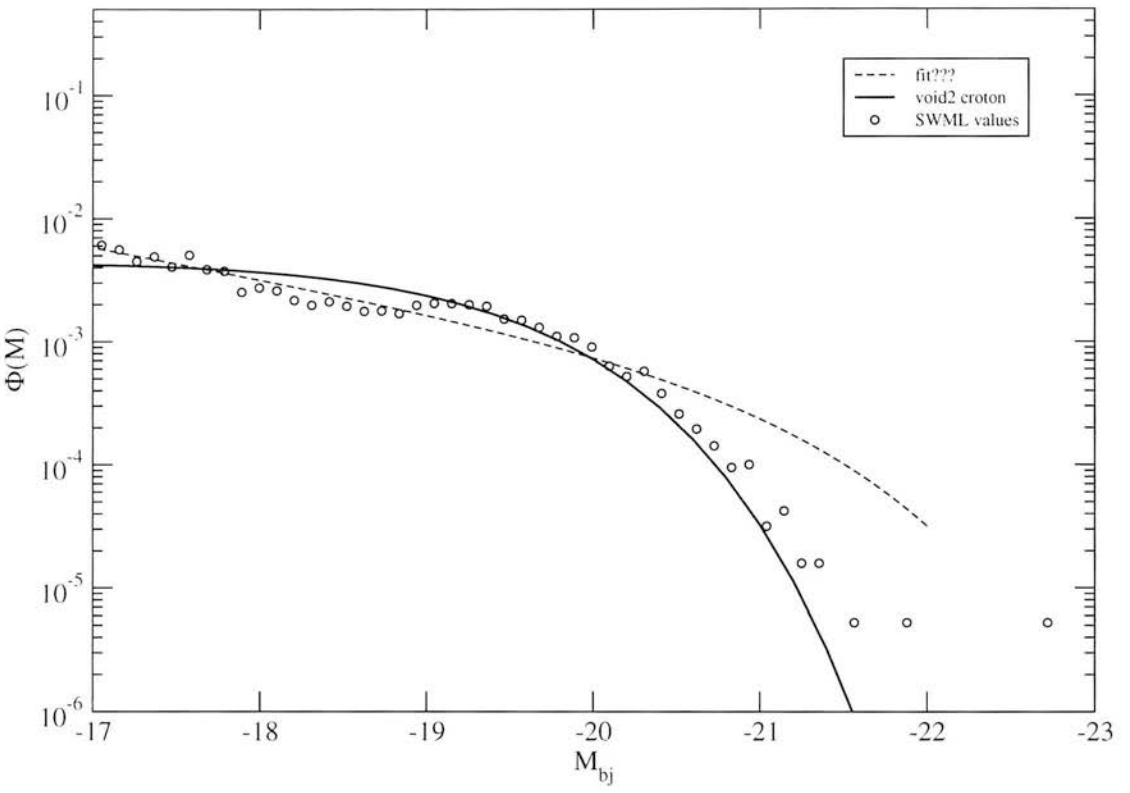

Figure 5.8: Comparison between the published results of Croton *et al.* (2005b) and the luminosity functions calculated using a combination of $V_{\rm max}$ and SWML estimators. The luminosity functions are for the second void region (table 5.1).

5.5 Radio galaxies in the 2dFGRS density field

5.5.1 Introduction

One important question that this chapter tries to address is the relationship between the radio emission and the underlying environment. In particular, is radio emission somehow influenced by different density regions? It is not clear as to how and why a galaxy becomes radio active and perhaps the local density is one of the catalysts for the creation of a radio galaxy. If this is true, then radio galaxies are expected to show preference for a certain density environment. Radio galaxy models suggest that the radio luminosity $L_{\rm rad}$ is higher when the the radio source is confined in denser environments (Scheuer, 1974; Falle, 1991; Kaiser & Alexander, 1997). Therefore, more powerful radio galaxies will populate the higher density regions. This implies another correlation between the black hole mass of the radio galaxies and the local density, more specifically, the radio galaxies with the highest black hole masses will be encountered in overdense regions.

Another possibility is that radio galaxies are created as the result of collisions between galaxies and galaxy mergers Heckman *et al.* (1986). This would imply a preference for higher density regions for radio galaxies once more, so as merging would be possible, but also that the radio galaxy population will not distribute the properties of the non-radio galaxies as far as any environment dependencies are concerned. This is contradictory to the expectation of the two populations displaying similar properties, if radio galaxies are a constant fraction of the total population. If that assumption holds true, then radio galaxies are simply a sub-sample of the total population, thus the distribution of radio galaxy black hole masses in various density regions would be similar to the total distribution of black hole masses in the same density regions.

5.5.2 The dependence of radio and non-radio galaxies on local density

The radio galaxies in the 2dFGRS have already been identified in a previous chapter and it is a simple matter to retrieve the overdensity region each radio galaxy belongs to. This will allow to compare various galactic properties between radio and non-radio galaxies.

In figures 5.9(a) and 5.9(b), the distribution of galactic type according to local density can be seen for the two populations. Normal (non-radio) galaxies are found mostly in mean overdensity regions of course, with the red population exhibiting a preference for slightly higher densities, with a small percentage of blue galaxies being present at high densities. The presence of blue galaxies (thus star-forming) mainly at low density regions agrees with previous results that indicate that star formation is heavily suppressed in high density environments (Hashimoto *et al.*, 1998).

Radio galaxies follow a similar trend. Apart from a concentration of radio galaxies in the red region of figure 5.9(b) which is expected given that most radio

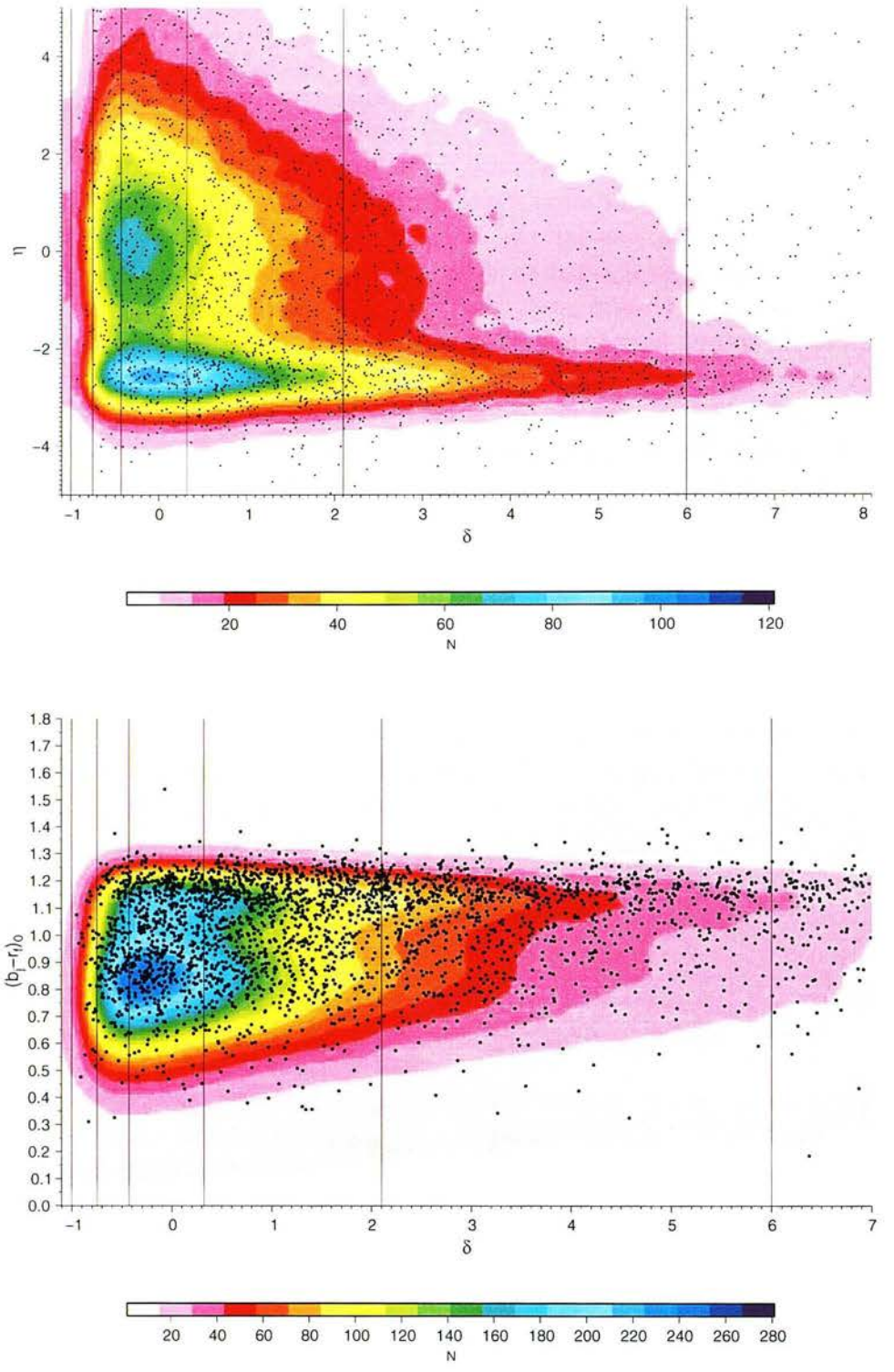

Figure 5.9: The $(\delta, (B_J - R_F)_0)$ and (δ, η) plane for the two populations. The background is a numerical density contour of all the galaxies in the 2dFGRS. The black dots identify the radio galaxies amongst them. The black horizontal lines separate the density regions (table 5.1).

galaxies are red, no trend can be identified between either η or colour with density. There seems to be a tendency for radio galaxies to concentrate on slightly denser regions than normal galaxies but it is not a heavily defined trend. The absence of a strong correlation between radio emission and local density agrees with the findings of Best (2004). The concentration of radio galaxies in dense regions but not in very dense clusters indicates that radio galaxies live at the edge of clusters.

In figures 5.10(a) and 5.10(b) the correlation between absolute magnitude and density as well as the dependence of central black hole mass on local density. It can also be seen that for a given density region, radio galaxies are always at the high end of luminosity and black hole mass amongst the distribution of galaxies in said region. This tendency can be better seen in figure 5.11. It can be seen that blue galaxies (figure 5.11(b)) are not showing a different behaviour that the normal galaxy population and span the mass range, the red galaxies are constantly amongst the galaxies with the highest black hole masses in any given density bin.

The observations regarding the distributions of normal and radio galaxies can be summarised as follows:

- Radio galaxies appear for the most part to follow the distribution of the non-radio galaxies. A small preference for the denser parts of the mean regions is exhibited, but it does not appear to exist a significant difference.
- Red radio galaxies have the highest black hole masses at any density bin.
- Blue galaxies avoid high density regions.
- Blue radio galaxies appear to follow the normal populations as well.

5.5.3 The Kolmogorov-Smirnov test

The test employed to decide if radio galaxies have as parent population the population of normal galaxies is the Kolmogorov-Smirnov test. The Kolmogorov-Smirnov test is a non parametric method that checks if a sample comes from a specific population. The main advantage of the test relies on the fact that it needs no assumption about the distribution of the underlying data. It is a distribution free test. The test can be used in order to compare if two distributions differ by a large degree.

The test is remarkably simple. Considering two data sets, A and B, with data set A being the parent or test population (or the theoretical distribution in case of one set against an expected distribution). The question arises as to whether B follows the same distribution as A. Let P_A and P_B be the empirical distribution function of A and B respectively. The empirical distribution function $P(x)$ gives the fraction of the the data that have values less than x, so

$$P(x) = \frac{n(x)}{N} \ , \tag{5.18}$$

where $n(x)$ is the number of data points with values less that x and N is the total number of data points. Obviously $P(x$ is a step function that asymptotically

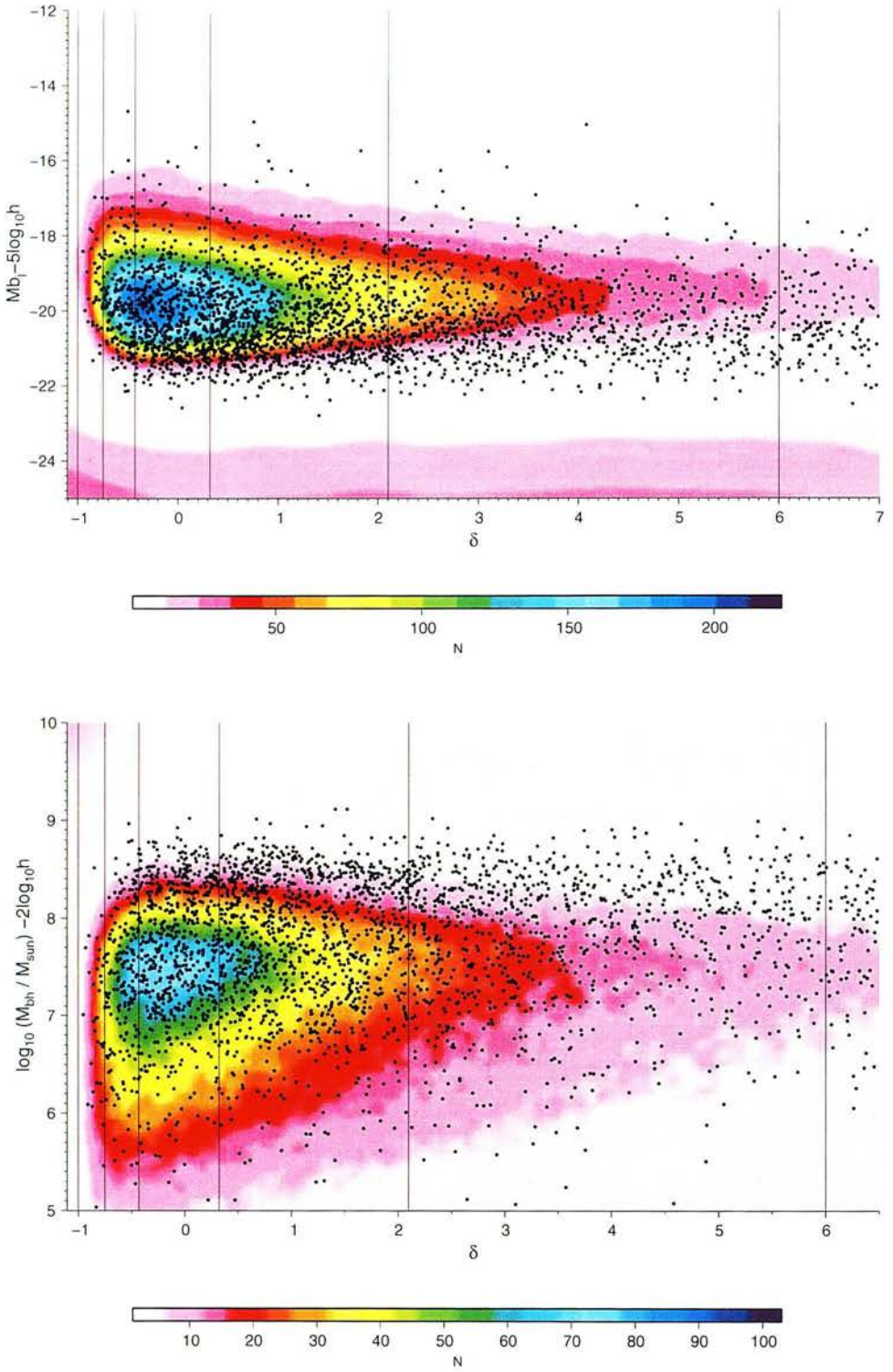

Figure 5.10: The (δ, M_{b_j}) and $(\delta, M_{\rm bh})$ plane for all the galaxies. The background is a numerical density contour of all the galaxies in the 2dFGRS. The black dots identify the radio galaxies amongst them. The black horizontal lines separate the density regions (table 5.1).

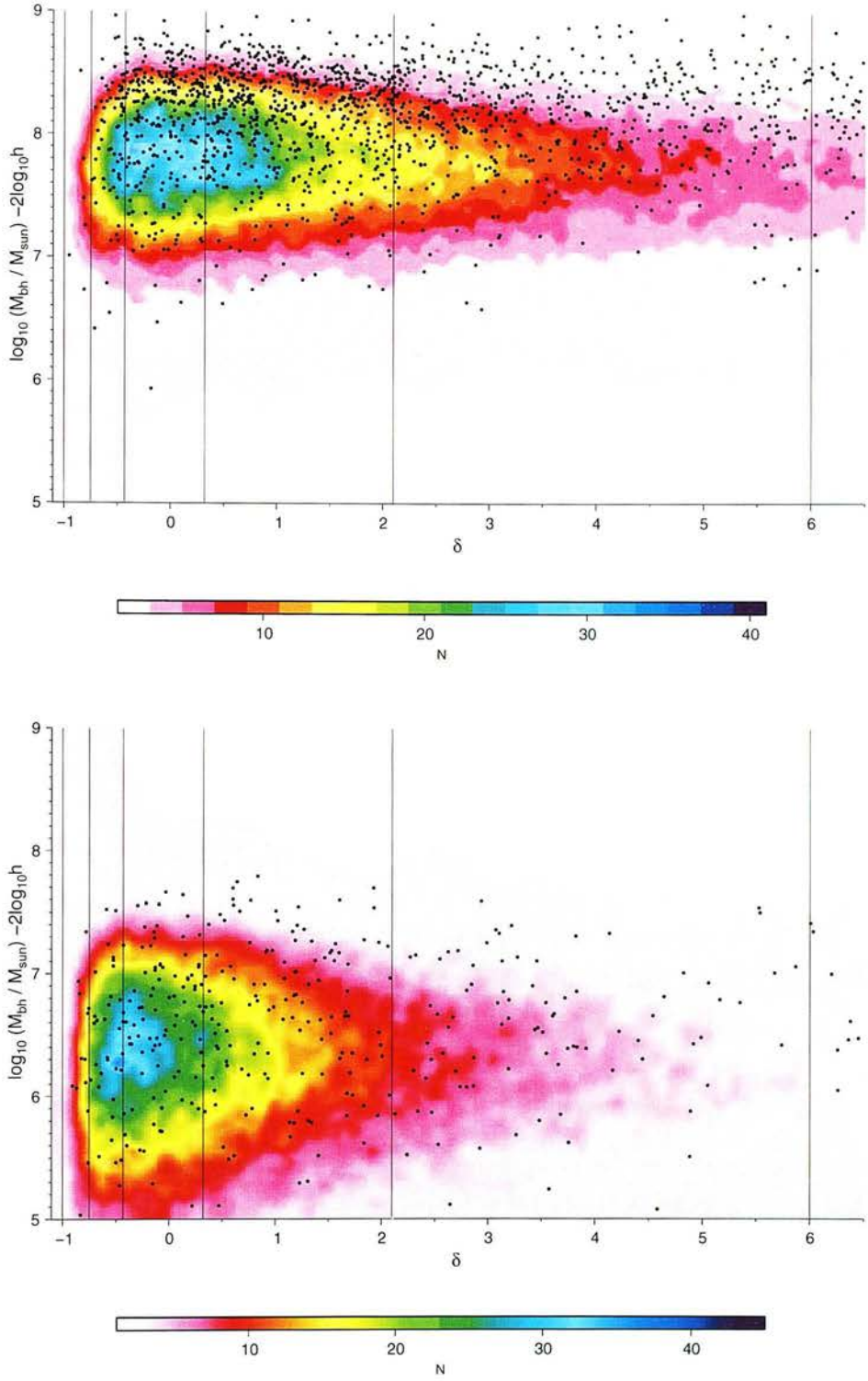

Figure 5.11: The $(\delta, M_{\rm bh})$ plane for red ($(b_j - r_f)_0 > 1.05$) galaxies (top) and blue ($(b_j - r_f)_0 < 0.8$) galaxies (bottom). The background is a numerical density contour of all the galaxies in the 2dFGRS. The black dots identify the radio galaxies amongst them. The black horizontal lines separate the density regions (table 5.1).

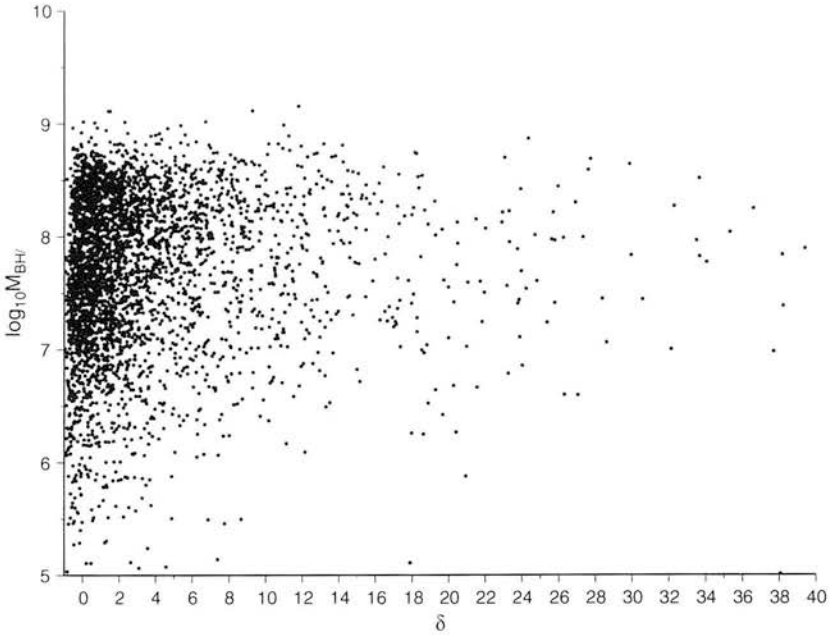

Figure 5.12: The distribution of radio galaxies black hole masses with regards to the density. There is no direct correlation with density although small mass black holes are not found in higher densities.

approaches $P = 1$, with an increase of $\frac{1}{N}$ per step. The KS statistic D is taken to be the maximum distance of P_A and P_B.

$$D = \max_{0 \leq i \leq N} |P_A(x_i) - P_B(x_i)| \tag{5.19}$$

To make the test approximately independent of sample size, the quantity $Z = \sqrt{\frac{n_A n_B}{n_A + n_B}} D$ is used (or in the case of a theoretical distribution and one data set $Z = \sqrt{N}$).

5.5.4 Conclusions

The results of the KS test seen in figures 5.14 5.15 and 5.16 are an indication that for the most parts radio galaxies are a subsample of the general population. Radio galaxies are amongst the galaxies with the largest black hole mass in the red population which indicates that the presence of a central black hole is a main factor in the creation of a radio galaxy. Radio galaxies with large black hole seem to prefer high density regions, although cluster regions do not have a higher number of radio galaxies than the other regions. This picture is consistent with the hypothesis that radio galaxies are the result of merger activity.Heckman *et al.* (1986). In order for mergers to take place, there must be a large number of galaxies, so it can only happen in high density systems. Really high density clusters do not encourage merger activity, whereas at the outskirt of clusters the conditions are optimised for galaxy interactions.

No direct correlation of local density with the size of the radio galaxy black hole was observed, although only medium to high mass black holes are found in

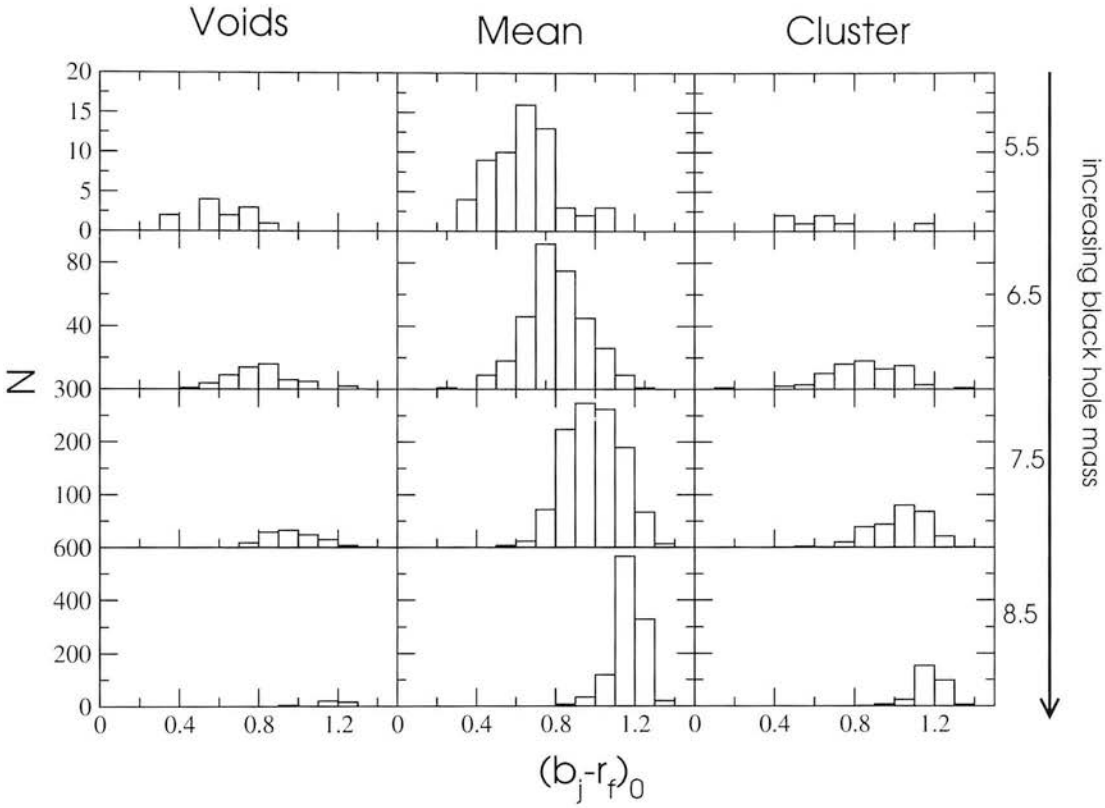

Figure 5.13: The distribution of radio galaxies according to their colour and black hole mass. The three regions are defined in table 5.1. The black hole mass bin is centred at the quoted value and has width $\Delta \log_{10} M = 1$. There is no obvious sift towards high density for larger black hole masses.

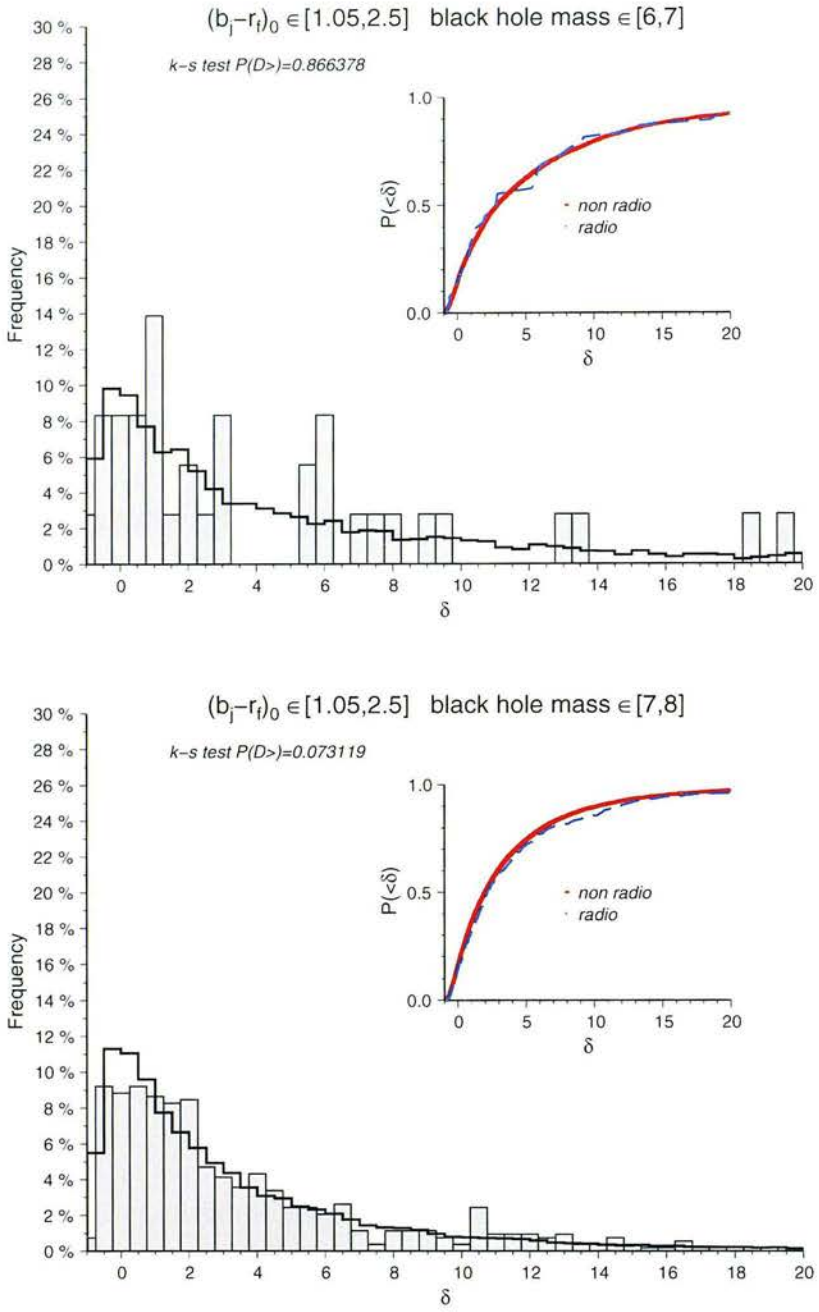

Figure 5.14: The result for the KS test for red galaxies with small black hole masses (top panel) and medium black hole masses (bottom panel). The small panel inside each figure shows the integral probability distribution for the two populations. The histograms are shown as frequency histograms in order to compare the shapes of the distributions. The KS test value is shown as well. The radio galaxies with small black hole masses do not differ by any significant amount from the normal population. In the higher mass bin there is a small difference in the two populations. The results suggest that radio galaxies in this black hole mass bin and colour come from the same population.

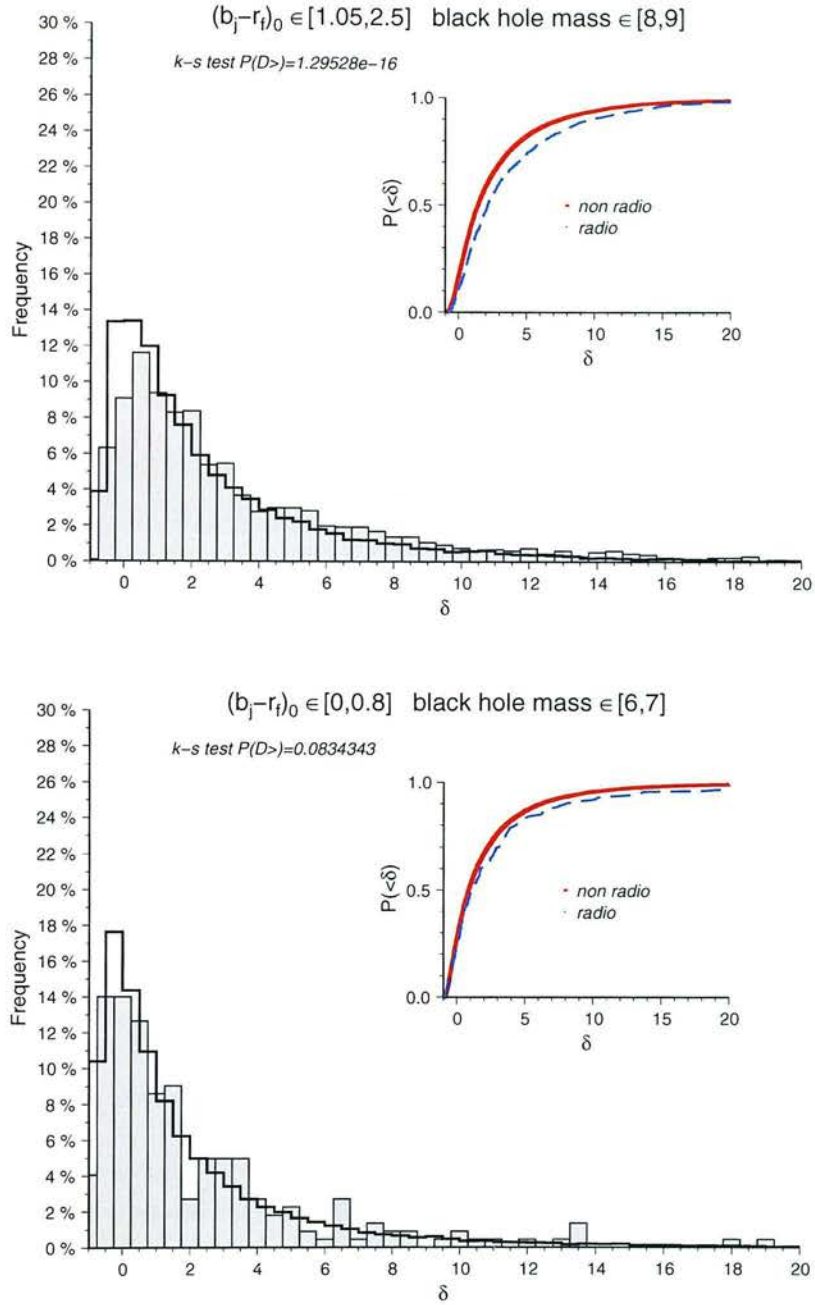

Figure 5.15: Top panel shows the result of the KS test for red galaxies with high black hole masses. Radio galaxies show a shift towards higher densities which makes the two distributions different. Blue galaxies display no such behaviour.

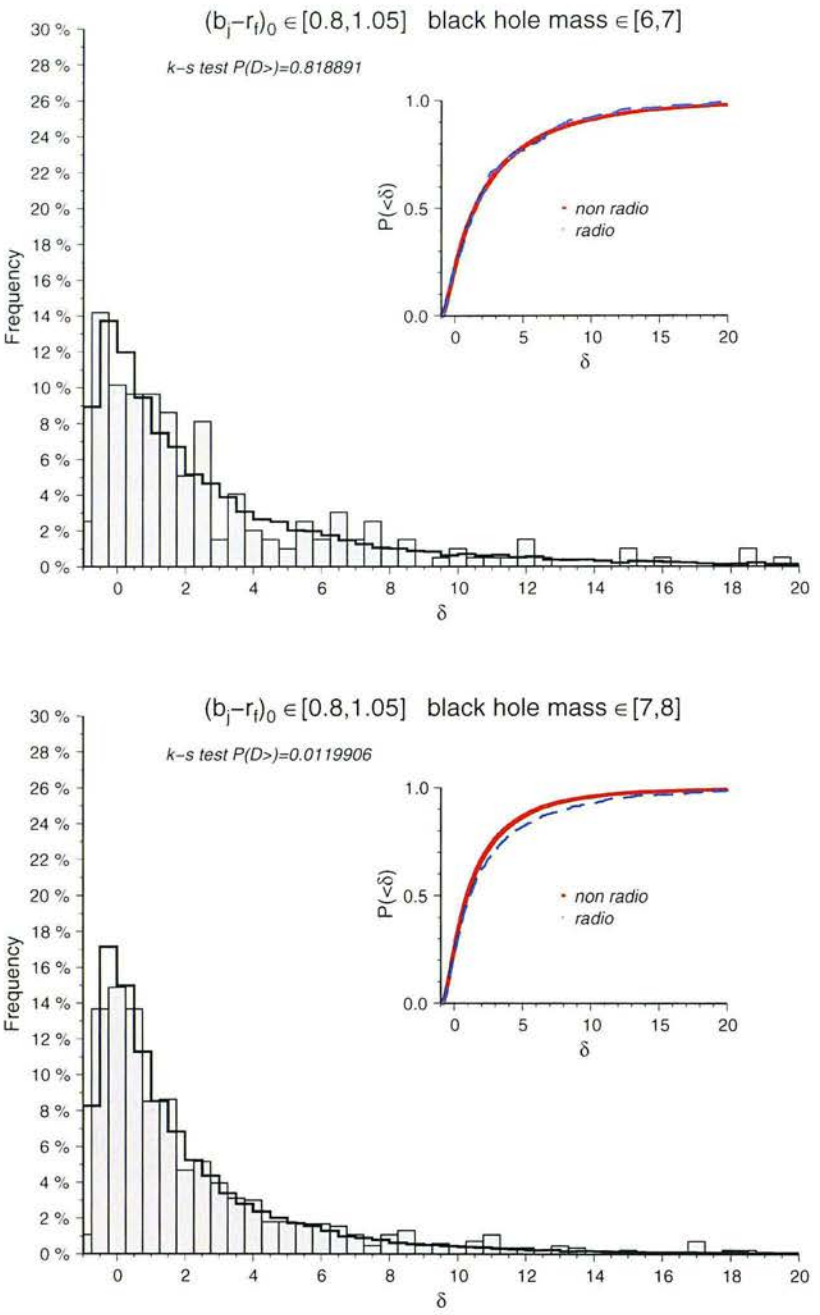

Figure 5.16: The KS test results for the lenticular galaxies. Once again, for the small black hole mass bin, there is no difference in the two population. For the medium black hole mass bin, a small difference is observed but the value of the KS test is not suggestive of a great significance, as can be readily observed in the two distributions.

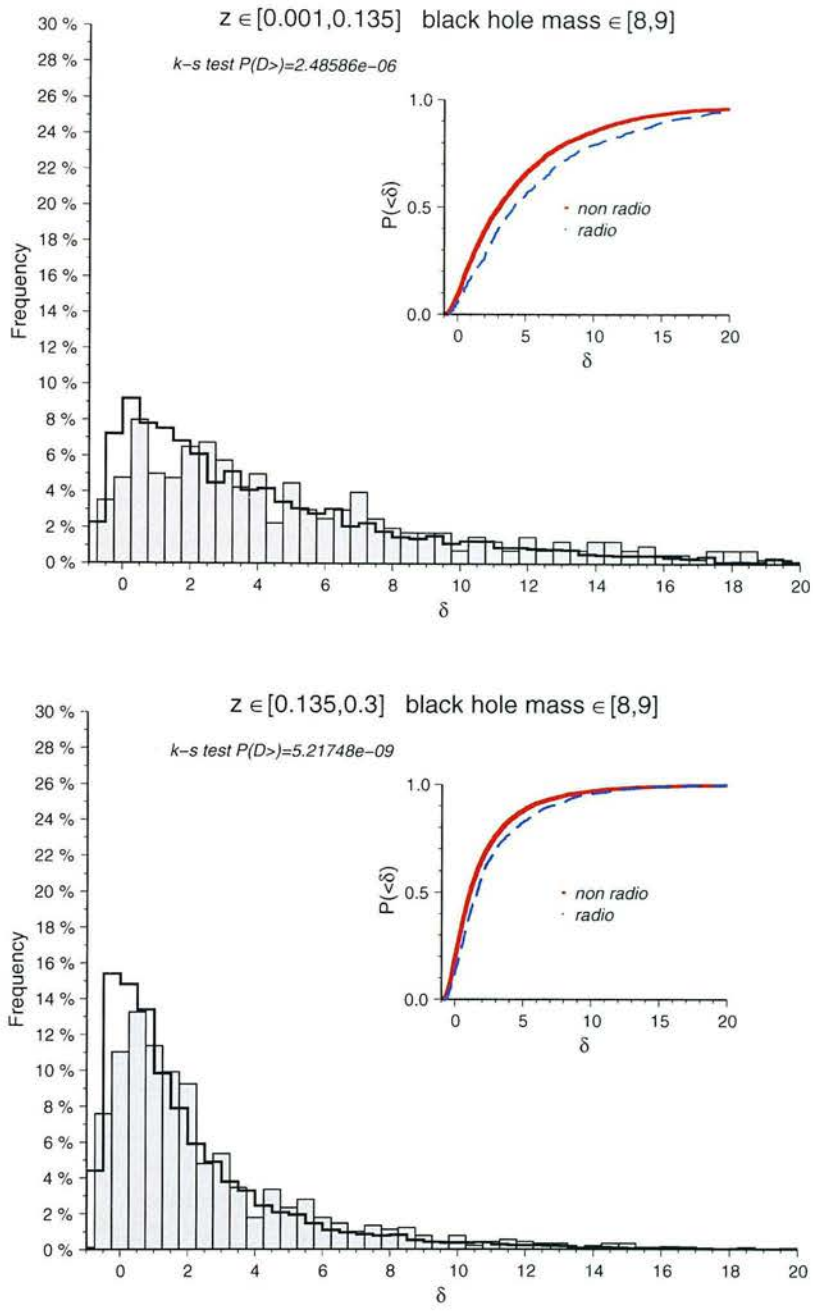

Figure 5.17: The KS test result for the red galaxies with a high black hole mass again, although this time is divided in two redshift bins, in order to investigate if the apparent difference in the population is affected by selection effects. The two different redshift bins display a very similar behaviour so selection effects can be ruled out.

dense regions. A high density environment explains the size of the black hole. The galaxies with the largest black hole masses tend to be in the denser regions since the presence of excess material will help the central engine to increase in size.

In order to better define the dependence of radio galaxies on local density, it is essential that higher redshift radio galaxies are included in the analysis. The more powerful radio sources are vital for a conclusive study of environmental effects. Another issue with the present density estimation is that in reality is not able to probe the local field in as fine detail as one would want. To better deal with high density regions and especially cluster regions, a finer grid is necessary, perhaps down to a few kpc scales, in order to observe any strong density effect on the galactic population.

As always, the answer will come to those who wait (for the next bigger and better survey). The behaviour and identity of galaxies is still an open question in astronomy and with the increase in size and depth of surveys local environment studies are going to a very active field for quite a while.

Chapter 6

Conclusions

In the closing chapter of this thesis a brief outline of the most important results and suggestions of future and follow up work will be presented.

In the first chapter, which was the most independent work of all the thesis, a method was presented that allows the extraction of information about the luminosity function of a deep survey without redshift information. The method relies on the hypothesis that faint galaxies are clustered around bright ones, therefore two surveys were combined in order to extract a sample of galaxies with faint magnitudes and distance indicators. The 2dFGRS survey galaxies were used as centre galaxies, whereas the galaxies of the MGC catalogue were used as the satellite galaxies that exist around the bright centers.

Eventhough the method proved accurate for luminosities in the M_* range, the uncertainty at the faint end did not allow an accurate determination of a faint end slope for the luminosity function. An upper limit was given of $\alpha = -1.7$ to the Schechter function fit at the faint end. This is an important result, since it provides an observational restriction to models of galaxy formation. Models that predict very steep slopes for the faint end and advocate the creation of a large number of low mass dark matter haloes are in contrast to this observation. In order to reduce the number of low mass haloes the models have to be altered in order to incorporate feedback processes that will restrict the creation of small galaxies.

The faint end of the luminosity function is a very important part of any galaxy formation model. If calculated accurately, it will allow CDM theory to finally settle one of the biggest challenges that are facing it; namely the missing dwarf galaxies problem. Sufficiently deep and wide redshift surveys,that will allow the calculation of the LF directly in the faint end, have yet to become available. The method proposed in this thesis is a viable alternative if its accuracy is improved. In order to do so, a bigger number of objects is needed, which translates in to the need for larger survey but without any redshift information, something that is more than viable. Furthermore, some criteria can be imposed on the centre galaxies themselves. It would be interesting to separate the galaxies according to their type or their local environment and proceed to calculate the LF taking into account only certain types. The accuracy of the calculated LF should increase when galaxies in clusters are used as centres, thus ensuring that the galaxies

observed in projection around them have a higher chance of being satellite galaxies in reality.

Of farther interest would be to investigate the population of dwarf galaxies themselves according to their galaxy types. Further results from the MGC survey are expected and it will allow the separations in different populations. Different slopes of the faint end of the LF for different dwarf galaxy populations would allow better restrictions to galaxy formation models.

The second chapter introduced the 2dFGRS b_j and r_f colours extracted from the SCSS survey. It also provided a new formula for calculating the k-corrections for the 2dFGRS survey. The colours were shown to be very accurate and a good statistical indicator of galaxy type. This enhances the quality and information of the final 2dFGRS results and provides a powerful tool to the astronomical community.

Using the Maggorian relation between the bulge luminosity and the black hole mass, the survey mass function was calculated and compared to similar work done using the more difficult to obtain relation between stellar velocity dispersions and black hole mass. The results were compatible in accuracy, which is further proof that the Maggorian relation is very accurate and can be used without introducing any bias.

On the next chapter, the radio galaxies of the 2dFGRS survey were identified by cross matching the 2dFGRS with the NVSS radio survey. The final sample of ≈ 3000 radio galaxies with colour and redshift information is one of the largest available and it allowed the calculation of the radio luminosity function with great accuracy. Investigation on the relation between black hole mass and radio output of galaxies did not reveal any direct relation. There was an indication of a relation of the form $L_{Radio} \sim M_{BH}^{2.4}$ as was previously reported from workers in the field, but it was shown that this is probably due to selection effects and not any real relationship. The bivariate luminosity function calculated using the black hole mass and the radio luminosity of the galaxies indicated that the radio emission is independent of black home mass size, farther proof that the quoted relation between radio output and black hole mass is not real.

There is a lot to be investigated in this chapter, especially regarding the origin of the radio emission. An effort was made to link H_a luminosity to radio emission from star forming galaxies but the scatter in the relation made it difficult to have any solid conclusion. Identification of SF galaxies using only one feature of their spectra is not possible. It would be interesting to do a similar investigation taking into account more spectral lines or using galaxies with information on the IR spectrum. Isolating radio emission from AGN galaxies accurately could settle the question whether the radio emission is linked to the black hole or not.

The final chapter introduced a local numerical density estimator based on Smooth Particle Hydrodynamics principles. The local density at each galaxy was calculated and separation of the 2dFGRS survey in different density areas became possible. The radio galaxy population was found to be similar to the normal galaxy population, regarding their placement in the local density field. This is strong indication that radio galaxies are not a product of a special process but simply a fraction of normal galaxies. There is indication of a small differentiation

in higher black hole masses and this should be investigated further. Examining the larger galaxies requires a deeper redshift survey. A next generation survey would allow a density estimator of real space density to be calculated instead of a redshift space. Using the 2dFGRS spectra does not allow for the calculation of peculiar velocities in order to eliminate redshift space effects but this should be made possible with more advanced surveys.

As a closing note, I would like to thank the people that made this work possible. My parents, George and Nina, who were always there for me. I hope this work makes them proud. I would also like to thank John Peacock, my supervisor, for his support and his belief in me as well as his enormous patience with my weird working methods. Without him I would have failed a long time ago. Finally, my examiners Peter Brand and Paul Hewett for making my viva a very pleasant experience. In my years in the Royal Observatory of Edinburgh, I was lucky to have met such great scientists and people.

Bibliography

Abazajian, K., Adelman-McCarthy, J. K., Agueros, M. A. *et al.*. *The Third Data Release of the Sloan Digital Sky Survey*. AJ, 2005. volume 129:1755–1759.

Akerib, D. S., Alvaro-Dean, J., Armel-Funkhouser, M. S. *et al.*. *First Results from the Cryogenic Dark Matter Search in the Soudan Underground Laboratory*. *Physical Review Letters*, 2004. volume 93(21):211301–+.

Aller, M. C. & Richstone, D. *The Cosmic Density of Massive Black Holes from Galaxy Velocity Dispersions*. AJ, 2002. volume 124:3035–3041.

Antonucci, R. *Unified models for active galactic nuclei and quasars*. ARA&A, 1993. volume 31:473–521.

Baade, W. & Minkowski, R. *Identification of the Radio Sources in Cassiopeia, Cygnus a, and Puppis a.*. ApJ, 1954. volume 119:206–+.

Baldry, I. K., Glazebrook, K., Brinkmann, J. *et al.*. *Quantifying the Bimodal Color-Magnitude Distribution of Galaxies*. ApJ, 2004. volume 600:681–694.

Bell, A. R. *The acceleration of cosmic rays in shock fronts. I*. MNRAS, 1978. volume 182:147–156.

Benoist, C., Maurogordato, S., da Costa, L. N. *et al.*. *Biasing in the Galaxy Distribution*. ApJ, 1996. volume 472:452–+.

Benson, A. J., Frenk, C. S., Baugh, C. M. *et al.*. *The effects of photoionization on galaxy formation - III. Environmental dependence in the luminosity function*. MNRAS, 2003. volume 343:679–691.

Benson, A. J., Pearce, F. R., Frenk, C. S. *et al.*. *A comparison of semi-analytic and smoothed particle hydrodynamics galaxy formation*. MNRAS, 2001. volume 320:261–280.

Best, P. N. *The environmental dependence of radio-loud AGN activity and star formation in the 2dFGRS*. MNRAS, 2004. volume 351:70–82.

Best, P. N., Kauffmann, G., Heckman, T. M. *et al.*. *The host galaxies of radio-loud active galactic nuclei: mass dependences, gas cooling and active galactic nuclei feedback*. MNRAS, 2005. volume 362:25–40.

Binggeli, B., Sandage, A. & Tammann, G. A. *The luminosity function of galaxies.* ARA&A, 1988. volume 26:509–560.

Binney & Merrifield. *Galactic Astronomy.* Princeton University Press, 1998.

Binney, J. & Mamon, G. A. *M/L and velocity anisotropy from observations of spherical galaxies, or must M87 have a massive black hole.* MNRAS, 1982. volume 200:361–375.

Blanton, M. R., Brinkmann, J., Csabai, I. *et al.*. *Estimating Fixed-Frame Galaxy Magnitudes in the Sloan Digital Sky Survey.* AJ, 2003. volume 125:2348–2360.

Blanton, M. R., Lupton, R. H., Schlegel, D. J. *et al.*. *The Properties and Luminosity Function of Extremely Low Luminosity Galaxies.* ApJ, 2005. volume 631:208–230.

Burstein, D. & Rubin, V. C. *The distribution of mass in spiral galaxies.* ApJ, 1985. volume 297:423–435.

Butkevich, A. G., Berdyugin, A. V. & Teerikorpi, P. *Statistical biases in stellar astronomy: the Malmquist bias revisited.* MNRAS, 2005. volume 362:321–330.

Cavaliere, A. & Padovani, P. *The connection between active and normal galaxies.* ApJ, 1989. volume 340:L5–L8.

Chokshi, A. & Turner, E. L. *Remnants of the quasars.* MNRAS, 1992. volume 259:421–424.

Cole, S., Lacey, C. G., Baugh, C. M. *et al.*. *Hierarchical galaxy formation.* MNRAS, 2000. volume 319:168–204.

Colless, M., Dalton, G., Maddox, S. *et al.*. *The 2dF Galaxy Redshift Survey: spectra and redshifts.* MNRAS, 2001. volume 328:1039–1063.

Condon, J. J. *Radio emission from normal galaxies.* ARA&A, 1992. volume 30:575–611.

Condon, J. J., Cotton, W. D., Greisen, E. W. *et al.*. *The NRAO VLA Sky Survey.* AJ, 1998. volume 115:1693–1716.

Croton, D. J., Farrar, G. R., Norberg, P. *et al.*. *The 2dF Galaxy Redshift Survey: luminosity functions by density environment and galaxy type.* MNRAS, 2005a. volume 356:1155–1167.

Croton, D. J., Farrar, G. R., Norberg, P. *et al.*. *The 2dF Galaxy Redshift Survey: luminosity functions by density environment and galaxy type.* MNRAS, 2005b. volume 356:1155–1167.

Davis, M. & Peebles, P. J. E. *A survey of galaxy redshifts. V - The two-point position and velocity correlations.* ApJ, 1983. volume 267:465–482.

de Paolis, F., Ingrosso, G., Jetzer, P. *et al.*. *Halo Dark Clusters of Brown Dwarfs and Molecular Clouds*. ApJ, 1998. volume 500:59–+.

de Sitter, W. *Einstein's theory of gravitation and its astronomical consequences*. MNRAS, 1916. volume 76:699–728.

Dressler, A. *Galaxy morphology in rich clusters - Implications for the formation and evolution of galaxies*. ApJ, 1980. volume 236:351–365.

Efstathiou, G. *A model of supernova feedback in galaxy formation*. MNRAS, 2000. volume 317:697–719.

Efstathiou, G., Ellis, R. S. & Peterson, B. A. *Analysis of a complete galaxy redshift survey. II - The field-galaxy luminosity function*. MNRAS, 1988. volume 232:431–461.

Efstathiou, G., Moody, S., Peacock, J. A. *et al.*. *Evidence for a non-zero Λ and a low matter density from a combined analysis of the 2dF Galaxy Redshift Survey and cosmic microwave background anisotropies*. MNRAS, 2002. volume 330:L29–L35.

Einstein, A. *Relativity: The Special and General Theory.*. Henry Holt and Company, 1920.

Erwin, P., Graham, A. W. & Caon, N. *The Correlation between Supermassive Black Hole Mass and the Structure of Ellipticals and Bulges*. 2004.

Falle, S. A. E. G. *Self-similar jets*. MNRAS, 1991. volume 250:581–596.

Felten, J. E. *On Schmidt's Vm estimator and other estimators of luminosity functions*. ApJ, 1976. volume 207:700–709.

Ferrarese, L. & Merritt, D. *A Fundamental Relation between Supermassive Black Holes and Their Host Galaxies*. ApJ, 2000. volume 539:L9–L12.

Franceschini, A., Vercellone, S. & Fabian, A. C. *Supermassive Black Holes in Early-Type Galaxies: Relationship with Radio Emission and Constraints on the Black Hole Mass Function*. MNRAS, 1998. volume 297:817–824.

Freedman, W. L., Madore, B. F., Gibson, B. K. *et al.*. *Final Results from the Hubble Space Telescope Key Project to Measure the Hubble Constant*. ApJ, 2001. volume 553:47–72.

Freeman, K. C. *On the Disks of Spiral and so Galaxies*. ApJ, 1970. volume 160:811–+.

Fukugita, M., Shimasaku, K. & Ichikawa, T. *Galaxy Colors in Various Photometric Band Systems*. PASP, 1995. volume 107:945–+.

Gaztañaga, E., Norberg, P., Baugh, C. M. *et al.*. *Statistical analysis of galaxy surveys - II. The three-point galaxy correlation function measured from the 2dFGRS*. MNRAS, 2005:921–+.

Gingold, R. A. & Monaghan, J. J. *Smoothed particle hydrodynamics - Theory and application to non-spherical stars*. MNRAS, 1977. volume 181:375–389.

Gnedin, N. Y. *Galaxy Formation in a CDM + Lambda Universe. I. Properties of Gas and Galaxies*. ApJ, 1996. volume 456:1–+.

Hambly, N. C., MacGillivray, H. T., Read, M. A. *et al.*. *The SuperCOSMOS Sky Survey - I. Introduction and description*. MNRAS, 2001. volume 326:1279–1294.

Hamilton, A. J. S. *Toward Better Ways to Measure the Galaxy Correlation Function*. ApJ, 1993. volume 417:19–+.

Hashimoto, Y., Oemler, A. J., Lin, H. *et al.*. *The Influence of Environment on the Star Formation Rates of Galaxies*. ApJ, 1998. volume 499:589–+.

Hawkins, E., Maddox, S., Cole, S. *et al.*. *The 2dF Galaxy Redshift Survey: correlation functions, peculiar velocities and the matter density of the Universe*. MNRAS, 2003. volume 346:78–96.

Heckman, T. M., Smith, E. P., Baum, S. A. *et al.*. *Galaxy collisions and mergers - The genesis of very powerful radio sources?*. ApJ, 1986. volume 311:526–547.

Ho, L. C. *On the Relationship between Radio Emission and Black Hole Mass in Galactic Nuclei*. ApJ, 2002. volume 564:120–132.

Hogg, D. W. *Distances measures in cosmology*. *astro-ph*, 2000. volume 9905116.

Hogg, D. W., Baldry, I. K., Blanton, M. R. *et al.*. *The k correction*. *astro-ph*, 2002. volume 0210394.

Hogg, D. W., Blanton, M. R., Eisenstein, D. J. *et al.*. *The Overdensities of Galaxy Environments as a Function of Luminosity and Color*. ApJ, 2003. volume 585:L5–L9.

Hubble, E. & Humason, M. L. *The Velocity-Distance Relation among Extra-Galactic Nebulae*. ApJ, 1931. volume 74:43–+.

Hubble, E. P. *Extragalactic nebulae.*. ApJ, 1926. volume 64:321–369.

Jennison, R. C. & Latham, V. *The brightness distribution within the radio sources Cygnus A (19N4A) and Cassiopeia A (23N5A)*. MNRAS, 1959. volume 119:174–+.

Kaiser, C. R. & Alexander, P. *A self-similar model for extragalactic radio sources*. MNRAS, 1997. volume 286:215–222.

Kambas, A., Davies, J. I., Smith, R. M. *et al.*. *The Low Surface Brightness Extent of the Fornax Cluster*. AJ, 2000. volume 120:1316–1324.

Kamionkowski, M. & Kurylov, A. *Generalized analysis of WIMP searches*. *New Astronomy Review*, 2005. volume 49:241–244.

Kauffmann, G. & Haehnelt, M. *A unified model for the evolution of galaxies and quasars*. MNRAS, 2000. volume 311:576–588.

Kauffmann, G., White, S. D. M. & Guiderdoni, B. *The Formation and Evolution of Galaxies Within Merging Dark Matter Haloes*. MNRAS, 1993. volume 264:201–+.

Kent, S. M. *CCD surface photometry of field Galaxies. II - Bulge/disk decompositions*. ApJS, 1985. volume 59:115–159.

Kormendy, J. & Gebhardt, K. *Supermassive Black Holes in Galactic Nuclei (Plenary Talk)*. 2001:363–+.

Landy, S. D. & Szalay, A. S. *Bias and variance of angular correlation functions*. ApJ, 1993. volume 412:64–71.

Lewis, I. J., Cannon, R. D., Taylor, K. *et al.*. *The Anglo-Australian Observatory 2dF facility*. MNRAS, 2002. volume 333:279–299.

Lia, C. & Carraro, G. *Parallel Tree-SPH: A Tool for Galaxy Formation*. Ap&SS, 2001. volume 276:1049–1056.

Liske, J., Lemon, D. J., Driver, S. P. *et al.*. *The Millennium Galaxy Catalogue: $16 \leq= B_{MGC} \leq 24$ galaxy counts and the calibration of the local galaxy luminosity function*. MNRAS, 2003. volume 344:307–324.

Loveday, J. *The Local Space Density of Dwarf Galaxies*. ApJ, 1997. volume 489:29–+.

Loveday, J., Peterson, B. A., Efstathiou, G. *et al.*. *The Stromlo-APM Redshift Survey. I - The luminosity function and space density of galaxies*. ApJ, 1992. volume 390:338–344.

Madgwick, D. S., Hawkins, E., Lahav, O. *et al.*. *The 2dF Galaxy Redshift Survey: galaxy clustering per spectral type*. MNRAS, 2003. volume 344:847–856.

Madgwick, D. S., Lahav, O., Baldry, I. K. *et al.*. *The 2dF Galaxy Redshift Survey: galaxy luminosity functions per spectral type*. MNRAS, 2002. volume 333:133–144.

Magliocchetti, M., Maddox, S. J., Lahav, O. *et al.*. *Variance and skewness in the FIRST survey*. MNRAS, 1998. volume 300:257–268.

Marconi, A., Risaliti, G., Gilli, R. *et al.*. *Local supermassive black holes, relics of active galactic nuclei and the X-ray background*. MNRAS, 2004. volume 351:169–185.

Marinho, E. P. & Lépine, J. R. D. *SPH simulations of clumps formation by dissipative collision of molecular clouds. I. Non magnetic case*. A&AS, 2000. volume 142:165–179.

Matthews, T. A. & Sandage, A. R. *Optical Identification of 3c 48, 3c 196, and 3c 286 with Stellar Objects.*. ApJ, 1963. volume 138:30–+.

McLure, R. J. & Dunlop, J. S. *On the black hole-bulge mass relation in active and inactive galaxies*. MNRAS, 2002. volume 331:795–804.

Melnick, J. & Sargent, W. L. W. *The radial distribution of morphological types of galaxies in X-ray clusters*. ApJ, 1977. volume 215:401–407.

Merritt, D. & Ferrarese, L. *Relationship of Black Holes to Bulges*. 2001:335–+.

Mo, H. J., Yang, X., van den Bosch, F. C. *et al.*. *The dependence of the galaxy luminosity function on large-scale environment*. MNRAS, 2004. volume 349:205–212.

Monaghan, J. J. *Smoothed particle hydrodynamics*. ARA&A, 1992. volume 30:543–574.

Netzer, H., Heller, A., Loinger, F. *et al.*. *Optical monitoring of luminous AGN - I. Radio-loud quasars*. MNRAS, 1996. volume 279:429–446.

Norberg, P., Baugh, C. M., Hawkins, E. *et al.*. *The 2dF Galaxy Redshift Survey: the dependence of galaxy clustering on luminosity and spectral type*. MNRAS, 2002. volume 332:827–838.

Oort, M. J. A. *Radio Galaxies at very low flux levels. PhD Thesis*, 1987.

Ostriker, J. P., Peebles, P. J. E. & Yahil, A. *The size and mass of galaxies, and the mass of the universe*. ApJ, 1974. volume 193:L1–L4.

Peacock, J. *Cosmological Physics*. Cambridge University Press, 1999.

Peacock, J. A. *Implications of 2d FGRS Results on Cosmic Structure*. 2003:275–290.

Pearce, F. R., Jenkins, A., Frenk, C. S. *et al.*. *A Simulation of Galaxy Formation and Clustering*. ApJ, 1999. volume 521:L99–L102.

Peebles, P. J. E. *Large-scale background temperature and mass fluctuations due to scale-invariant primeval perturbations*. ApJ, 1982. volume 263:L1–L5.

Peterson, B. M. *Reverberation mapping of active galactic nuclei*. PASP, 1993. volume 105:247–268.

Phillipps, S. *A Possible Geometric Measurement of the Cosmological Constant*. MNRAS, 1994. volume 269:1077–+.

Phillipps, S. & Shanks, T. *Galaxy correlations and the luminosity function*. MNRAS, 1987. volume 227:115–121.

Pretzl, K. *Direct Detection of Dark Matter WIMPs. Space Science Reviews*, 2002. volume 100:209–220.

Reber, G. *Notes: Cosmic Static.*. ApJ, 1940. volume 91:621–624.

Reber, G. *Cosmic Static.*. ApJ, 1944. volume 100:279–+.

Richstone, D., Ajhar, E. A., Bender, R. *et al.*. *Supermassive black holes and the evolution of galaxies.*. Nature, 1998. volume 395:A14+.

Roberts, M. S. & Haynes, M. P. *Physical Parameters along the Hubble Sequence.* ARA&A, 1994. volume 32:115–152.

Robinson, I., Schild, A. & Schucking, E. L. *Quasi-stellar sources and gravitational collapse.* 1965.

Rodmann, J. *Book Review: Practical statistics for astronomers / Cambridge University Press, Cambridge, 2003, XVI+178 pp., ISBN 0-521-45616-9.*. *Sterne und Weltraum*, 2004. volume 43(8):88–+.

Rubin, V. C., Thonnard, N. & Ford, W. K. *Rotational properties of 21 SC galaxies with a large range of luminosities and radii, from NGC 4605 /R = 4kpc/ to UGC 2885 /R = 122 kpc/.* ApJ, 1980. volume 238:471–487.

Sabatini, S., Davies, J., Scaramella, R. *et al.*. *The dwarf LSB galaxy population of the Virgo cluster - I. The faint-end slope of the luminosity function.* MNRAS, 2003. volume 341:981–992.

Sadler, E. M., Jackson, C. A., Cannon, R. D. *et al.*. *Radio sources in the 2dF Galaxy Redshift Survey - II. Local radio luminosity functions for AGN and star-forming galaxies at 1.4 GHz.* MNRAS, 2002. volume 329:227–245.

Salucci, P., Szuszkiewicz, E., Monaco, P. *et al.*. *Mass function of dormant black holes and the evolution of active galactic nuclei.* MNRAS, 1999. volume 307:637–644.

Schechter, P. *An analytic expression for the luminosity function for galaxies.*. ApJ, 1976. volume 203:297–306.

Scheuer, P. A. G. *Models of extragalactic radio sources with a continuous energy supply from a central object.* MNRAS, 1974. volume 166:513–528.

Schmidt, M. *3C 273: a star-like object with large red-shift.*. Nature, 1963. volume 197:1040–1040.

Seyfert, C. K. *Nuclear Emission in Spiral Nebulae.*. ApJ, 1943. volume 97:28–+.

Shane, C. D. & Wirtanen, C. A. *The distribution of galaxies.* Lick Observatory Publications, 1967.

Shapley, H. & Ames, A. *A survey of the external galaxies brighter than the thirteenth magnitude.* Annals of Harvard College Observatory, Cambridge, Mass.: Astronomical Observatory of Harvard College, 1932, 1932.

Sheth, R. K., Mo, H. J. & Tormen, G. *Ellipsoidal collapse and an improved model for the number and spatial distribution of dark matter haloes*. MNRAS, 2001. volume 323:1–12.

Sheth, R. K. & Tormen, G. *An excursion set model of hierarchical clustering: ellipsoidal collapse and the moving barrier*. MNRAS, 2002. volume 329:61–75.

Silk, J. & Rees, M. J. *Quasars and galaxy formation*. A&A, 1998. volume 331:L1–L4.

Smith, J. A., Tucker, D. L., Kent, S. *et al.*. *The u'g'r'i'z' Standard-Star System*. AJ, 2002. volume 123:2121–2144.

Smith, S. *The Mass of the Virgo Cluster*. ApJ, 1936. volume 83:23–+.

Soltan, A. *Masses of quasars*. MNRAS, 1982. volume 200:115–122.

Spergel, D. N., Verde, L., Peiris, H. V. *et al.*. *First-Year Wilkinson Microwave Anisotropy Probe (WMAP) Observations: Determination of Cosmological Parameters*. ApJS, 2003. volume 148:175–194.

Spitzer, L. J. & Baade, W. *Stellar Populations and Collisions of Galaxies.*. ApJ, 1951. volume 113:413–+.

Takeuchi, T. T., Yoshikawa, K. & Ishii, T. T. *Tests of Statistical Methods for Estimating Galaxy Luminosity Function and Applications to the Hubble Deep Field*. ApJS, 2000. volume 129:1–31.

Tonry, J. L. *Evidence for a central mass concentration in M32*. ApJ, 1984. volume 283:L27+.

Trentham, N. & Tully, R. B. *The faint end of the galaxy luminosity function*. MNRAS, 2002. volume 335:712–732.

Tully, R. B. *Light-to-Mass Variations with Environment*. ApJ, 2005. volume 618:214–226.

Urry, C. M. & Padovani, P. *Unified Schemes for Radio-Loud Active Galactic Nuclei*. PASP, 1995. volume 107:803–+.

Vaucouleurs, D., Vaucouleurs, D., Corwin *et al.*. *Third reference catalogue of bright galaxies*. 1991.

Verde, L., Heavens, A. F., Percival, W. J. *et al.*. *The 2dF Galaxy Redshift Survey: the bias of galaxies and the density of the Universe*. MNRAS, 2002. volume 335:432–440.

Waldrop, M. M. *The case of the missing matter*. *Air and Space*, 1993. volume 7:58–67.

Weedman, D. W. *Luminosities of Seyfert galaxies and QSOs*. ApJ, 1976. volume 208:30–36.

Whitmore, B. C., Gilmore, D. M. & Jones, C. *What determines the morphological fractions in clusters of galaxies?*. ApJ, 1993. volume 407:489–509.

Windhorst, R. A., Burstein, D., Mathis, D. F. *et al.*. *The discovery of a young radio galaxy at Z = 2.390 - Probing initial star formation at Z less than approximately 3.0*. ApJ, 1991. volume 380:362–383.

Woltjer, L. *Emission Nuclei in Galaxies.*. ApJ, 1959. volume 130:38–+.

Wyse, R. F. G., Gilmore, G. & Franx, M. *Galactic Bulges*. ARA&A, 1997. volume 35:637–675.

Yoo, J., Chanamé, J. & Gould, A. *The End of the MACHO Era: Limits on Halo Dark Matter from Stellar Halo Wide Binaries*. ApJ, 2004. volume 601:311–318.

Yoshii, Y., Peterson, B. A. & Takahara, F. *On the angular correlation function of faint galaxies*. ApJ, 1993. volume 414:431–435.

Yu, Q. & Tremaine, S. *Observational constraints on growth of massive black holes*. MNRAS, 2002. volume 335:965–976.

Zucca, E., Zamorani, G., Vettolani, G. *et al.*. *The ESO Slice Project (ESP) galaxy redshift survey. II. The luminosity function and mean galaxy density.*. A&A, 1997. volume 326:477–488.

Zwicky, F. *On the Masses of Nebulae and of Clusters of Nebulae*. ApJ, 1937. volume 86:217–+.

Zwicky, F., Herzog, E. & Wild, P. *Catalogue of galaxies and of clusters of galaxies*. Pasadena: California Institute of Technology (CIT), 1961-1968, 1968.